NASA CR-72720
GE R70-AEG 223

EVALUATION OF RANGE AND DISTORTION TOLERANCE FOR HIGH MACH NUMBER TRANSONIC STAGES

by

V.L. Doyle and C.C. Koch

GENERAL ELECTRIC COMPANY

prepared for

NATIONAL AERONAUTICS AND SPACE ADMINISTRATION

NASA-Lewis Research Center
Contract NAS 3-11157
Charles H. Voit, Project Manager

NASA CR-72720
GE R70 AEG 223

DESIGN REPORT

EVALUATION OF RANGE AND DISTORTION TOLERANCE FOR HIGH MACH NUMBER TRANSONIC STAGES

By

V.L. Doyle and C.C. Koch

GENERAL ELECTRIC COMPANY
Aircraft Engine Group
Cincinnati, Ohio 45215

Prepared For

NATIONAL AERONAUTICS AND SPACE ADMINISTRATION

July 23, 1970

Contract NAS 3-11157

NASA-Lewis Research Center
Cleveland, Ohio 44135
Charles H. Voit, Project Manager
Fluid System Components Division

TABLE OF CONTENTS

TABLE OF CONTENTS (Concluded)

LIST OF ILLUSTRATIONS

LIST OF TABLES

ABSTRACT

Two transonic single-stage compressors were designed to investigate the efficiency, weight flow range, and distortion tolerance of high-tip-speed fan stages and to determine the ability of variable-geometry blading to improve off-design performance. The first compressor, the Task I Stage, used an existing 1400 ft/sec-tip-speed, multiple-circular-arc rotor and a new matching stator. The Task II Stage consisted of a variable-camber inlet guide vane, a 1500-ft/sec-tip-speed rotor and a variable-stagger stator. Both stages had a rotor inlet tip diameter of 36.5 inches and a rotor inlet hub:tip radius ratio of 0.5. Both stages used the same stator vanes, had identical flowpaths, and used many of the same test vehicle components. The Task I Stage design total-pressure ratio was 1.617 at a weight flow of 219.4 lbs/sec; the Task II Stage design total-pressure ratio was 1.659 at a weight flow of 226 lbs/sec.

SECTION I

SUMMARY

Two transonic single-stage compressors were designed to investigate the efficiency, weight flow range, and tolerance to distorted inlet airflows of high-tip-speed fan stages, and to determine the ability of variable-geometry blading to improve off-design performance and distortion tolerance.

The Task I Stage consisted of the 1400-ft/sec-tip-speed Rotor 1B, previously tested as an isolated blade row under NASA Contract NAS 3-7617, and a set of new stator vanes. The resulting Task I Stage was predicted to have a total-pressure ratio of 1.617 and an adiabatic efficiency of 0.873 at an inlet corrected weight flow of 219.4 lbs/sec and 1400 ft/sec tip speed. The Task II Stage was a new design, consisting of a 1500-ft/sec-tip-speed rotor, a variable-camber inlet guide vane and a variable stagger stator. Design total-pressure ratio for the Task II Stage was 1.659 with an adiabatic efficiency of 0.854 at an inlet corrected weight flow of 226 lbs/sec. Both stages had a rotor inlet tip diameter of 36.5 inches, and both had a rotor inlet hub:tip radius ratio of 0.50. A preliminary design study indicated that by designing the Task II Stage for the same tip diameter and radius ratio as the Task I Stage, and by properly selecting the Task II rotor total-pressure ratio, both stages could use the same stator vanes, have the same flowpath contours, and use a large amount of common test vehicle hardware. As a result, all blading was designed for the aerodynamic conditions of the Task II Stage, and yet the Task II stator could be used with Rotor 1B to form the Task I Stage.

The 1500-ft/sec-tip-speed rotor designed for the Task II Stage had an inlet specific weight flow (corrected to standard day rotor inlet conditions) of 41.62 lbs/sec-sq ft of annulus area, and a relative inlet Mach number of 1.526 at the tip with zero inlet guide vane turning. Tip diffusion factor was 0.368 with a tip solidity of 1.40. The rotor mass-averaged design total-pressure ratio was 1.686, approximately constant with radius. Radially varying relative total-pressure losses were assumed, resulting in a rotor mass-weighted adiabatic efficiency of 0.883. Fully arbitrary blade sections were used in order to better control throat areas and suction surface Mach numbers. Chord length was varied slightly, increasing from hub to tip in order to obtain the desired solidity values. The aspect ratio of the rotor was 2.36 based on the pitchline chord. A part-span shroud was used to insure aeromechanical stability.

The common stator vane was designed to accept the flow leaving the 1500-ft/sec-tip-speed Task II rotor, and also to be compatible with the 1400-ft/sec-tip-speed Task I rotor. The stator returned the flow leaving the

rotor to the axial direction. Hub diffusion factor was 0.435 at an inlet Mach number of 0.77, with a hub solidity of 2.156. Radially-varying losses were assumed; the mass-weighted total pressure loss was 1.22 percent. Stator vane aspect ratio was 2.065 based on pitchline chord. Double-circular-arc vane sections were specified in the outer part of the vane, and arbitrary sections were generated near the hub for better control of surface Mach numbers.

A preliminary off-design analysis was conducted to identify optimum off-design inlet guide vane and stator settings for the Task II Stage. This study examined operation at 70 percent corrected speed and 54 percent design corrected weight flow, an operating point typical of Mach 3 flight. It was determined that approximately 30-35 degrees of inlet guide vane turning, radially constant, and an increase of 8 degrees in stator stagger angle would allow reasonable performance to be maintained.

The inlet guide vane for the Task II Stage was designed to have variable camber so that it would allow axial flow to enter the rotor at the design point and would turn the flow to at least 35 degrees for off-design operation. This vane was made up of an uncambered nose section fixed in the axial direction, and an uncambered rear flap which was hinged to provide the camber variation. The chord of the flap was approximately four times that of the nose. The vane solidity, based on the sum of nose and flap chords, varied from 1.788 at the hub to 1.299 at the tip. In the cambered position, the vane sections became oriented so as to form a slot between the nose and the flap. The axially-oriented nose and the slot were intended to minimize losses due to incidence and turning and to extend the low-loss range of turning angles beyond that obtained with conventional adjustable guide vanes.

Additional test equipment was designed to permit the study of the effects of inlet flow distortions. Screening was specified to produce radial and circumferential inlet distortion patterns, and provision was made to rotate the circumferential distortion screen past the instrumentation for detailed surveys of the flow. Detailed aeromechanical analysis was performed in the design of each blade row to assure reliability of the test hardware.

SECTION II

INTRODUCTION

The need to reduce the size and weight of gas turbine engines for advanced military and commercial aircraft has led to the use of high-tip-speed fan and compressor stages. Such stages frequently are required to operate satisfactorily at off-design conditions and with distorted inlet flows. A turbofan engine for a Mach 3 aircraft, for example, would need fan stages meeting severe performance requirements at both design and off-design corrected speeds, and also could encounter severely distorted inlet airflows. It is therefore worthwhile to obtain data on the efficiency, weight-flow range, and distortion tolerance of high-tip-speed stages and to investigate the use of variable-geometry features to maintain performance at off-design operating conditions. This research program, NASA Contract NAS 3-11157, was instituted in response to these needs. The program involved the design and testing of two single-stage compressors designed for rotor tip speeds of 1400 and 1500 ft/sec using a common variable-stagger stator. The higher-speed stage was also provided with variable-geometry inlet guide vanes.

The Task I Stage used an existing 1400-ft/sec-tip-speed rotor from NASA Contract NAS 3-7617 and a new matching stator. The rotor (Rotor 1B in references 1-3) had been tested previously as an isolated blade row and demonstrated excellent efficiency and weight-flow range. The Task I test objectives were to determine the efficiency and flow range potential of this stage, to evaluate any effect the new stator might have on the rotor performance, and to obtain blade element data on both the rotor and the stator. The Task II Stage had a 1500-ft/sec-tip-speed rotor, a variable-camber inlet guide vane, and an adjustable stator. Objectives of Task II Stage tests were to obtain blade element data and to evaluate the effectiveness of the variable-geometry blading at several key points in an operating envelope typical of an engine for a Mach 3 aircraft. Another major objective of both Task I and II was to determine the tolerance of each compressor stage to distorted inlet flows and to obtain extensive data on the structure of the distorted flow fields. The inlet flow distortion testing with the Task II stage was also intended to evaluate the effectiveness of variable-geometry blading in improving stable operating range with inlet flow distortions.

This report documents the considerations involved in selecting design parameters for each stage, the detailed aerodynamic design of the Task II rotor and stator blading, the preliminary study to define requirements for the Task II variable-geometry features, and the aerodynamic design of the variable-camber inlet guide vanes for the Task II stage. Also included in this report are descriptions of the mechanical and aeromechanical design of the test vehicle and compressor blading.

SECTION III

PRELIMINARY DESIGN OF TASK I AND TASK II COMPRESSOR STAGES

The basic requirement for the Task I Stage compressor was to provide a stator to match the flow conditions leaving Rotor 1B, a high-performance, 1400-ft/sec-tip-speed, multiple-circular-arc rotor tested previously without inlet guide vanes or stators under NASA Contract NAS 3-7617 (references 1-3). In this report, the rotor for the Task I Stage is referred to as Rotor 1B, in order to be consistent with Contract NAS 3-7617 terminology. Since the rotor blading, inlet ducting, frames, shafts, and bearings for the Task I Stage were to be existing hardware used in earlier Rotor 1B testing, the Task I Stage design effort involved only the provision of stator vanes and stator flowpath hardware needed to produce axial flow at the compressor discharge. The existing hardware had a rotor inlet tip diameter of 36.5 inches with an inlet hub:tip radius ratio of 0.50.

Operating requirements for the stator for the Task I Stage were established at a rotor inlet corrected weight flow of 219.4 lbs/sec, a rotor total-pressure ratio of 1.636, and a rotor adiabatic efficiency of 0.8915. This rotor operating condition is shown on the performance map for Rotor 1B, figure 1, and corresponds to a 100-percent design corrected speed data point from Rotor 1B testing (reading 52, documented in reference 2). At this point, the rotor stall margin was 21.5 percent, and the rotor adiabatic efficiency was nearly maximum for design speed operation. Blade element data obtained during reading 52 of the Rotor 1B testing, reference 2, indicated that rotor trailing edge absolute air angles were in the range from 37 degrees near the tip to 46 degrees near the hub. The stator vanes for the Task I Stage would be required to remove approximately this level of swirl.

The Task II Stage for this program was to consist of a 1500-ft/sec-tip-speed rotor plus variable-geometry inlet guide vanes and variable-stagger stators. The variable-geometry blading was to be used to improve off-design operating range. The Task II inlet guide vanes were required to impart no swirl to the inlet flow at the stage design point, and the stators were required to remove all swirl from the stage exit flow. Variable-geometry requirements for the Task II inlet guide vanes and stators were defined in a study of off-design operation. Variable-geometry requirements did not directly influence the detailed design of the Task II rotor or stator, because it was believed that designing for acceptable performance at 1500 ft/sec tip speed would be difficult enough without the introduction of additional considerations. The inlet guide vane design, however, was based primarily on off-design requirements. Additional design requirements for the Task II Stage were a rotor tip diffusion factor of approximately 0.35, a rotor hub:tip radius ratio of 0.5 maximum, and a rotor inlet tip diameter of 30 inches minimum.

Early in the preliminary design phase, it became clear that a considerable cost saving would result if the Task II Stage design point could be selected so as to enable it to use the same flowpath, and possibly the same stator vanes, as the Task I Stage. The Task II Stage rotor inlet tip diameter and hub:tip radius ratio were, therefore, made the same as in the Task I Stage, 36.5 inches and 0.50, respectively. The inlet corrected weight flow of the Task II Stage was selected to be 226 lbs/sec, the flow passed by Rotor 1B when operated overspeed at 1500-ft/sec tip speed. Resulting Task II rotor inlet specific weight flow was 41.62 lbs/sec-sq ft of annulus area. The required Task II rotor tip diffusion factor of 0.35 and the rotor tip speed of 1500 ft/sec dictated that the Task II rotor total-pressure ratio be just under 1.7. Examination of figure 1 shows that the design point of the Task II rotor was very nearly on a constant throttle line passing through the point at which Rotor 1B was matched for the design of the Task I Stage. Therefore, it appeared that the same flowpath contours would be acceptable for both stages.

Figure 2 shows the common flowpath that was developed for the two stages. The outer casing contours were made identical to those used in Rotor 1B tests under NASA Contract NAS 3-7617 throughout the length of the compressor, and hub contours were the same as in the previous contract from the compressor inlet to the rotor trailing-edge station. New stator hub contours were developed to provide annulus convergence across the stator vane row. It was decided that the Task II Stage inlet guide vanes would be designed as a subassembly which could be removed and replaced by smooth hub and casing spool pieces for Task I Stage testing.

Preliminary aeromechanical analysis was conducted and indicated that a reliable Task II Stage rotor blade could be designed with the same hub axial projection as the Rotor 1B used in the Task I Stage, thus assuring that a common flowpath could be used for both compressor stages. The selected flowpath allowed use of existing inlet ducting, rear casings, frames, bearings, and shafts from previous NASA contracts.

Preliminary axisymmetric flow calculations were performed for each compressor stage using the common flowpath contours in order to confirm that the same stator vanes could be used in both the Task I Stage and the Task II Stage without significant compromise. The analysis for the Task I Stage used Rotor 1B blade element data to specify radial distributions of rotor total-pressure ratio and relative total-pressure loss coefficient at the selected 100-percent speed stage design point. Figure 3 shows rotor exit station absolute air angles, β 1.50, resulting from the axisymmetric flow calculations, and compares these to rotor trailing edge absolute air angles, β_2, determined from blade element data testing on Rotor 1B at the same operating condition. The agreement is generally good between calculated and measured values; differences are due to the

different axial locations associated with the data, the different hub contours aft of the rotor trailing edge, and the influence of the rotor part-span shroud wake on the test data. Similar preliminary axisymmetric calculations were performed for the Task II Stage at its inlet corrected weight flow of 226 lbs/sec. It was determined that a rotor total-pressure ratio of 1.686 would produce absolute flow angles at the stator inlet calculation station that were nearly identical to those expected in the Task I Stage. The close agreement in Task II Stage and Task I Stage stator inlet air angles, β 1.60, is shown in figure 3. The Task II rotor total-pressure ratio was therefore fixed at 1.686, so that the same stator vanes could be used in both compressor stages.

Since the preliminary study indicated that the same stator vanes could be used in both the Task I Stage and the Task II Stage, it was decided to design the stator vanes specifically for the Task II Stage flow conditions and to use this stator in the Task I Stage without performing further design work related to the Task I Stage. This decision not only simplified the design procedure, but also allowed the stator vanes to be designed for the generally higher Mach numbers of the Task II Stage. All blading designed under this contract is, therefore, referred to as Task II blading in the following sections. Details of the stator aerodynamic conditions expected in the Task I Stage at its design point are compared to stator design quantities in certain of the figures related to the aerodynamic design of the Task II stator vanes. A summary of general design features and predicted performance for both the Task I Stage and the Task II Stage is given in table I.

In summary, the preliminary design effort resulted in the selection of a design point for the 1500-ft/sec-tip-speed Task II rotor compatible with an overspeed operating point for the 1400-ft/sec-tip-speed Rotor 1B from Task I. The flowpath for the Task II rotor was made identical to that of Rotor 1B. The primary difference between the new Task II rotor and Rotor 1B was that new blade section shapes and solidities were selected in order to precisely match the flow conditions at the higher speed Task II rotor design point. At 1500-ft/sec tip speed, or 107 percent of design speed, the Rotor 1B, operating with adequate stall margin, would have an adiabatic efficiency of 0.86 to 0.87 as indicated in figure 1, considerably below the 0.915 attainable at 90 percent design speed. It was believed that the new Task II rotor design, having blading specifically designed for the 1500-ft/sec-tip-speed operating condition, would produce a higher efficiency than that attained by Rotor 1B at the Task II design tip speed. The more advanced technology to be developed in the design of the Task II rotor, and the opportunity to obtain performance comparisons between the Task II rotor and Rotor 1B, were expected to be of significant value.

SECTION IV

TASK II ROTOR AERODYNAMIC DESIGN

1. AXISYMMETRIC FLOW CALCULATIONS

The preliminary phase of the aerodynamic design effort, described in the previous section of this report, established the basic design specifications of the Task II rotor. These specifications, as well as certain rotor performance parameters, are summarized in table I.

Flowpath contours for the Task II Stage are shown in figure 2. Hub and casing contours between the rotor leading edge and trailing edge, calculation stations 1.0 and 1.5 respectively, were made identical to those of the Rotor 1B compressor from NASA Contract NAS 3-7617. Five calculation stations were placed inside the rotor blade row between the rotor leading edge and trailing edge stations, to stabilize the axisymmetric flow calculations and to facilitate the selection of rotor blade-section shapes. The General Electric Compressor Axisymmetric Flow Determination computer program described in reference 1 was used to establish flow conditions throughout the stage. The flow was analyzed along nine streamlines, numbered 1 (at the tip) through 9 (at the hub). These streamlines passed approximately through radial positions at 0, 5, 10, 30, 50, 70, 90, 95, and 100 percent of annulus height from the tip at station 1.51, the rotor exit instrumentation plane. Table II lists the radial position of each streamline at the major calculation stations throughout the flowpath.

The wall boundary layer blockage distribution, denoted by the effective-area coefficient (K_{bl}), was modified slightly from that used in the Rotor 1B design, due to Rotor 1B performance test results which suggested that the actual boundary layer blockage was less than the assumed design values (reference 3). The adjustment used in the Task II rotor design was applied from ahead of the inlet guide vane to the rotor exit, station 1.50.

The boundary layer blockage effective area coefficient was assumed equal to 0.990 at compressor inlet and gradually decreased through the inlet guide vane to 0.985 at IGV exit station 0.50. It was then maintained at that level to the rotor inlet, station 1.0, then reduced to 0.96 at rotor exit. The remainder of the flowpath boundary layer blockage aft of the rotor was estimated from past experience with similar compressors. An adjustment to the K_{bl} distribution, to account for part-span shroud blockage of approximately 1.60 percent maximum, was uniformly distributed over the rotor annulus area at the rotor internal calculation stations. Figure 4 is a plot of boundary layer blockage effective area coefficient, K_{bl}, including the part-span shroud blockage adjustment, versus axial distance along the flowpath. Axisymmetric calculations to account for blade thickness blockage effects

were carried out as part of an iterative design process explained below, in which accurate determination of blade blockage depended on obtaining an accurate definition of the rotor blade section shapes. The blade blockage, denoted by the effective area coefficient (K_b), was accounted for at rotor internal calculation stations. This was determined by letting blade thickness be distributed along the chord length of the rotor on each streamline section according to quarter-sine-wave functions between each edge thickness and the maximum thickness. The radial distributions of maximum thickness and of leading and trailing edge thickness are shown in figure 5. The location of maximum section thickness, as a percent of "cascade" chord length, is given in figure 6.

The design relative total-pressure loss coefficients for the Task II rotor were based on Rotor 1B test data at design speed near peak efficiency, reading 52 found in reference 2, and adjusted upwards slightly to account for increased shock losses at the 1500-ft/sec tip speed. The results were consistent with the projected improvement in efficiency compared-to the overspeed performance of Rotor 1B. Figure 7 shows the design relative total-pressure loss coefficient distribution for the Task II rotor plus the Rotor 1B test data. Rotor total-pressure ratio was specified as 1.686, approximately constant from tip to hub. The total pressures and total temperatures within the axial extent of the rotor were estimated by varying the angular momentum along streamsurfaces, as a sine function raised to the 1.5 power, while maintaining a constant value of polytropic efficiency equal to the overall value.

Axial velocity, axial velocity ratio, and relative Mach number distributions at the blade leading and trailing edges are shown in figures 8, 9, and 10. The number of blades, 44, was the same as for Rotor 1B used in Task I. The nonlinear chord distribution shown in figure 11 was established by aeromechanical requirements and the tip solidity considerations mentioned below. The aspect ratio, based on mean span and pitchline chord, was 2.36 compared to 2.5 for Rotor 1B. The hub solidity of 2.443 was the same as Rotor 1B, but the tip solidity was increased to 1.40 to reduce Mach number losses and tip diffusion factor. Figure 12 shows the final solidity distribution, and figure 13 shows the resulting diffusion factors. The tip diffusion factor was 0.368 from leading edge to trailing edge as compared to a Rotor 1B design tip diffusion factor of 0.350.

2. ROTOR BLADE SECTION SHAPE SELECTION

The initial step required in selecting rotor blade section shapes was to establish leading and trailing edge meanline angles. In order to do this, the axial location of the rotor leading and trailing edges on each streamline and the airflow angles at each edge were required. The axial projection of the rotor blade, however, could only be determined after the blade

meanline angles had been specified and the rotor sections had been stacked radially on centers of gravity. In addition, the axial projection of the blade was needed in order to properly specify blade thickness blockages, enthalpy gradients, and entropy gradients in the axisymmetric flow calculations from which the leading and trailing edge air angles were obtained. In practice, the design procedure consisted of estimating the axial projection, using this to obtain the axisymmetric flow calculations, using these results to specify preliminary blade sections, and obtaining a new axial projection. The process was repeated several times until acceptable blade section shapes were obtained and until the axial projection used in performing the axisymmetric flow calculations was in agreement with that resulting from the final selected blade sections.

Blade setting calculations and specification of section shapes were performed along "cascade" projections in which the blade was cut along axisymmetric streamsurfaces and these cut sections were viewed along the blade axis, a radial line in this case. The rotor relative air angles at the blade leading and trailing edges, in the "cascade" projection, are shown in figure 14. The relative turning angle of the flow from leading edge to trailing edge is plotted versus radius ratio in figure 15.

Design incidence angles for the Task II rotor, figure 16, were selected from examination of Rotor 1B test data at 100 percent design speed near the peak efficiency point. Task II rotor tip incidence of 3 degrees was approximately equal to the Rotor 1B test results. The hub incidence angle for the Task II rotor was reduced by approximately 2 degrees from the level indicated by the Rotor 1B test data. This was done in an effort to avoid the greater-than-design hub deviation angle and low hub total-pressure ratio produced by Rotor 1B which were attributed to leading edge separation due to excessive incidence.

The deviation angles, $\delta°$, were obtained from a modification to Carter's rule for circular arc meanlines as explained in reference 1. An equivalent two-dimensional cascade of the same circulation as the streamline section under study was used to obtain an equivalent rotor outlet relative flow angle and, thus, an equivalent relative turning angle. Carter's rule was employed using the equivalent relative turning angle plus an empirical adjustment, X, based on past experience with similar blades, primarily Rotor 1B. The empirical adjustment was increased at the hub from the Rotor 1B value because the Rotor 1B test data, reference 2, showed a need for more camber than its design value. The resulting design deviation angles, and the X-factors assumed in obtaining the deviation angles, are shown in figure 17. Resulting blade-edge meanline angles are shown in figure 18, and the camber distribution of the rotor is shown in figure 19.

As mentioned earlier, the blade setting procedure was carried out simultaneously with the selection of blade section meanline angle distri-

butions between leading and trailing edges. In order to allow more flexibility in designing the blade sections for leading edge suction surface contours properly matched to the entering flow, for low suction surface Mach numbers near the expected shock location, and for proper passage area distributions, the blade sections were allowed to be of arbitrary shape.

As discussed in reference 4, the entry region of a supersonic rotor passage is critical to the ability of the rotor to accept its design weight flow. Essentially, the entry requirement for rotor sections having supersonic relative and subsonic axial Mach numbers is that the net effect of all disturbances produced forward of the first Mach wave which intersects the leading edge of the adjacent blade must be zero. In designing the suction surface contours of the Task II rotor to meet this entry requirement, it was required that leading edge meanline incidence angles consistent with past experience would still be retained. A free-flow streamline direction and Mach number were calculated at several axial positions within the rotor passage to define the flow field which would exist if there were no blade forces or blade-induced losses present. The average angle of the suction surface in the entry region was offset slightly from the average free-flow streamline direction to account for the effects of leading edge thickness, bow wave losses, and blade boundary layer buildup. The amount by which the suction surface was offset and the amount of blade meanline curvature specified in the entry region were adjusted to allow entry requirements to be met consistent with the selected incidence angles, figure 16.

Another objective to be met in the selection of rotor blade section shapes was to design for suction surface Mach numbers that were as low as possible consistent with adequate flow area. For streamlines 1-6, for which the inlet relative Mach numbers were supersonic, the suction surface Mach numbers were calculated by assuming a Prandtl-Meyer expansion or compression process between the local free-flow air angle and Mach number and the local blade suction surface angle. These calculations were performed at points between the leading edge and the approximate passage shock position on the suction surface; the resulting distributions are given in figure 20. The passage shock position was estimated as being the point on the suction surface from which a line normal to that surface would intersect the leading edge of the adjacent blade. As seen in figure 20, the suction surface Mach numbers for tip streamlines 1-3 at the estimated shock location did not exceed the value of the leading edge relative Mach number. This was achieved by the use of some negative camber in the forward part of the airfoil. Rotor 1B, by comparison, had zero camber near its leading edge at the tip and, thus, should have had suction surface Mach numbers greater than the tip relative inlet Mach number. For streamlines 4-6, passage throat area requirements necessitated some camber in the blade near the shock location; and, suction surface Mach numbers higher than the leading edge relative Mach number resulted.

Surface Mach number distributions for the rotor hub section (streamline 9) could not be determined by the method used for streamlines 1-6, because the inlet relative Mach number was subsonic (0.907). An analysis of the hub section was made, however, using the General Electric Compressible Fluxplot Computer Program. This analysis method predicts surface Mach numbers for arbitrary blades in cascade and is an extension of the Rayleigh-Janzen technique of adding compressibility disturbances, formulated in terms of powers of a reference Mach number, to an incompressible solution. The extension of the method involves iteration techniques to improve the convergence of the solution at high subsonic inlet Mach numbers. The Compressible Fluxplot Program is formulated in terms of the stream function instead of the more usual potential function, in order to simplify the specification of boundary conditions. Also, the continuity equation is automatically satisfied by the use of the stream function. The Euler equations, which reduce to the irrotationality condition when subject to the condition of constant total pressure throughout the flow, is expressed as a second-order partial differential equation in terms of the stream function. A system of finite-difference equations in terms of the stream function is formed at the intersections of a Cartesian grid, and a simultaneous solution of the system of equations yields the solution to the differential equation. The periodic nature of the cascade flow field is enforced by relating stream function values on parallel boundaries surrounding a single airfoil. The program may account for annulus area convergence through the cascade by allowing for variable streamtube thickness. Variations in fluid total properties due to losses or radius change in a rotating cascade are not accounted for, however. In general, reliable results are obtained for cases in which the local Mach numbers do not exceed 0.95.

Figure 21 shows the surface Mach number distributions for the rotor hub blade section at an inlet relative Mach number of 0.70. Reliable solutions could not be obtained at the design relative inlet Mach number of 0.907 because supersonic local suction surface Mach numbers were calculated. It was assumed, however, that the distributions at the design condition would be similar to those obtained at 0.70 Mach number but at an overall higher level. A rotor hub blade section was developed to give acceptable surface Mach number distributions, and the meanline shapes for streamline sections 7 and 8 were selected to form a smooth transition between the supersonic portion of the rotor blade and the hub section.

Streamline passage area distributions resulted from the selected meanline angle distributions and the quarter-sine-wave thickness distributions (figures 5 and 6). Figure 22 shows axial distributions of the ratio of passage area to capture area for streamlines 1, 4, 5, and 9. The calculated passage area: capture area ratio includes the effects of channel width, streamtube height, and the change in relative fluid properties due to radius change. The ratio of minimum passage area, or throat area, to capture area for each streamline is shown in figure 23. This figure also

indicates the choke margin above the minimum area ratio possible for the inlet relative Mach number of each streamline. Design objectives for choke margin were selected on the basis of past experience, such as the design of Rotor 1B, reference 1. At the tip, streamline 1, choke margin was set at 4 percent, a value believed to be just sufficient to pass the design weight flow with some allowance for blade boundary layer formation. Choke margin in the pitchline region, streamlines 4 and 5, was set somewhat higher (5.5%) to allow for the blockage created by the part-span shroud. A choke margin of 5 percent was allowed at the hub, streamline 9. In general, the location of the throat was kept aft of the estimated passage shock location. The throat was located near the trailing edge for tip sections where the exit relative Mach number was near unity, and was located at the leading edge for the hub sections which had subsonic inlet and exit relative Mach numbers. Choke margin was virtually the same as in Rotor 1B design; but, because of the higher design inlet relative Mach numbers, the throat area:capture area ratios were smaller in the Task II rotor than in Rotor 1B.

Blade sections having the design incidence and deviation angles, and with meanline angle distributions selected according to the criteria discussed above, were developed along each of the nine axisymmetric streamsurfaces. Figure 24 shows the shape of the final tip, pitch, and hub sections. Stagger angles resulting from the selected meanline shapes are given in figure 25. Final design values of meanline angle and section thickness distributions are given in table III, and a summary of rotor design aerodynamic data is given in table IV.

In summary, by designing the Task II rotor at 7 percent higher tip speed than Rotor 1B, the resulting design had a higher tip solidity, some negative camber near the leading edge at the tip, and smaller throat-area:capture-area ratios. In addition, the Task II rotor section thicknesses were less than used in Rotor 1B. Therefore, although both rotors had the same flowpath contours, and nearly the same operating conditions at 1500-ft/sec tip speed, the two rotors had noticeably different blade geometry and were expected to produce distinctly different performance.

SECTION V

TASK II STATOR AERODYNAMIC DESIGN

1. AXISYMMETRIC FLOW CALCULATIONS

Design specifications for the Task II stator vanes were defined during the preliminary phase of the design effort and are summarized in table I. The detailed stator design was based on the flow conditions calculated for the Task II stage; but, because both compressor stages used the same flowpath and because the Task II rotor total-pressure ratio was selected to produce the same stator inlet air angles as the Task I rotor (figure 3), the stator vanes could also be used in the Task I Stage. Operating conditions of the stator as used in the Task I Stage are shown on certain of the figures in this section for comparison with Task II Stage design conditions. For use in the Task II Stage off-design investigations, the stator was designed with variable-stagger capability.

The flowpath for the stator, figure 2, was established during the preliminary design phase. Tip contours were made identical to those used in Rotor 1B tests in NASA Contract NAS 3-7617. Hub contours were selected to have annulus area convergence, slopes, and curvatures sufficient to control the hub diffusion factor. Calculation stations 1.60 and 2.0 were located at stator leading and trailing edges, respectively; and, station 1.65 was placed inside the vane row at the stacking axis in order to stabilize the axisymmetric flow calculations.

Stator inlet and exit flow conditions were obtained from axisymmetric flow calculations for the Task II Stage using the General Electric Compressor Axisymmetric Flow Determination computer program. The inputs to the calculation procedure for the stator vane row specified axial flow direction at stator exit and total-pressure loss coefficients. Flow conditions for the stator were calculated along the 9 streamlines used in the design of the Task II rotor. Boundary layer blockage effective-area coefficients were specified in the stator region as shown in figure 4. Vane thickness blockages were input to the compressor axisymmetric flow determination computer program at station 1.65. The maximum thickness was used to obtain internal blade blockages, since station 1.65 was the stacking axis location (defined as the 50-percent-chord point on the meanline) and the thickness was maximum at 50 percent chord. The t_m/C distribution varied linearly from a hub value of 0.045 to 0.065 at the tip. Total-pressure loss coefficients for the stator were based on blade element data given in NASA SP-36, reference 5. A 15-percent increase in loss was applied to the hub and tip regions to account for end wall effects. The stator loss distribution is shown in figure 26.

The axial velocity and Mach number distributions at stator inlet and exit stations resulting from the axisymmetric flow calculations are shown in figures 27 and 28. The low hub axial velocities in the Task I Stage were due to the low hub total-pressure ratio produced by Rotor 1B. An objective of the Task II Stage design was to produce a radially-constant, total-pressure ratio in order to avoid low velocities along the hub surface.

An approximately linear chord distribution, shown in figure 29, was specified, which varied from 3.650 inches at the tip to 3.184 inches at the hub. The stator vane aspect ratio, based on mean blade height and pitchline chord, was 2.065. Chord length and aspect ratio were primarily determined by aeromechanical considerations. A total of 46 stator vanes were used, giving a distribution of solidity (figure 30) which varied from 2.156 at the hub to 1.498 at the tip. Acceptable stator vane diffusion factors, shown in figure 31, resulted from this solidity distribution.

2. STATOR VANE SECTION SHAPE SELECTION

The design procedure used for the selection of the stator vane section shapes did not require an iteration process to find the axial projection of the vane. Since the stator leading and trailing edges were nearly radial, fluid conditions at the vane edges were assumed equal to those at calculation stations 1.60 and 2.00.

Vane setting parameters of incidence, deviation, and resulting meanline angles at the vane edges were required. The design incidence, i, was based on past experience and Compressible Fluxplot investigations of the stator vane sections. The final design incidence angle distribution is shown in figure 32. The stator deviation angle, $\delta°$, was calculated from the same equivalent cascade modification to Carter's Rule as had been used for the rotor. The empirical deviation angle adjustment, X, for the stator was obtained from prior experience with similar vanes of this general type. Figure 33 shows the deviation angle and empirical adjustment distributions for the stator. The stator leading and trailing edge meanline angles, resulting from the selection of incidence and deviation, are shown in figure 34. The camber distribution for cascade sections is shown in figure 35.

Double-circular-arc airfoils in the cascade projection were selected for the outer half of the vane. An arbitrary airfoil section was developed for the hub to obtain lower suction surface Mach numbers than produced by a double-circular-arc hub section. The vane sections between the arbitrary hub and double-circular-arc pitchline sections were selected to form a smooth transition.

In order to completely specify the vane section shapes, the distribution of vane thickness, t/t_m, had to be specified versus percent chord length. By using double-circular-arc sections in the outer part of the stator vane, and having specified maximum thickness and edge thickness, the t/t_m distributions

could be determined. The t/t_m distributions for the arbitrary sections between the hub and the pitch-line were obtained by letting thickness vary as quarter sine waves along the chord length between the edge values and the maximum thickness. The location of maximum thickness for the arbitrary sections was slightly aft of the mid-chord point at approximately 52 percent chord.

Surface Mach number distributions for the double-circular-arc tip and pitch-line sections are shown in figures 36 and 37, as obtained from the General Electric Compressible Fluxplot computer analysis. The design inlet tip Mach number was 0.61, while at the pitchline the Mach number was 0.66. Double-circular-arc sections were tried in the hub region, but resulting suction surface Mach numbers were unnecessarily high. The curvature in the forward portion of the blade was therefore reduced in order to reduce the suction surface Mach numbers. Surface Mach number distributions for the arbitrary hub section can be seen in figure 38. The design stator hub Mach number was 0.77. A Compressible Fluxplot analysis at this inlet Mach number was attempted but was believed to be somewhat inaccurate. The fluxplot analysis and the optimization of the hub section were therefore done at 0.70 Mach number, with the assumption that, if satisfactory surface Mach numbers could be obtained, a satisfactory blade would result for the higher design Mach number.

Cascade sections selected for the stator tip, pitch, and hub are shown in figure 39. With the determination of final stator vane section shapes, the stagger angle distribution could be calculated. The radial variation of stagger angle, in the cascade projection, is shown in figure 40.

Stator choke margin values calculated for the tip, pitch, and hub sections (streamlines 1, 5 and 9) are shown in figure 41. Stator hub sections are generally most critical to choking below the design point on the performance map; and, although the Task II stator hub choke margin of 6.2 percent was less than at other sections, this was believed adequate to avoid choking at the design point.

The final Task II stage stator design is documented in table V (which lists meanline angle and thickness distributions versus percent chord on cylindrical sections) and table VI (which lists aerodynamic data for each streamline).

SECTION VI

PRELIMINARY OFF-DESIGN ANALYSIS

1. OBJECTIVES AND METHODS

A major objective of this contract was to investigate the use of variable geometry inlet guide vanes and stators as a means of obtaining high performance at operating conditions typical of both takeoff and of Mach 3 cruise at high altitude.

The Task II Stage to be used in this investigation consisted of a 1500-ft/sec-tip-speed rotor, a variable-stagger stator (whose designs have been discussed in previous sections), and a variable-camber inlet guide vane. The design point of this stage, 1500 ft/sec corrected rotor tip speed and a corrected weight flow of 226 lbs/sec, was taken as representing the take-off condition. A contractual requirement was that, at this design point, the inlet guide vane should produce no swirl in the flow entering the rotor and that the stator should remove all swirl from the flow at the stage discharge.

A review of several advanced engine systems under development by the General Electric Company for use in high-Mach-number aircraft indicated that the compressors of these engines typically operate at approximately 70 percent of their take-off corrected speed and 54 percent of take-off corrected weight flow at high-Mach-number cruise. In the Task II Stage, this corresponds to 1050 ft/sec corrected rotor tip speed and 122 lbs/sec corrected weight flow; this operating condition was selected as the high-Mach-number cruise off-design point. As shown in figure 1, however, Rotor 1B used in the Task I Stage could only be throttled to 54.5 percent of design flow at 70 percent design speed without stalling. By analogy then, it was anticipated that the Task II Stage would require variable-geometry blading in order to operate at this high-Mach-number cruise condition with adequate stall margin.

An analysis of the operation of the Task II Stage at this off-design condition was undertaken in order to define a range of inlet guide vane and stator settings which would assure low losses and acceptable stall margin at high-Mach-number operation. An additional purpose of this analysis was to aid in defining the type of variable-camber arrangement to be incorporated into the design of the inlet guide vane. Finally, the analysis was to provide an estimate of the effect that would be produced by any adjustment of the inlet guide vane and stator of the Task II Stage on the inlet conditions of a hypothetical second stage.

The compressor analyzed in this study was a two-stage unit. The inlet region and the first stage were identical to the Task II Stage. The hypothetical second stage had the same percentage area contraction across each blade row as the first stage, and both its rotor and its stator had solidity distributions and design-point loss coefficients identical to the corresponding blade in the Task II Stage. The total-pressure ratio of the second stage, at the design weight flow of 226 lbs/sec and the design first-rotor tip speed of 1500 ft/sec, was 1.40. The flowpath for the compressor used in this analysis is shown in figure 42.

The off-design analysis made extensive use of the General Electric Compressor Axisymmetric Flow Determination computer program to predict radial and axial variations in fluid conditions. Blade row total-pressure loss coefficients and exit air angles were input to the program as functions of incidence angle as determined by General Electric experience. The most important outputs from the program for purposes of this study were values of blade row diffusion factor and inlet relative air angles. An iterative process was used to obtain convergence between calculated incidence angles and those input quantities which varied with incidence.

2. RESULTS

a. OPTIMUM INLET GUIDE VANE TURNING

The first step in this investigation was to identify a range of inlet guide vane discharge air angles which would result in satisfactory first-rotor relative inlet angles and diffusion factors at off-design operation. Attention was focused on radially-constant guide vane turning distributions. Because zero camber at all radii was required at the design condition, mechanical design of the inlet guide vane would be facilitated by a design approach that avoided nonuniform camber for off-design conditions.

In the analysis, flow angles of 25, 30, 35, and 40 degrees, radially constant, were assumed to be produced by the inlet guide vane at station 0.50 (figure 40). During this first step, the stators were assumed to be closed 10 degrees. It proved impossible to analyze the 25- and 40-degree guide vane turning cases using the axisymmetric flow computer program. With 25 degrees of inlet swirl, the program predicted a stall at the hub of the first stator; with 40 degrees of inlet swirl, the computer program indicated that the first rotor hub could produce no work input. Neither case could be adequately processed by the computer program.

Inlet guide vane turning angles of 30-35 degrees, however, were processed without any indications of stall or turbining and produced first-rotor inlet-air-angle and loading distributions which were considered acceptable. Figures 43 and 44 show first-rotor inlet-relative-air angle and diffusion factor

distributions, respectively, for the cases of 30- and 35 degrees of inlet swirl at 70 percent corrected speed and 54 percent corrected weight flow. Also shown on these figures are distributions of the same quantities at the 100-percent-speed design point and at 70 percent corrected speed and 68.5 percent corrected weight flow, with zero inlet swirl and stators in their nominal position in each case. This latter reference condition represents a satisfactory operating point at 70 percent speed with the nominal, or take-off, guide vane and stator settings. In Rotor 1B testing, figure 1, a rotor efficiency of approximately 0.90 and a stall margin of 26 percent were obtained at this 70-percent speed reference condition.

Figures 43 and 44 show that, with inlet swirl of 30-35 degrees, high incidence angles and normal loadings exist at the tip of the first rotor, with low incidence angles and low loadings at the hub as compared to the 100 percent and 70-percent speed reference cases. Based on Rotor 1B test results, reference 2, the 70-percent speed operating range of this type of rotor is expected to be quite broad, and the distributions shown in figures 43 and 44 should be tolerable for the rotor of the Task II Stage.

b. OPTIMUM STATOR SETTING

Having determined that inlet guide vane exit swirl angles of 30-35 degrees would produce acceptable first-rotor inlet conditions and loadings, the next step was to determine the optimum stator adjustment. An investigation was made of various stator setting angles at 70-percent corrected speed and 54-percent corrected weight flow with inlet guide vane turning of 30 degrees. To do this, increases in stator stagger of 10 degrees, 8 degrees, and 6 degrees were assumed. Stator deviation angles and blade row losses were obtained for each case as functions of incidence angle in an iterative procedure.

Figure 45 shows resulting radial distributions of stator incidence for the three cases investigated and also shows incidence angles at the two reference conditions for comparison. High incidence angles were encountered at the tip and low values at the hub. A stator adjustment of 8 degrees gave the best average distribution of incidence, and it was believed that acceptable performance could be obtained. Although not calculated, the estimated curve in figure 45 (for a stator setting of 0 degrees) shows that unacceptably-high stator tip incidence angles would have resulted at the design stator setting. It was also determined that stator adjustments in the range shown in figure 45 had no significant effect on first-rotor inlet relative air angles or diffusion factors. Figure 46 shows the radial variation of stator diffusion factor for a guide vane turning of 30 degrees and a stator adjustment of 8 degrees, and compares this to distributions at the reference conditions. The stator loadings were not greatly affected by stator adjustment, and the curve for an 8 degree adjustment is typical. Although the diffusion factors are higher than the design values, adequate performance is expected of the stator at these levels of diffusion.

c. SECOND-ROTOR INLET CONDITIONS.

At the selected off-design condition of 70 degrees corrected speed and 54 degrees corrected weight flow, the previous steps in the investigation showed that inlet guide vane exit air angles of 30-35 degrees and a stator adjustment of about 8 degrees were required in order for the first stage to produce acceptable performance. It remained to be determined if the inlet relative air angles of the hypothetical second stage would be acceptable at these operating conditions with the vane settings required by the first stage.

The second rotor inlet relative air angles are shown in figure 47 at the off-design condition with the 30-degree inlet guide vane and 8-degree stator settings. Inlet angles were approximately equal to the 100-percent speed design point values, and were only approximately 5 degrees higher than predicted at the 70-percent speed, 68.5-percent weight flow reference condition with nominal guide vane and stator settings. The second-rotor inlet conditions were not affected significantly by changing the inlet guide vane turning from 30 degrees to 35 degrees or by using stator stagger increases of 6 degrees and 10 degrees.

The distribution of air angles shown in figure 47 is therefore typical. The performance of a hypothetical second stage should thus be acceptable at the optimum first-stage off-design guide vane and stator settings.

3. SUMMARY OF OFF-DESIGN ANALYSIS

The primary conclusion of the preliminary off-design analysis was that acceptable performance could be achieved by the Task II Stage at 70 percent speed and 54 percent flow by using a variable-stagger stator and an inlet guide vane which produced a radially-uniform swirl angle distribution at its exit station. The importance of this was that a relatively simple mechanical design could be used for the inlet guide vane, one which did not require radially-varying camber at off-design settings while having zero camber at the design setting.

A second conclusion was that good off-design performance should be obtainable with guide vane exit air angles of 30-35 degrees and stator settings of about 8 degrees higher stagger angle than design. This conclusion will be checked during the shakedown test of the Task II Stage, and the final optimization of the guide vane and stator settings will be performed at that time. For mechanical design purposes, the stator was required to have an adjustment range of +20 degrees to -15 degrees from its design stagger angle. The inlet guide vane was designed for a 30-degree exit air angle, but mechanical provision for resetting the IGV to 45 degrees was incorporated.

Finally, the preliminary analysis demonstrated that the Task II Stage, operated with an inlet swirl angle of 30 degrees and its stator set at a stagger angle 8 degrees above design, could produce exit conditions compatible with a typical second stage. The Task II Stage could, therefore, serve as the first stage in a multistage fan or compressor used in a Mach-3 altitude cruise turbofan or turbojet engine.

SECTION VII

TASK II VARIABLE CAMBER INLET GUIDE VANE DESIGN

1. AXISYMMETRIC FLOW CALCULATIONS

The primary objective in designing the variable camber inlet guide vane was to minimize losses while varying the swirl angle at the exit of the guide vane. The results of the preliminary off-design analysis established that, at a 70-percent speed, 54-degree flow operating condition, the guide vane would be required to impart 30-35 degrees of swirl to the flow at all radii. It was required by the contract that, at the 100-percent speed, 100-percent flow design point of the Task II Stage, the guide vane should produce no turning of the flow.

The flowpath in the region of the inlet guide vane can be seen in figure 2. The guide vane was located relatively far forward of the rotor to provide space for instrumentation. The assumed wall boundary layer blockage coefficient distribution is shown in figure 4. Fluid properties and vector diagrams at station 0.40 (the guide vane inlet) and station 0.50 (the guide vane exit) were calculated using the Compressor Axisymmetric Flow Determination computer program. The nine design streamlines, along which calculations were performed, were the same as those used in the Task II rotor and stator design calculations.

Guide vane inlet and exit axial velocities are shown in figure 48 for the design condition with zero camber, and for the off-design condition with 30 degrees of camber. The total-pressure loss coefficient distribution is shown in figure 49 for these same two operating points. Losses were obtained from cascade tests of a similar variable-camber guide vane performed by General Electric under another contract.

2. AIRFOIL SECTION SHAPE SELECTION

In order to minimize losses, the variable camber vane was designed to have a leading edge blade angle of 0 degrees at all conditions and a trailing edge blade angle that could be varied from 0 degrees to at least 35 degrees. The discharge air angle could then be varied without incurring excessive losses from high incidence angles. A vane made up of two parts was selected to accomplish the camber variation. The nose part was fixed in the axial direction, while the rear flap could be rotated to vary the trailing edge angle. Figure 50 indicates the way in which the two parts of the guide vane were aligned in the uncambered position at the design point, and in the cambered position for off-design operation.

A total of 24 inlet guide vanes was specified, or approximately half the number of stator vanes (46). With 24 inlet guide vanes, the stator exit

wake rakes (which spanned two stator passages) also spanned approximately one guide vane passage. Thus, the total-pressure losses contributed by the guide vane and stator wakes would be measured in the proper proportion by the stage discharge instrumentation. Use of 23 guide vanes was considered, but rejected, because of the possibility that a guide vane wake might impinge on every other stator vane and cause stall. The selected number of 24 guide vanes avoided wake interference but still allowed accurate data acquisition.

Having specified the use of 24 inlet guide vanes, the radial distribution of chord length was selected so as to obtain the desired solidity distribution. The solidity, based on the sum of the nose and flap chords (figure 51), ranged from 1.299 at the tip to 1.788 at the hub. The range of guide vane solidity was chosen so as to bracket a value of 1.50, because the similar vanes which had been tested in cascade produced good performance at this level of solidity. A linear variation of the sum of chord lengths from hub to tip was used as shown in figure 52. Also shown in figure 52 are nose and flap chords separately. The cascade tests also showed that deviation angles in this type of design were very small. Accordingly, deviation angles of zero degrees were assumed in designing the guide vane for the Task II Stage.

The guide vane airfoil sections were made geometrically similar at all radii by scaling a single master section. This master section was derived from an airfoil having an uncambered meanline with a NACA 65-008 thickness distribution scaled up to a maximum thickness/chord ratio of 10 percent. Leading and trailing edge thickness of the 65-series airfoil were 1.0 percent and 1.5 percent of chord, respectively. The nose and flap portions of the guide vane were formed by dividing the 65-series airfoil into two parts, figure 50. The chord of the nose was 25.7 percent of the chord length of the flap and the sum of nose and flap chords was slightly less than the overall chord of the original 65-series airfoil. The maximum thickness of the resulting master vane section was 10.2 percent of the sum of nose and flap chords and was located 18.1 percent of the sum of chords from the flap leading edge.

Contours around the rear part of the nose and the leading edge of the flap were chosen so that a slot would be formed when the vane was in a cambered configuration. At 30 degrees of turning, the slot at the tip was a converging channel with a minimum width of 1.5 percent of the sum of chords. Acceptable slot shapes were formed at the tip with as little as 10 degrees of turning and as much as 40 degrees of turning. In the hub region, the aerodynamics of the slot had to be compromised to provide clearance between the nose and the flap in the cambered position. Although not analyzed in great detail, this slot was expected to assist in maintaining low losses at off-design operating conditions. The section shown in figure 50 indicates the airfoil contours and the shape of the slot at the tip section. Table VII presents a list of chord lengths and solidities, plus dimensions Z_N and Z_F from figure 50, which locate the nose and flap with respect to the axis of rotation of the flap.

SECTION VIII

TEST VEHICLE DESIGN

The inlet ducting for Contract NAS 3-11157 was the same as that used for Rotor 1B tests with uniform inlet flow under Contract NAS 3-7616. An incompressible fluxplot analysis of the inlet contraction region was made during the design phase of Contract NAS 3-7616, reference 1, and showed no adverse velocity gradients on either hub or casing contours. Zero swirl inlet conditions with a relatively thin casing boundary layer were found to exist during Rotor 1B testing, reference 2.

The same types of radial and circumferential distortion screens used in the Rotor 1B testing, conducted under Contract NAS 3-7617, will be incorporated for use in both Task I and II of Contract NAS 3-11157. The radial screen covered the outer 40 percent of the annulus area, while the circumferential screen spanned a 90-degree arc from hub to tip. Both screens were 20 mesh and had a 0.016-inch wire diameter corresponding to a screen solidity of 0.54. The distortion parameter for this screen material, $(P_{max.}-P_{min.})/P_{max.}$, was determined previously from test data to be 0.20 at the Task I Stage design weight flow. The support screen was designed to be rotated through 360 degrees for circumferential inlet distortion testing. The support screen was designed to separate into halves, to facilitate rapid installation, and was made of one-inch square mesh, 0.092-inch diameter wire with an open area of 83.4 percent. The distortion screens were located one-rotor diameter forward of the rotor leading edge and were mounted in a cylindrical section 30 inches long inserted into the test vehicle during distortion testing, as shown in figure 53.

Identical flowpath wall contours were specified for both Task I and Task II Stages, and the interchangeability of the test vehicle hardware can be seen in figure 53. The variable-geometry inlet guide vane assembly of the Task II Stage was designed to replace filler spools used in Task I.

Details of the mechanical arrangement of the inlet guide vane and stator vane supports and the actuation systems can be seen in figures 53, 54, and 61. The axis of rotation of the IGV flap was placed near the center of pressure of the flap, approximately at the point of maximum thickness, in order to reduce actuation loads and stress concentrations. This, however, required that the nose piece be displaced in the circumferential direction as the flap was rotated. Therefore, the nose was mounted into moveable rings set flush with the hub and casing walls. These rings were supported on bearings and were driven by the actuation system that rotated the flap. Table VII contains a listing for each guide vane section of the parameter $\Delta r\theta^\circ/\sin\phi^\circ$, where $\Delta r\theta^\circ$ is the circumferential displacement of the nose piece in inches, and ϕ° is the camber angle of the vane. Provision for up to 45 degrees of camber was

made in the mechanical design of the inlet guide vane. Stator variable-geometry capability allowed for +20 to -15 degrees of stagger angle adjustment with respect to the design setting.

Performance tests will be conducted in General Electric's house compressor test facility in Lynn, Massachusetts. The test compressor draws atmospheric air through two banks of filters. The first filter bank is intended to remove 22 percent of the particles larger than 3-5 microns (dust spot test), and the second filter bank is intended to remove 90-95 percent of the remaining particles down to the same size. The air then passes through a coarse-wire inlet screen, into the bellmouth, and then through the compressor. In the exit assembly, the compressor discharge flow is split into two concentric streams. The inner air stream is passed into an exit pipe containing a flow straightener and a venturi flow meter, and then is exhausted to the atmosphere. The outer air stream passes through a slide cylindrical throttle valve into a collector. Two pipes, each of which contains a flow straightener and a venturi flow meter, then discharge the outer stream to the atmosphere. Power to drive the test compressor is provided by a high-pressure noncondensing steam turbine rated at 15,000 horsepower.

APPENDIX I

TASK II BLADING AEROMECHANICAL DESIGN

BY J.E. Baker

The NASA Task II single-stage compressor is intended to provide aerodynamic data at tip speeds in excess of those explored by the Task I design, the Task II design speed being 9418 rpm for standard day inlet temperature of 59°F. It incorporates an inlet guide vane, a new rotor blade design, and the same stator vane as the Task I Vehicle. For the sake of economy, most of the Task I nonrotating hardware was retained. The new blading was thus designed within this constraint. This section of the design report deals with the aeromechanical design of the blading and the associated aeromechanical design guidelines.

Terminology which may not be of common understanding, and/or is peculiar to the General Electric Company, is defined below:

Aeromechanics — The technical discipline that considers the interaction of the aerodynamic environment with the elastic and mechanical properties of a turbomachine component, such as rotor blades or stator vanes.

Integral-Order Resonance — This type of blade vibration exists when a natural frequency corresponding to a "mode" of vibration is induced to respond at an integral multiple of rotor speed. These multiples are referred to as "orders" or "per-Rev's." Such resonances can occur when a blade natural frequency crosses each per-Rev.

Vibration Mode — Identification of a variety of ways in which a structure can vibrate, each of which has its own natural frequency. Examples in blading are:

- First flex: vibration normal to the least-moment axis with a node (zero motion) only at the root.
- Second flex: same as first flex except there are two nodes, one at the root and another at some point on the blade.
- First torsion: vibration having a twisting motion with a node running radially along the blade near its mid-chord location.

- System mode: one in which vibratory coupling occurs between blades as well as between the blades and the disc. The disc involvement involves radial nodes which are called nodal diameters. The disc involvement generally induces lower system mode frequencies than for the corresponding blade modes; and, like blade resonances, system mode resonances to excitations fixed in space (distortion, struts, etc.) can occur when the number of nodal diameters coincides with corresponding integral orders. See Chapter VI of Den Hartog, reference 6, for more details.

Limit-Cycle Instability

The vibration mechanism is self-excitation (excitation provided by the blade motion), occurring as a single degree-of-freedom vibration, and is associated with high angles of attack on the airfoil. It occurs as an essentially pure sinusoidal response of constant amplitude at one of the blade's natural frequencies.

Reduced Velocity

This parameter was developed originally for use in classical flutter work and is defined as follows:

$$V_R = V/(\omega_t \, C/2)$$

where, V = air velocity

C = chord length

ω_t = torsional frequency in radians per sec

Endurance Limit

Vibratory stress above which fatigue failure will occur in 10^7 cycles, or less

1. INLET GUIDE VANE

a. GENERAL CONSIDERATIONS

To satisfy aerodynamic requirements, this inlet guide vane design incorporates a variable-camber concept. Its construction is similar to the slotted flap commonly used on aircraft wings, where the rear airfoil can be pivoted and the forward airfoil remains aligned with the direction of airflow (see figure 54). In order to maintain a slot between the two airfoils, pins extending forward from the rear vane stems induce the forward vane actuation ring to move circumferentially as the rear vane is rotated.

The aeromechanical design of these vanes was predicated satisfying aerodynamic requirements, while at the same time maintaining structural integrity. Reuse of existing casings established the available axial length and the inner and outer diameters. The t_m/C and chord distributions, solidity requirements, and airfoil section shape were determined by aerodynamic requirements; this configuration was then evaluated for aeromechanical adequacy. The significant areas which were considered in this analysis, as well as the corresponding design criteria, are summarized as follows:

- Steady-State Stress: Design stresses should be sufficiently low to allow the use of readily obtainable, inexpensive, and easily machined material and still permit allowable vibratory stresses of at least 20-30 kpsi-single amplitude.

- Integral-Order Resonance: The lowest vane natural frequencies should be greater than twice rotor speed (2/Rev) in the operating speed range to assure against appreciable response to mechanical excitation (1/Rev) due to rotor unbalance. The natural frequencies, for the first 3 or 4 modes, should be sufficiently low to pass through resonance with rotor-blade passing excitation (44/Rev due to the use of 44 rotor blades) in the low- to mid-speed range. Reduced excitation forces to be expected at these lower speeds will guard against excessive vane vibration levels.

- Limit-Cycle Instability: For blading subjected to high angles of attack, General Electric Company experience indicates that limit-cycle instability will be avoided by designing the blading such that the reduced-velocity will not exceed 1.0-1.2 in the operating speed range.

b. DESIGN DEFINITION

The vane configuration and associated design data are summarized in table VIII and figures 55 and 56. Details pertaining to the aeromechanical adequacy of this configuration are provided in the next section.

c. DISCUSSION OF CRITICAL DESIGN PARAMETERS

This section describes the degree to which the design goals were achieved by the vane configuration selected for this compressor vehicle.

- Integral-Order Resonance: The natural frequencies for the first four vibration modes are tabulated in table VIII, and these plus higher modes are plotted in figures 55 and 56. Resonance with 44/Rev rotor blade passing excitation in the first four modes will fall below 4500 rpm where excitation energy will be moderate. The lowest frequency mode is first flex, the natural frequency of the forward vane being lower than that of the rear vane. This frequency for both the forward and rear vane sections is approximately equal to 3/Rev resonance in the high-speed range, thus providing adequate margin from 1/Rev and 2/Rev.

- Steady-State Stress: The steady stresses in the flap, nose, and actuating pins were calculated at the expected maximum steady aerodynamic loading on the IGV, a weight flow of 226 lbs/sec, and a flap rotation of 30 degrees from the axial direction (in the direction of rotation). The loading of the nose was estimated by aerodynamicists to be about 20 percent of the total vane load. These calculations yielded a maximum effective steady stress of 12 kpsi, this being on the rear vane adjacent to the inner diameter platform. Such low bending stresses made it unnecessary to use a sophisticated vane material. Thus, AISI 410 stainless steel was chosen for its availability and machinability as well as for its high endurance limit stress. As shown in figure 57, the allowable vibratory stress corresponding to 12 kpsi steady-state stress was about 60 kpsi - single amplitude, thus making it possible for sizeable vibratory stresses to occur without danger of vane fatigue failures.

- Limit-Cycle Instability: The possibility of encountering limit-cycle instability at any operating condition was adequately avoided since the maximum reduced velocity was less than 1.0. Thus, inlet guide vane instability will not limit the ability to acquire the aerodynamic data for which this program was designed.

2. ROTOR BLADE

a. GENERAL CONSIDERATIONS

The Task II rotor blade configuration, although aerodynamically different from that used in Rotor 1B, did not have to be greatly different geometrically. Thus, it too required use of a mid-span shroud. Details of the configuration and supporting design effort are provided in the following paragraphs.

To achieve commonality with much of the Task I vehicle hardware, many of the Task II rotor parameters had to be practically the same as those for the Rotor 1B design which was used in the Task I vehicle. Flowpath geometry set the axial length available, and thus fixed the chord lengths that could be used. Aerodynamic requirements for rotor tip solidity dictated the number of blades at 44. It was also preferable to keep the blade shroud below 65 percent span, so that the shroud wake and shock pattern would not disturb aerodynamic measurements in the outer portion of the blade. Within these restraints, the rotor blade was designed to avoid mechanical distress in the aerodynamic and mechanical environments expected to be encountered during testing. The more important design criteria considered are detailed as follows:

- Steady-State Stress: Blade steady-state stresses should be minimized in regions of anticipated high vibratory stresses in order to permit vibratory stresses of at least 20 kpsi - single amplitude. This allowance is necessary in order to assure that vibratory response of blading to inlet flow distortion and rotating stall will not exceed safe levels.

- Integral-Order Resonances: The most critical resonances to be considered for fan-type rotor blade vibration are the low orders (1, 2, and 3/Rev). Not only is mechanical rotor unbalance excitation (basic 1/Rev) important, but so also is excitation from 1/Rev circumferential inlet flow distortion, the investigation of which is a part of the planned program. Since the 2/Rev and 3/Rev harmonics can be appreciable, blade natural frequencies of the lower vibration modes should not be resonant with these per/Rev's in the mid-to-high-speed range.

  Resonant response to stator-passing excitation is not normally a significant aeromechanical consideration for shrouded blading. Vibration modes subject to such resonant excitation in the high-speed range are usually complex, and this, plus shroud damping, tend to keep vibratory response at low-stress levels.

- Limit-Cycle Instability: Although the aeromechanical design guidelines described in the inlet guide vane section also apply to rotor blades, it is more difficult to achieve reduced velocities below 1.0 for rotor blades. However, it is possible to design for higher values of reduced velocity if it can be determined that rotating stall will be reached prior to instability. The relationships on which such a design practice can be based have been determined from General Electric Company's design experience.

b. DESIGN DEFINITION

The blade geometry and pertinent design data are summarized in table IX and figures 58-60, with additional details provided in figures 5 and 11. The final design was primarily predicated on the avoidance of limit-cycle instability, since this consideration provided the most stringent limitation on blade size and shroud location. The Task II blades incorporate shrouds integral with the airfoil which are located at 63 percent span. The shrouds have an elliptical cross section in order to reduce aerodynamic losses. Blade material was chosen to be Ti-6Al-4V, primarily for its high strength-to-density ratio, a necessity for high-tip-speed fan blades; it also has long experience as a gas turbine engine blading material and is readily available.

c. DISCUSSION OF CRITICAL DESIGN PARAMETERS

The design geometrical constraints were such that the variables available for optimizing the blade design were chord distribution between the shroud and the blade tip, t_m/C distribution, and radial location and size of the shroud. The following paragraphs provide pertinent details of the final blade design in each of the critical areas.

- Limit-Cycle Instability: The combination of higher relative velocities and revised blade cascade definitions for the Task II rotor, as compared to Rotor 1B, made it necessary to refine the chord and t_m/C distribution as well as shroud radial location in order to keep the reduced velocity from falling appreciably above that of Rotor 1B. To accomplish this, local chord and t_m/C increases in the shroud region were necessary (figures 11 and 5) as well as moving the shroud from 58 percent span (Rotor 1B) to 63 percent span. These refinements increased the torsional frequency and the chord terms in the reduced velocity parameter, resulting in a value of 1.38. This compares with a value of 1.33 for Rotor 1B at design point operating conditions. With the possible exception of operation with inlet distortion, this blade design should be free of instability at unstalled operating conditions. As with Rotor 1B, there is the possibility of encountering instability near stall in the 83 percent speed range. However, since instability was absent during previous Rotor 1B testing, it will very probably remain absent for Task II as well.

- Steady-State Stress: In minimizing steady-state stresses, there are three regions of primary concern. They are the blade root, the shroud, and the blade section just above the part-span shroud. One of these three locations usually contains the maximum vibratory stress point in the lower modes of vibration. Stresses in these areas were minimized on the Task II rotor blade as much as feasible without compromising the aerodynamic design. Calculated steady-state stress values at 100 percent design speed are listed in table IX. According to the stress range diagram in figure 60, allowable vibratory stresses for this design (using the minimum material properties for Ti-6Al-4V) are:

Blade Root	49 kpsi - single amplitude
Above the Shroud	57 kpsi - single amplitude
On the Shroud	31 kpsi - single amplitude

  The rather large allowable vibratory stresses demonstrate that a high degree of aeromechanical safety was built into this blade design.

- Integral-Order Resonance: The primary integral-order vibration stimulus for the Task II rotor will be inlet distortion. Some degree of integral-order excitation is normally present in the airflow, but it will be at a maximum when purposely introduced during distortion tests. Past experience has indicated that, for shrouded rotors, the more serious blade response in distortion has been in system mode vibration rather than individual blade modes. To prevent the possibility of excessive vibration, it is generally advisable to avoid the low integral-order flexural system mode resonances in the high-speed range (i.e., 1, 2, and 3/Rev). Blade excitation at higher

orders by inlet distortion is less severe, since the magnitude of the higher harmonics of the 1/Rev basic circumferential distortion decreases with system order. The Task II rotor was designed to have its 3-nodal-diameter system mode frequency fall 9 percent above the corresponding 3/Rev frequency at 100 percent speed, and the 4-nodal-diameter mode fall 8 percent below 4/Rev (see figure 59). Thus, system mode resonant response at 100 percent speed should be low. With respect to the 4/Rev, 4-nodal-diameter system mode resonance at 8400 rpm, the combination of relatively weak excitation strength of the 4/Rev harmonic to be expected from basic 1/Rev circumferential distortion should limit the vibratory stresses to tolerable levels.

Resonant response to stator-passing excitation in the mid-to-high-speed range will be possible only in high-frequency complex blade modes (see figure 59). Accordingly, vibratory stresses are expected to be tolerably low. This conclusion is based on Rotor 1B blade vibration characteristics as well as other experience with this type of blade design.

3. STATOR VANES

a. GENERAL CONSIDERATIONS

The stator vanes were designed to provide the capability of varying the vane angle settings. Because of the wide range of possible air incidence angles (including negative values) that might be encountered during tests, they were designed to be very conservative aeromechanically.

Compatibility of the stator vane casing flowpath with other existing hardware established the vane length and the inner and outer diameters. The t_m/C distribution with span, vane solidity, and airfoil shape were determined by aerodynamic requirements. The resulting design was then evaluated for aeromechanical adequacy. The areas considered in this analysis were identical to those for the inlet guide vanes. They included consideration of the steady-state stresses, integral-order resonances, and limit-cycle instability.

b. DESIGN DEFINITION

The stator geometry and pertinent design details are summarized in table X and figure 61, with natural frequencies provided in figure 62. The final design was predicated on the avoidance of limit-cycle stability, all other considerations being less critical because of the generally conservative design. A novel feature was the addition of a ring inside the hub flowpath with vane lever arms attached to it, the objective being to assure that vane first torsional frequency was adequately high. The vane material was chosen to be AISI 410 for the same reasons as for the inlet guide vanes.

c. DISCUSSION OF CRITICAL DESIGN PARAMETERS

The stator vane design, as generated to satisfy flowpath and aerodynamic requirements, was such that only the addition of the inside diameter trunnion

restraint was necessary to make the design aeromechanically acceptable. Details on the critical design areas are as follows:

- Steady-State Stresses: The maximum steady-state stress on the stator vane was sufficiently low that it was possible to use a low-cost and easily-machineable material (AISI 410) and still safely allow for relatively large vibratory stresses. The calculated maximum steady-state stress is given in table X. At this stress level, 10.56 kpsi, the stress range curve of figure 57 indicates that the allowable vibratory stress using minimum material properties is 60 ksi - single amplitude. Thus, more-than-adequate allowance was provided for vane vibration.

- Integral-Order Response: The natural frequency for the lowest four outlet guide vane modes is shown in table X. A Campbell diagram of these and higher modes is shown in figure 62. All of the modes lie above 5/Rev at 100 percent design speed. The vane excitation at these higher per-Rev's from the basic 1/Rev mechanical excitation source should be very weak and, accordingly, will not excite appreciable vibratory stresses. Vane resonance with the 44/Rev rotor-blade passing frequency in the high-speed range, where appreciable excitation energy is to be expected, will be possible only in the high-frequency complex vibration modes. Thus, it is unlikely that significant vibratory stresses will be encountered.

- Limit-Cycle Instability: The stator vane on this vehicle can be subject to a wide range of air incidence angles during tests. The vanes as designed, but without torsional restraint on the inside-diameter trunnion, could be subject to limit-cycle instability at the maximum incidence angles expected, based on previous General Electric experience. To eliminate this possibility, the vane stems at the inner-diameter end were ganged together by an actuation ring (see figure 61). This effectively provided a torsional restraint for the first torsional vibratory mode and lowered the reduced velocity to such a value that, based on past experience, instability should not occur. The ganged actuation ring, while providing a torsional vibratory restraint, still allowed for varying the vane stagger angles since it was free to rotate.

APPENDIX II

SYMBOLS

Symbol	Description	Units
A	Annulus or streamtube area	$in.^2$
A_I	Streamtube capture area at blade row inlet calculation station	$in.^2$
A_T	Streamtube throat area	$in.^2$
C	Chord length of cylindrical section	in.
C_c	Chord length of "cascade" section	in.
D	Diffusion factor $D_{rotor} = 1 - \frac{V'_2}{V'_1} + \frac{r_2 V_{\theta 2} - r_1 V_{\theta 1}}{2\bar{r}\,\sigma\, V'_1}$ $D_{stator} = 1 - \frac{V_2}{V_1} + \frac{r_1 V_{\theta 1} - r_2 V_{\theta 2}}{2\bar{r}\,\sigma\, V_1}$	---
i	Incidence angle, difference between air angle and camber line angle at leading edge in cascade projection	deg
K_b	Effective-area coefficient due to blade thickness blockage	---
K_{bl}	Effective-area coefficient due to wall boundary layer blockage	---
M	Mach number	---
N	Rotational speed	rpm
P	Total or stagnation pressure	psia
p	Static pressure	psia
r	Radius	in.
$\bar{r}$	Mean radius, average of streamline leading and trailing edge radii	in.

Symbol	Description	Units
S	Spacing between blades	in.
SL	Streamline	---
T	Total or stagnation temperature	°R
t	Airfoil thickness	in.
U	Rotor speed	ft/sec
V	Air velocity	ft/sec
W	Weight flow	lbs/sec
X	Empirical adjustment to deviation angle	deg
Z	Displacement along compressor axis	in.
β	Air angle, angle whose tangent is the ratio of tangential to axial velocity	deg
$\Delta\beta$	Air turning angle	deg
$\gamma°$	Blade-chord angle (stagger), angle in cascade projection between blade chord and axial direction	deg
$\delta°$	Deviation angle, difference between air angle and camber line angle at trailing edge in cascade projection	deg
δ	Pressure correction, $\frac{P_{actual}}{14.696 \text{ psia}}$	---
$\Delta r\theta°$	Circumferential displacement about compressor axis (figure 50)	in.
θ	Temperature correction, $\frac{T_{actual}}{518.7°R}$	---
η_{ad}	Adiabatic efficiency	---
k°	Angle between tangent to blade camber line and the axial direction	deg
Σ	Summation	---

Symbol	Description	Units
σ	Solidity, ratio of cylindrical shord to spacing	---
ϕ°	Camber angle, difference between angles in cascade projection of tangents to camber line at extremes of camber line arc	deg
$\bar{\omega}$	Total-pressure loss coefficient Rotor, $\bar{\omega}' = \frac{P'_{2id} - P'_2}{P'_1 - p_1}$, Stator $\bar{\omega} = \frac{P_1 - P_2}{P_1 - p_1}$	---

Subscripts

e	Edge of blade
F	Flap portion of inlet guide vane
id	Ideal
N	Nose portion of inlet guide vane
m	Point of camber line where maximum thickness occurs
t	Tip at station 1.0
z	Axial direction
θ	Tangential direction
1	Leading edge
2	Trailing edge
0.4, 0.5, 1.0, 1.5, 1.6, 2.0	Calculation station designations (figure 2)

Superscript

'	Relative to rotor

REFERENCES

1. Seyler, D.R. and Smith, L.H., Jr.: Single Stage Experimental Evaluation of High Mach Number Compressor Rotor Blading, Part 1 - Design of Rotor Blading, NASA CR-54581, April 1, 1967.

2. Seyler, D.R. and Gostelow, J.P.: Single Stage Experimental Evaluation of High Mach Number Compressor Rotor Blading, Part 2 - Performance of Rotor 1B, NASA CR-54582, September 22, 1967.

3. Gostelow, J.P., Krabacher, K.W., and Smith, L.H., Jr.: Performance Comparisons of High Mach Number Compressor Rotor Blading, NASA CR-1256, December 1968.

4. Reddy, J.L. and Klapproth, J.F.: Advanced Fan Development for High Bypass Engines, AIAA Paper No. 68-563, June 10, 1968.

5. NASA: Aerodynamic Design of Axial-Flow Compressors, Revised NASA SP-36, 1965.

6. Den Hartog, J.P.: Mechanical Vibrations, New York: McGraw Hill Book Company, 1947.

Table I. Summary of Stage Design Specifications and Performance

Parameter	Task I Stage	Task II Stage
Rotor Inlet Corrected Tip Speed, Ft/Sec	1400	1500
Stage Inlet Corrected Weight Flow, Lbs/Sec	219.4	226.0
Stage Total-Pressure Ratio	1.617	1.659
Stage Adiabatic Efficiency	0.873	0.854
Number of Inlet Guide Vanes	0	24
Inlet Guide Vane Total-Pressure Loss, Percent Inlet Total Pressure	0	0.37
Inlet Guide Vane Exit Flow Angle, Degrees	0	0
Rotor Inlet Tip Diameter, Inches	36.5	36.5
Rotor Inlet Hub:Tip Radius Ratio	0.5	0.5
Rotor Inlet Corrected Weight Flow Per Unit Annulus Area, Lbs/Sec-Ft^2	40.25	41.62
Rotor Inlet Tip Relative Mach Number	1.414	1.526
Rotor Tip Diffusion Factor	0.382	0.368
Rotor Total-Pressure Ratio	1.636	1.686
Rotor Adiabatic Efficiency	0.8915	0.883
Rotor Tip Solidity	1.3	1.4
Rotor Aspect Ratio	2.5	2.36
Number of Rotor Blades	44	44
Stator Inlet Hub Absolute Mach Number	0.684	0.766
Stator Exit Flow Angle, Degrees	0	0
Stator Hub Diffusion Factor	0.474	0.435
Stator Total-Pressure Loss, Percent Stator Inlet Total Pressure	1.17	1.22
Stator Hub Solidity	2.156	2.156
Stator Aspect Ratio	2.065	2.065
Number of Stator Vanes	46	46

Table II. Streamline Radial Positions

Calculation Station	Streamline Radius, Inches								
	Tip SL 1	SL 2	SL 3	SL 4	SL 5	SL 6	SL 7	SL 8	Hub SL 9
0.09	18.412	17.892	17.435	15.387	13.267	11.022	8.495	7.761	7.099
0.40	18.408	17.880	17.417	15.370	13.273	11.055	8.525	7.778	7.099
0.45	18.390	17.878	17.432	15.471	13.489	11.419	9.059	8.347	7.680
0.50	18.370	17.867	17.430	15.521	13.612	11.640	9.442	8.805	8.230
0.95	18.323	17.830	17.403	15.560	13.738	11.874	9.832	9.253	8.737
1.00	18.250	17.766	17.350	15.577	13 833	12.063	10.148	9.606	9.125
1.50	17.845	17.447	17.099	15.560	14.030	12.500	10.923	10.504	10.141
1.51	17.838	17.434	17.084	15.562	14.060	12.570	11.043	10.637	10.287
1.60	17.836	17.432	17.083	15.586	14.132	12.706	11.263	10.882	10.553
2.00	17.836	17.454	17.123	15.697	14.325	13.005	11.715	11.386	11.109
2.20	17.836	17.459	17.132	15.725	14.370	13.064	11.781	11.449	11.167

Table III. Rotor Meanline Angle and Thickness Distributions

Percent Cascade Chord $\%C_c$	Streamline								
	Tip SL 1	SL 2	SL 3	SL 4	SL 5	SL 6	SL 7	SL 8	Hub SL 9
$k^{\circ\prime}$ Distribution Along Streamline Sections									
0	63.30	61.28	60.22	57.02	53.75	50.70	48.50	48.00	47.50
10	63.29	61.46	60.41	56.86	52.96	49.02	45.89	45.18	44.56
20	63.33	61.68	60.62	56.81	52.73	47.94	42.80	41.67	40.70
30	63.40	61.94	60.85	56.88	52.55	46.93	39.20	37.50	35.96
40	63.51	62.22	61.09	56.48	51.79	45.30	35.14	32.82	30.62
50	63.66	62.53	61.36	55.68	49.64	41.86	30.77	28.07	25.43
60	63.37	62.31	61.17	54.84	46.69	37.13	26.54	23.56	20.55
70	61.59	60.44	59.46	54.12	46.50	35.13	23.02	19.46	15.81
80	58.98	58.13	57.53	53.53	46.63	35.01	20.29	15 94	11.64
90	57.80	57.58	57.20	53.10	46.35	35.01	18.21	12.90	7.92
100	57.27	57.53	57.18	52.85	46.10	35.05	16.84	10.35	4.56
t/tm Distribution Along Streamline Sections									
0	0.2475	0.2307	0.2138	0.1630	0.1400	0.1345	0.1294	0.1267	0.1248
10	0.4318	0.4407	0.4277	0.4009	0.3211	0.2897	0.3195	0.3285	0.3111
20	0.6046	0.6281	0.6197	0.6062	0.5245	0.4895	0.5265	0.5400	0.5172
30	0.7569	0.7846	0.7804	0.7745	0.7171	0.6853	0.7245	0.7372	0.7170
40	0.8787	0.9025	0.9018	0.9005	0.8729	0.8540	0.8841	0.8928	0.8799
50	0.9606	0.9748	0.9758	0.9773	0.9702	0.9629	0.9759	0.9788	0.9746
60	0.9932	0.9943	0.9945	0.9931	0.9866	0.9829	0.9751	0.9730	0.9757
70	0.9645	0.9508	0.9474	0.9334	0.8979	0.8887	0.8694	0.8649	0.8712
80	0.8496	0.8222	0.8136	0.7838	0.7081	0.6862	0.6667	0.6629	0.6684
90	0.6161	0.6459	0.5719	0.5303	0.4399	0.4136	0.4003	0.3980	0.3998
100	0.2392	0.2236	0.2087	0.1616	0.1407	0.1360	0.1305	0.1277	0.1262

Table IV. Rotor Aerodynamic Design Parameters (Number of Blades = 44)

Design Parameter	Streamline									Units
	Tip SL 1	SL 2	SL 3	SL 4	SL 5	SL 6	SL 7	SL 8	Hub SL 9	
$\bar{r}$	18.032	17.600	17.224	15.574	13.934	12.282	10.538	10.057	9.635	Inches
$\bar{r}/rt$	0.9881	0.9644	0.9438	0.8534	0.7635	0.6730	0.5774	0.5511	0.5279	---
r_1	18.173	17.706	17.308	15.581	13.860	12.097	10.171	9.620	9.128	Inches
r_1/rt	0.9958	0.9702	0.9484	0.8538	0.7595	0.6628	0.5573	0.5271	0.5002	---
r_2	17.891	17.493	17.139	15.567	14.008	12.466	10.904	10.493	10.141	Inches
r_2/rt	0.9803	0.9585	0.9391	0.8530	0.7676	0.6831	0.5975	0.5750	0.5557	---
V'_1	1852	1610	1591	1452	1345	1208	1042	996	945	Ft/Sec
V'_2	1200	1164	1132	998	868	746	643	622	610	Ft/Sec
M'_1	1.526	1.510	1.490	1.374	1.258	1.130	0.983	0.941	0.907	---
M'_2	1.023	0.992	0.966	0.856	0.747	0.648	0.571	0.557	0.551	---
$\bar{\omega}'$	0.1634	0.1486	0.1355	0.1004	0.0803	0.0668	0.0707	0.0766	0.0821	---
C	3.601	3.599	3.596	3.587	3.527	3.446	3.388	3.377	3.361	Inches
σ	1.400	1.431	1.462	1.610	1.777	1.967	2.251	2.331	2.443	---
i_m/C	0.0227	0.0259	0.0287	0.0437	0.0562	0.0660	0.0747	0.0768	0.0785	---
D	0.368	0.372	0.380	0.409	0.456	0.495	0.514	0.515	0.501	---
β'_1	66.3	64.4	63.5	60.9	58.2	55.7	53.4	52.7	51.7	Degrees
β'_2	59.3	59.5	59.3	56.1	50.6	42.0	27.9	22.9	18.4	Degrees
$\Delta\beta'$	7.0	4.9	4.2	4.8	7.6	13.7	25.5	29.8	33.3	Degrees
$k°_1'$	63.30	61.28	60.22	57.01	53.75	50.70	48.50	48.00	47.50	Degrees
$k°_2'$	57.27	57.52	57.18	52.85	46.10	35.05	16.84	10.35	4.56	Degrees
i	3.00	3.12	3.28	3.89	4.45	5.00	4.90	4.70	4.20	Degrees
$\delta°$	2.03	1.98	2.12	3.25	4.50	6.95	11.06	12.55	13.84	Degrees
$\gamma°$	61.94	60.79	59.85	55.32	49.56	41.59	31.46	28.65	25.95	Degrees
$\phi°$	6.03	3.76	3.04	4.16	7.65	15.65	31.66	37.65	42.94	Degrees

Table V. Stator Meanline Angle and Thickness Distributions

Percent Chord, %C	Section Radius, Inches								
	17.836	17.500	17.100	15.700	14.300	12.850	11.489	11.130	10.815
k° Distribution Along Cylindrical Sections									
0	40.1	39.5	39.1	39.0	39.7	40.8	42.0	42.4	43.0
10	34.6	34.3	34.0	33.9	34.8	36.4	38.1	38.6	39.5
20	29.2	29.2	29.0	28.7	29.8	31.7	34.0	35.6	35.1
30	24.0	24.1	24.0	23.7	25.0	27.0	29.4	30.0	30.6
40	18.6	19.0	19.1	19.0	20.3	22.3	24.6	25.2	25.7
50	13.5	14.1	14.3	14.2	15.6	17.4	19.4	19.7	20.5
60	8.3	9.2	9.5	9.6	10.9	12.2	13.9	14.2	14.3
70	3.1	4.0	4.4	5.0	6.2	7.0	8.1	8.2	8.0
80	- 2.2	- 1.0	- 0.3	0.4	1.2	1.9	2.4	1.9	1.1
90	- 7.6	- 6.2	- 5.2	- 4.1	- 3.7	- 3.6	- 4.2	- 5.0	- 6.4
100	-13.1	-11.2	-10.0	- 8.9	- 8.8	- 9.1	-11.2	-12.7	-14.6
t/tm Distribution Along Cylindrical Sections									
0	0.1231	0.1250	0.1272	0.1361	0.1460	0.1598	0.1709	0.1747	0.1778
10	0.4385	0.4391	0.4404	0.4490	0.4489	0.4615	0.4701	0.4694	0.4711
20	0.6846	0.6859	0.6852	0.6905	0.6934	0.6923	0.6923	0.6921	0.6911
30	0.8585	0.8594	0.8553	0.8605	0.8668	0.8521	0.8397	0.8406	0.8378
40	0.9646	0.9656	0.9650	0.9660	0.9672	0.9546	0.9444	0.9410	0.9378
50	1.0	1.0	1.0	1.0	1.0	1.0	0.9936	0.9934	0.9911
60	0.9646	0.9656	0.9650	0.9660	0.9672	0.9665	0.9679	0.9672	0.9661
70	0.8585	0.8594	0.8553	0.8605	0.8668	0.8619	0.8675	0.8646	0.8711
80	0.6846	0.6859	0.6852	0.6905	0.6934	0.6982	0.7030	0.7031	0.7020
90	0.4385	0.4391	0.4404	0.4490	0.4489	0.4675	0.4701	0.4694	0.4711
100	0.1231	0.1250	0.1272	0.1391	0.1460	0.1598	0.1709	0.1747	0.1778

Table VI. Stator Aerodynamic Design Parameters (Number of Blades = 46)

Design Parameter	Streamline									Units
	Tip SL 1	SL 2	SL 3	SL 4	SL 5	SL 6	SL 7	SL 8	Hub SL 9	
$\bar{r}$	17.836	17.443	17.103	15.642	14.228	12.855	11.489	11.134	10.831	Inches
$\bar{r}/rt$	0.9773	0.9558	0.9372	0.8571	0.7796	0.7044	0.6295	0.6101	0.5935	---
$r_{1.6}$	17.836	17.432	17.083	15.586	14.132	12.706	11.263	10.882	10.553	Inches
$r_{1.6}/rt$	0.9773	0.9552	0.9361	0.8540	0.7744	0.6962	0.6172	0.5963	0.5782	---
$r_{2.0}$	17.836	17.454	17.123	15.697	14.325	13.005	11.715	11.386	11.109	Inches
$r_{2.0}/rt$	0.9773	0.9564	0.9382	0.8601	0.7849	0.7126	0.6419	0.6239	0.6087	---
$V_{1.6}$	725	729	732	744	764	796	844	860	874	Ft/Sec
$V_{2.0}$	597	596	595	595	598	605	621	627	634	Ft/Sec
$M_{1.6}$	0.615	0.620	0.624	0.639	0.659	0.690	0.737	0.753	0.766	---
$M_{2.0}$	0.500	0.500	0.501	0.503	0.507	0.515	0.529	0.535	0.541	---
$\bar{\omega}$	0.0404	0.0393	0.0383	0.0396	0.0451	0.0520	0.0650	0.0707	0.0754	---
C	3.650	3.628	3.605	3.489	3.390	3.299	3.224	3.199	3.184	Inches
σ	1.4983	1.5176	1.5434	1.6269	1.7355	1.8794	2.0549	2.1045	2.1557	---
t_m/C	0.0650	0.0640	0.0629	0.0588	0.0548	0.0507	0.0468	0.0458	0.0450	---
D	0.3784	0.3790	0.3787	0.3847	0.3954	0.4100	0.4273	0.4317	0.4346	---
β_1	37.12	36.73	36.48	37.00	38.57	40.52	43.43	44.45	45.43	Degrees
β_2	0	0	0	0	0	0	0	0	0	Degrees
$k°_1$	40.09	39.48	39.06	39.10	40.15	41.24	42.85	43.55	44.00	Degrees
$k°_2$	-13.11	-10.99	-10.21	- 8.94	- 8.80	- 9.17	-10.41	-11.31	-12.54	Degrees
i	-2.97	-2.75	-2.58	-2.10	-1.58	-0.72	0.58	0.90	1.43	Degrees
$\delta°$	13.11	10.99	10.21	8.94	8.80	9.17	10.41	11.31	12.54	Degrees
$\gamma°$	13.46	14.21	14.24	14.58	15.76	16.99	18.89	19.43	19.62	Degrees
$\phi°$	53.20	50.47	49.27	48.04	48.95	50.41	53.26	54.86	56.54	Degrees

Table VII. Inlet Guide Vane Design Parameters (Number of Vanes = 24)

Design Parameter	Manufacturing Section									Units
	1	2	3	4	5	6	7	8	9	
r	18.389	17.885	17.435	15.485	13.465	11.375	8.940	8.100	7.390	Inches
r/rt	1.0076	0.9800	0.9553	0.8485	0.7378	0.6233	0.4899	0.4438	0.4049	---
C_N	1.280	1.254	1.230	1.129	1.024	0.915	0.788	0.745	0.708	Inches
C_F	4.975	4.873	4.782	4.388	3.979	3.557	3.064	2.894	2.751	Inches
ΣC	6.255	6.127	6.012	5.517	5.003	4.472	3.852	3.639	3.459	Inches
σ	1.299	1.309	1.317	1.361	1.419	1.502	1.646	1.716	1.788	Inches
Z_N	2.706	2.658	2.613	2.425	2.228	2.028	1.793	1.711	1.642	Inches
Z_F	1.279	1.253	1.230	1.128	1.023	0.914	0.788	0.744	0.707	Inches
$\Delta r\theta/\delta m\phi°$	1.1800	1.1477	1.1188	0.9936	0.8640	0.7299	0.5737	0.5198	0.4742	Inches

Table VIII. Aeromechanical Data for the Task II Variable-Camber Inlet Guide Vane

Item	Forward Vane (Nose)	Aft Vane (Flap)
No. of Vanes	24	24
Vane Material	AISI 410 Stainless Steel	AISI 410 Stainless Steel
Vane Aeromechanical Chord at OD, In.	1.6845	5.0394
Vane Aeromechanical Chord at ID, In.	0.9354	2.798
Vane Maximum Thickness at OD, In.	0.4292	0.6398
Vane Maximum Thickness at ID, In.	0.2388	0.355
Outer Casing Radius, In.	18.39	18.39
Inner Hub Radius, In.	7.39	7.39
Vane Span, In.	11.01	11.01
Outer Spindle Diameter	Dovetailed	0.6398 In.
Inner Spindle Diameter	Dovetailed	0.355 In.
Aspect Ratio*	6.56	2.194
Airfoil Type	See Aerodynamic Design Section.	
Vane Natural Frequencies (CPS)		
First Torsional	2841	1053
First Flexural	477	500
Second Flexural	1216	1540
Third Mode	2400 (3 Flex.)	2100 (2 Torsional)
Reduced Velocity at Design Point (See Notes)	0.669**	0.730***
Maximum Steady-State Bending Stresses (KPSI)	5 at Leading Edge, Inner End	11.86 at Spindle, Outer End
Maximum Steady-State Shear Stress (KPSI)	0.616 at Max. Thickness, Inner End	1.586 at Spindle, Inner End
Maximum Steady-State Actuation Pin Bending Stress (KPSI)	9.0 at Outer Pin	---

* Based on vane chord at the outer diameter.

Notes (1) In reduced velocity calculations, V = 615 fps was assumed.
(2) Forward vane: fixed-fixed. Aft vane: fixed-fixed in bend and cantilevered from OD in torsion.

** Based on chord at 60% span below outer diameter (approximate location of maximum torsional deflection).

*** Based on chord at 87.5% span below outer diameter. (This is considered to be a representative section for limit-cycle instability considerations for airfoils having no torsional restraint at one end - the inner end in this case.)

Table IX. Aeromechanical Data for the Task II Rotor

Design RPM	9418
Design Tip Speed (Ft/Sec)	1500
Blade Material	Ti-6Al-4V
Number of Blades	44
Tip Diameter (Inches)*	36.075
Root Diameter (Inches)*	19.25
Chord	See figure 11
Aspect Ratio (Average Length/Root Chord)	2.5
Chord Taper Ratio (Tip Chord/Root Chord)	1.07
t_m/C Distribution	See figure 5
Steady-State Stresses at Design Speed (KPSI)	
Average Root Centrifugal Stress	34.600
Stresses at Root Locations (Centrifugal and Aerodynamic)	
Convex Side*	43.000
Concave Side*	16.500
Leading Edge	26.000
Trailing Edge	19.200 Compression
Stresses Adjacent to Shroud	
Convex Side*	13.850
Concave Side*	16.770
Leading Edge	21.460
Trailing Edge	21.460
Maximum Shroud Stress	83.000
Tip Untwist at Design Speed (Degrees)	0.93
Blade Natural Frequencies at Design Speed (CPS)**	
First Flexural	623
Second Flexural	1837
First Torsional	1186
Reduced Velocity at Design Point	1.38

* At Mid-Chord
** With Shroud Restraint

Table X.—Aeromechanical Data for the Task II Stator

Parameter	Data
Number of Vanes	46
Material	AISI 410 Stainless Steel
Vane Chord at OD (Inches)	3.650
Vane Chord at ID (Inches)	3.184
t_m/C at OD	0.065
t_m/C at ID	0.045
Vane Length (Inches)	7.02*
Outer Diameter (Inches)	35.68
Inner Diameter (Inches)	21.64
Reduced Velocity at Design Point	0.72
First Torsional Frequency (CPS)	1072
First Flexural Frequency (CPS)	939
Second Torsional Frequency (CPS)	2216
Second Flexural Frequency (CPS)	2215
Maximum Steady-State Stress (KPSI)	10.560 (at Vane ID)

* At Mid-Chord

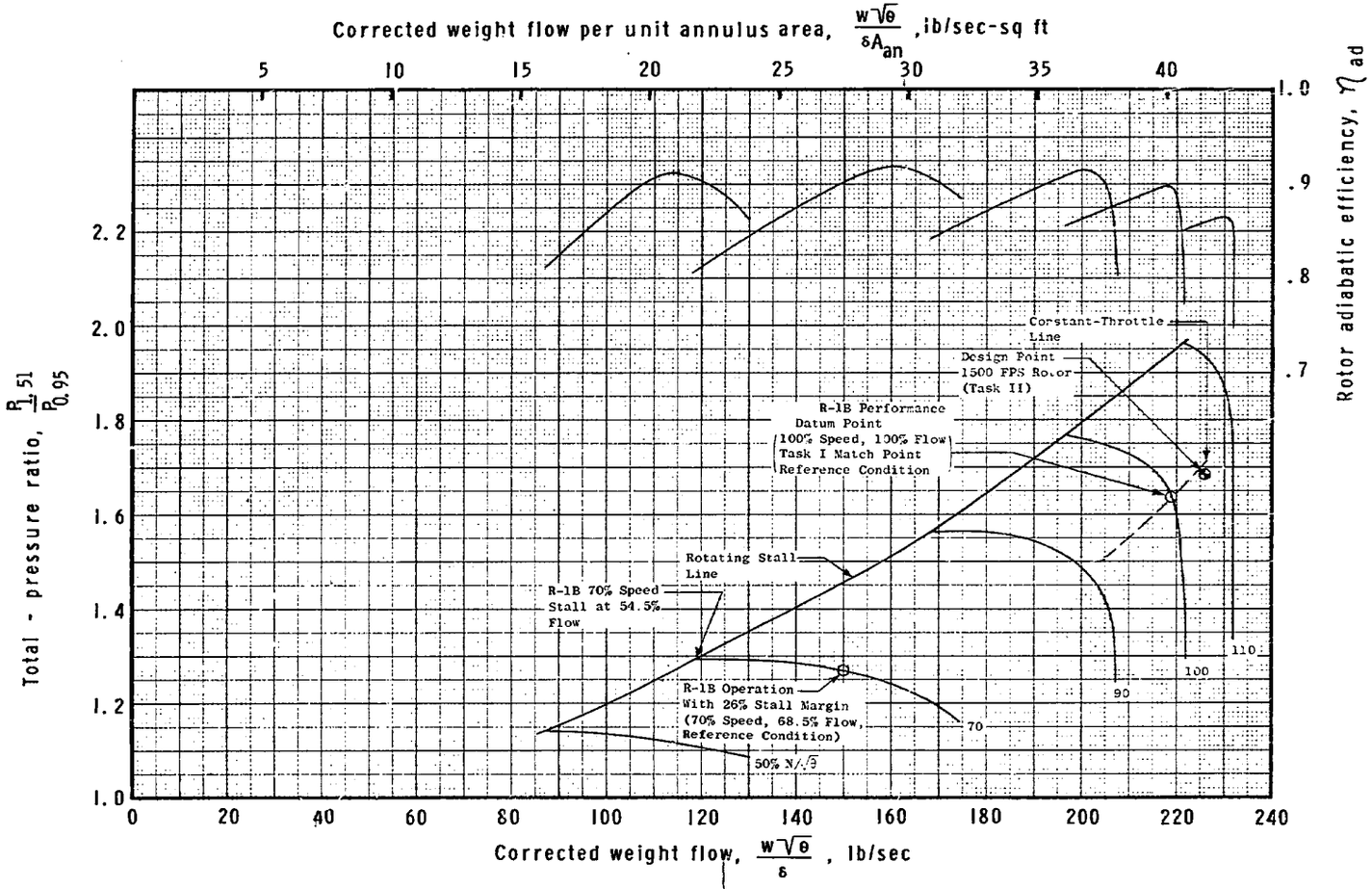

Figure 1. Rotor 1B Compressor Performance Map

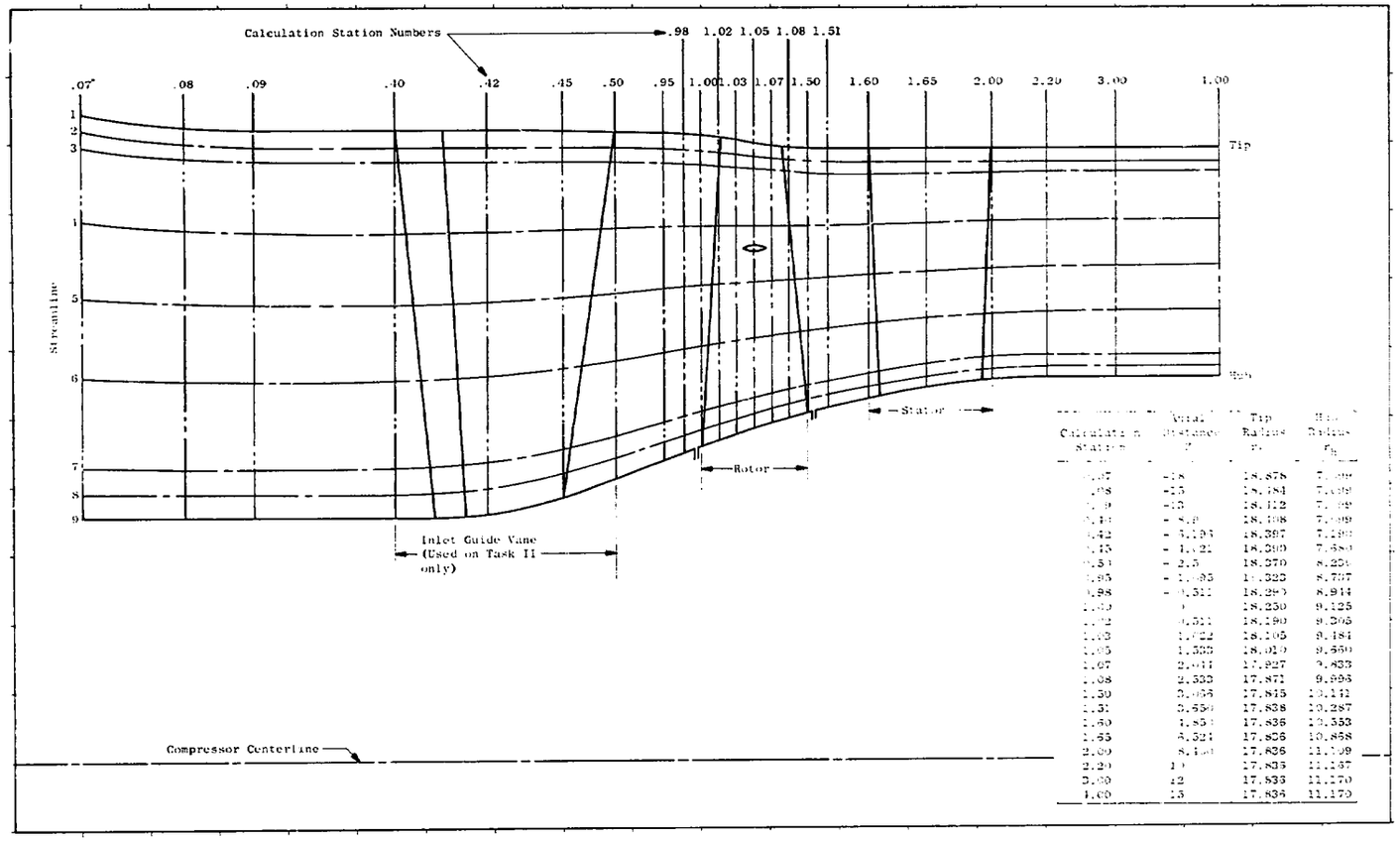

Calculation Station	Axial Distance z	Tip Radius r_t	Hub Radius r_h
.07	-1.8	18.875	7.[illegible]
.08	-1.5	18.784	7.[illegible]
.09	-1.0	18.112	7.[illegible]
.40	- .8	18.108	7.[illegible]
.42	- .1193	18.387	7.[illegible]
.45	- .121	18.[illegible]	7.[illegible]
.51	- .5	18.570	8.[illegible]
.95	- 1.[illegible]95	18.[illegible]	8.707
.98	- .511	18.[illegible]	8.914
1.00	0	18.250	9.125
1.02	.511	18.190	9.305
1.03	1.022	18.105	9.484
1.05	1.533	18.019	9.660
1.07	2.044	17.927	9.833
1.08	2.533	17.871	9.996
1.50	2.[illegible]66	17.815	10.141
1.51	2.554	17.838	10.287
1.60	1.85[illegible]	17.836	10.353
1.65	1.521	17.836	10.858
2.00	1.[illegible]00	17.836	11.[illegible]09
2.20	1.[illegible]	17.835	11.137
3.00	.[illegible]2	17.835	11.170
1.00	.15	17.836	11.170

Figure 2. Compressor Flowpath

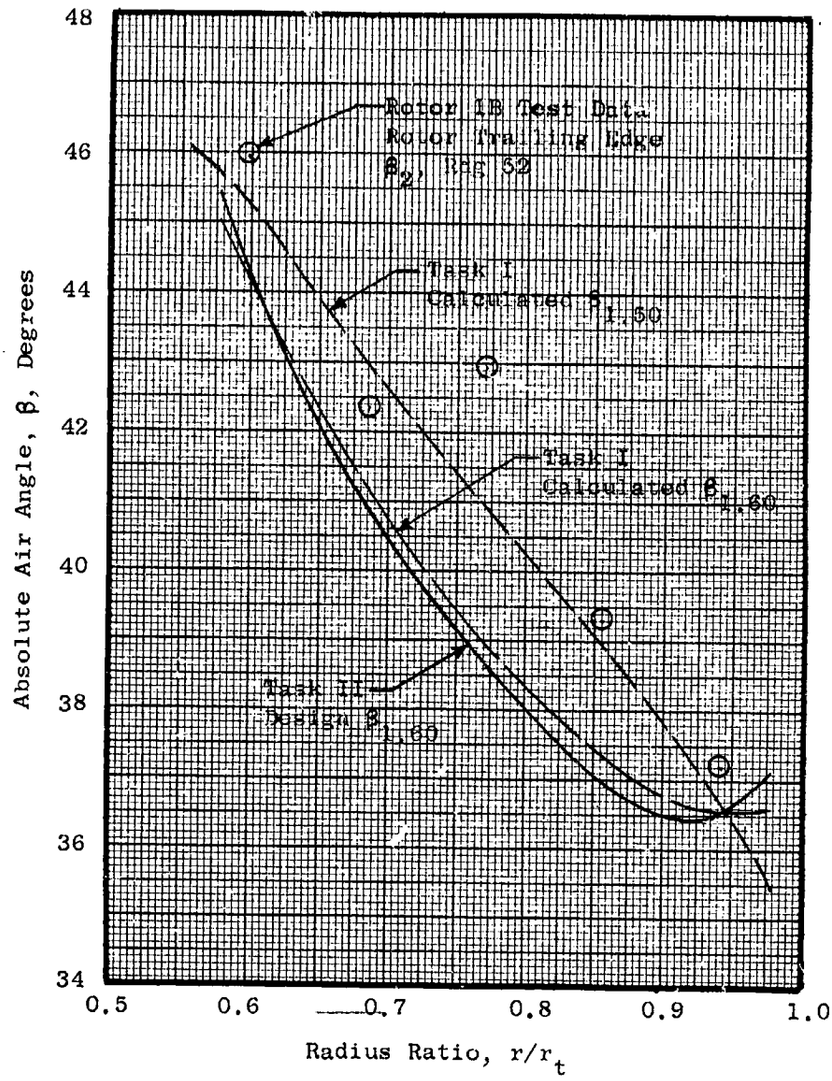

Figure 3. Stator Inlet Air Angle Distributions

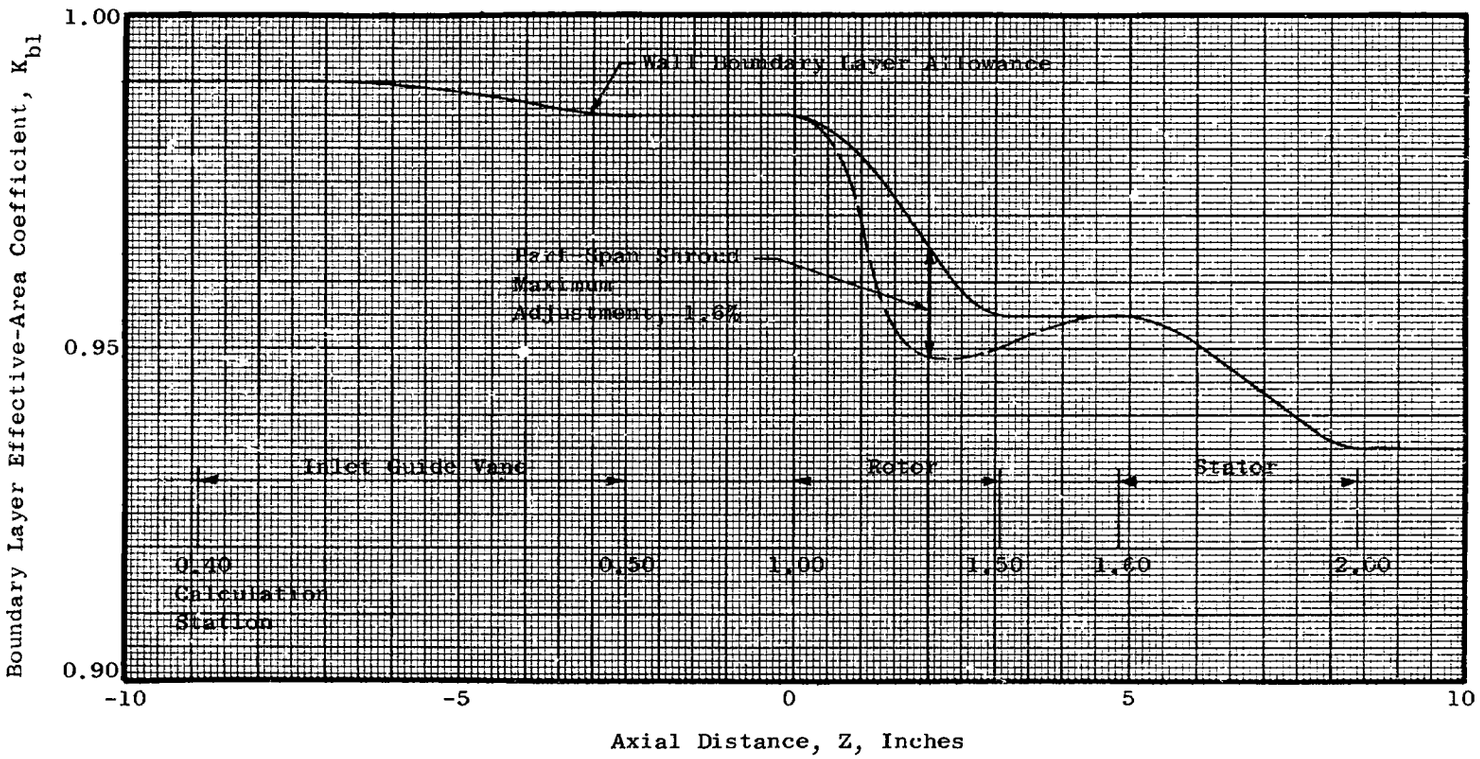

Figure 4. Boundary Layer Effective-Area Coefficient

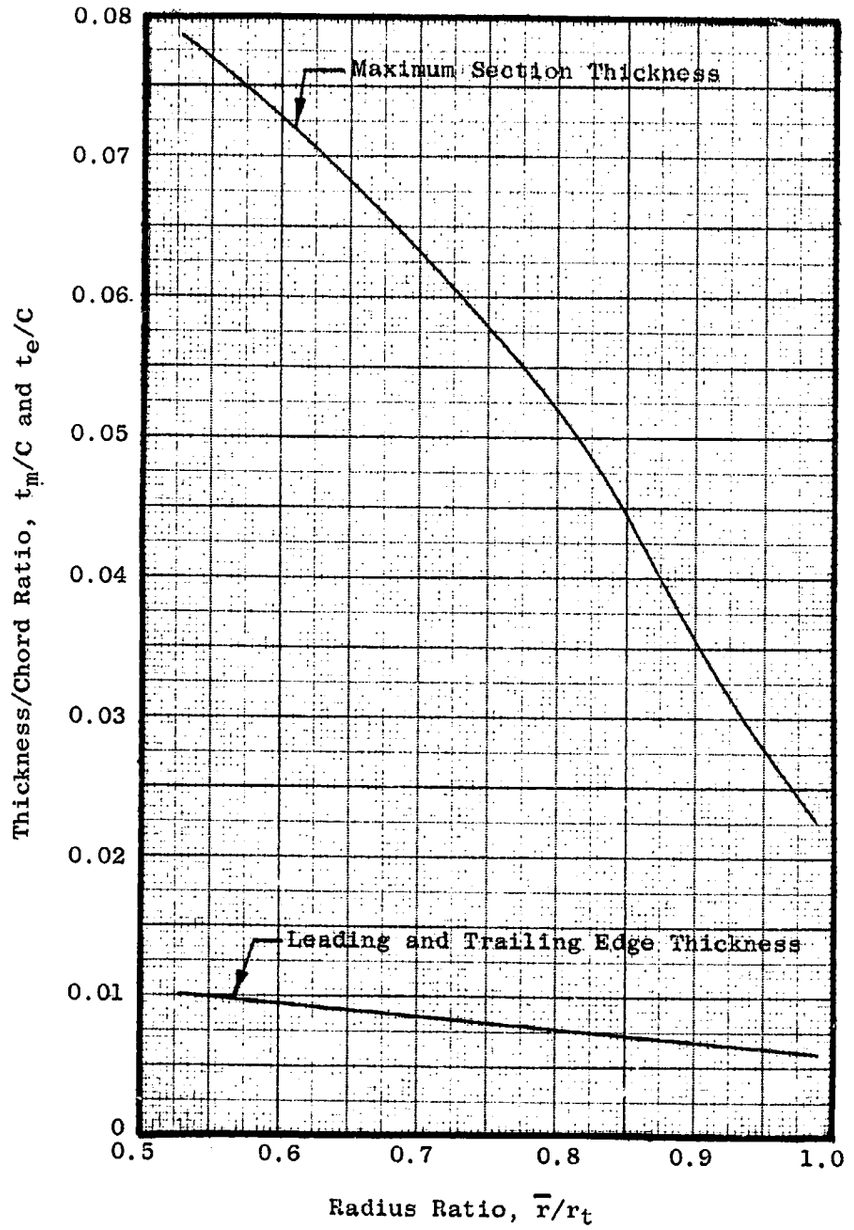

Figure 5. Rotor Maximum and Edge Thickness Distributions

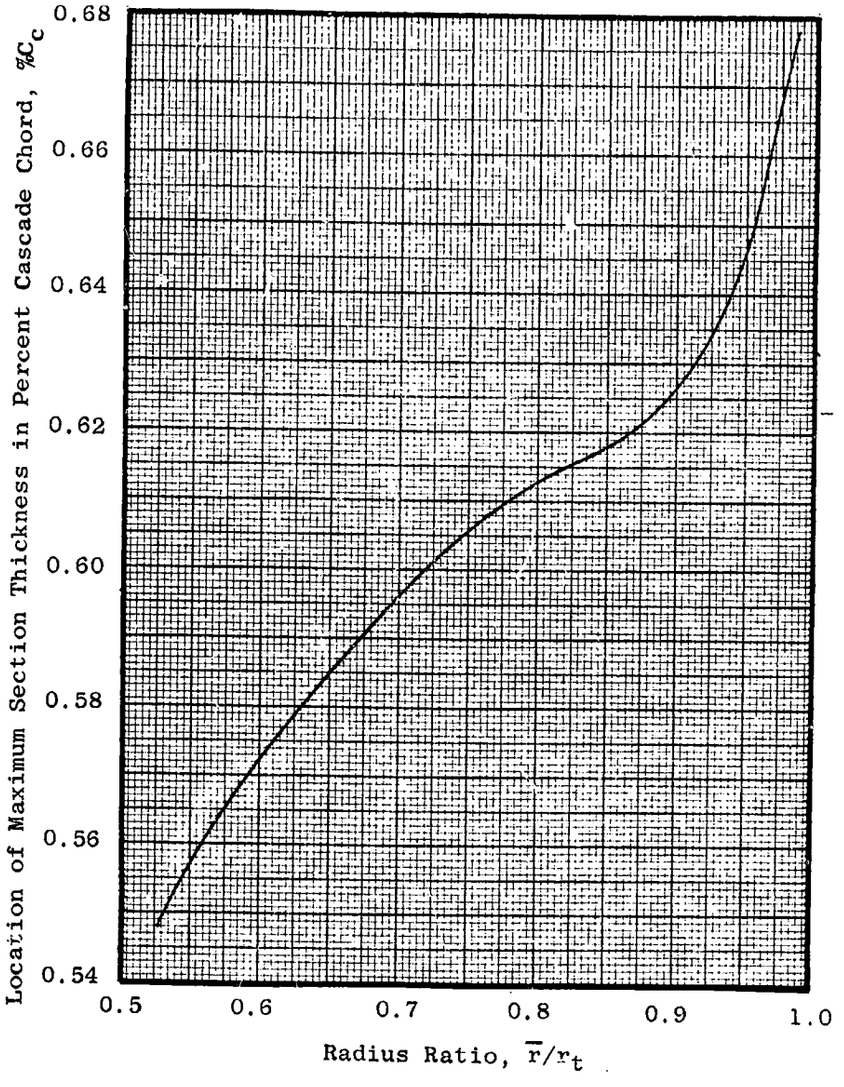

Figure 6. Chordwise Location of Rotor Maximum Thickness

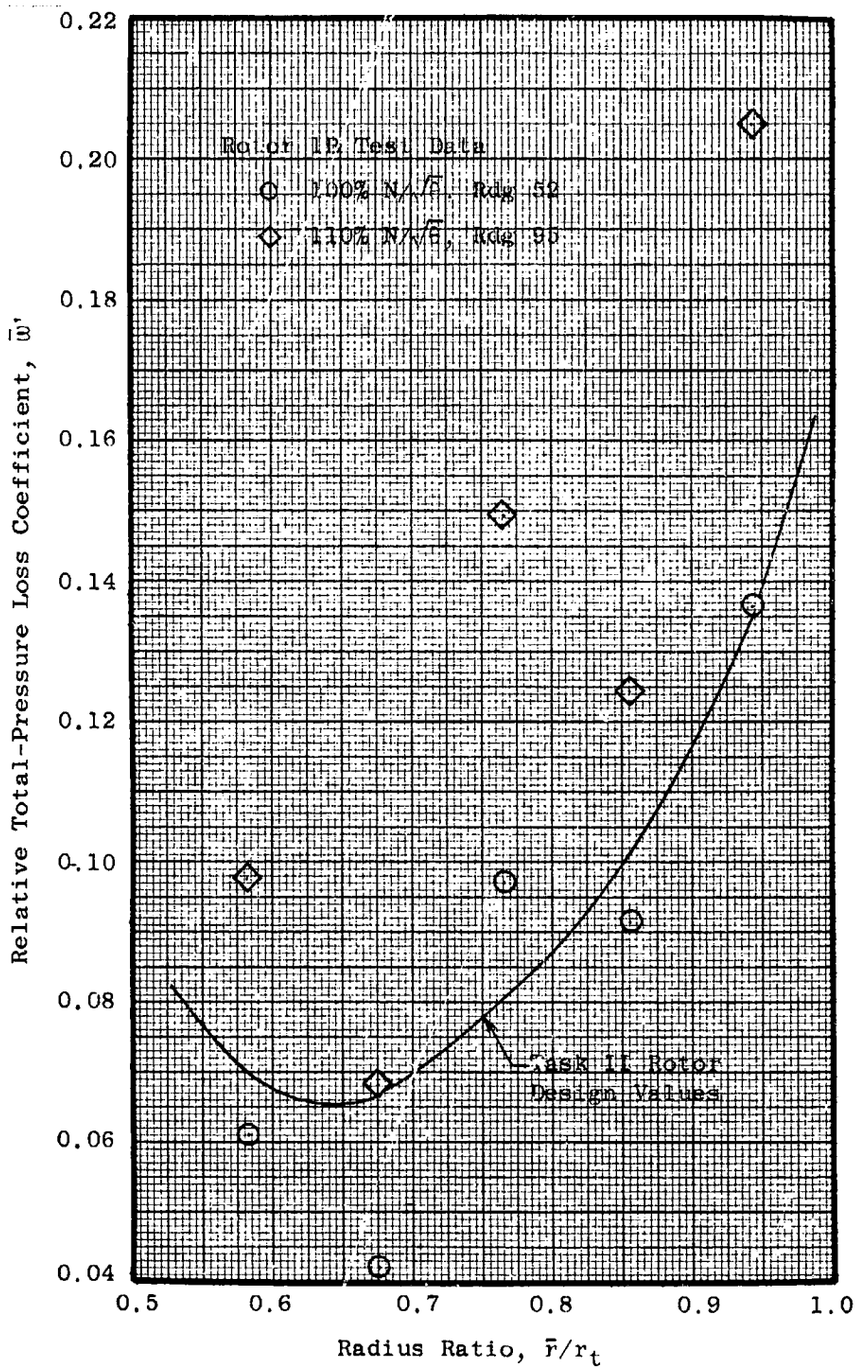

Figure 7. Rotor Relative Total-Pressure Loss Coefficient Distribution

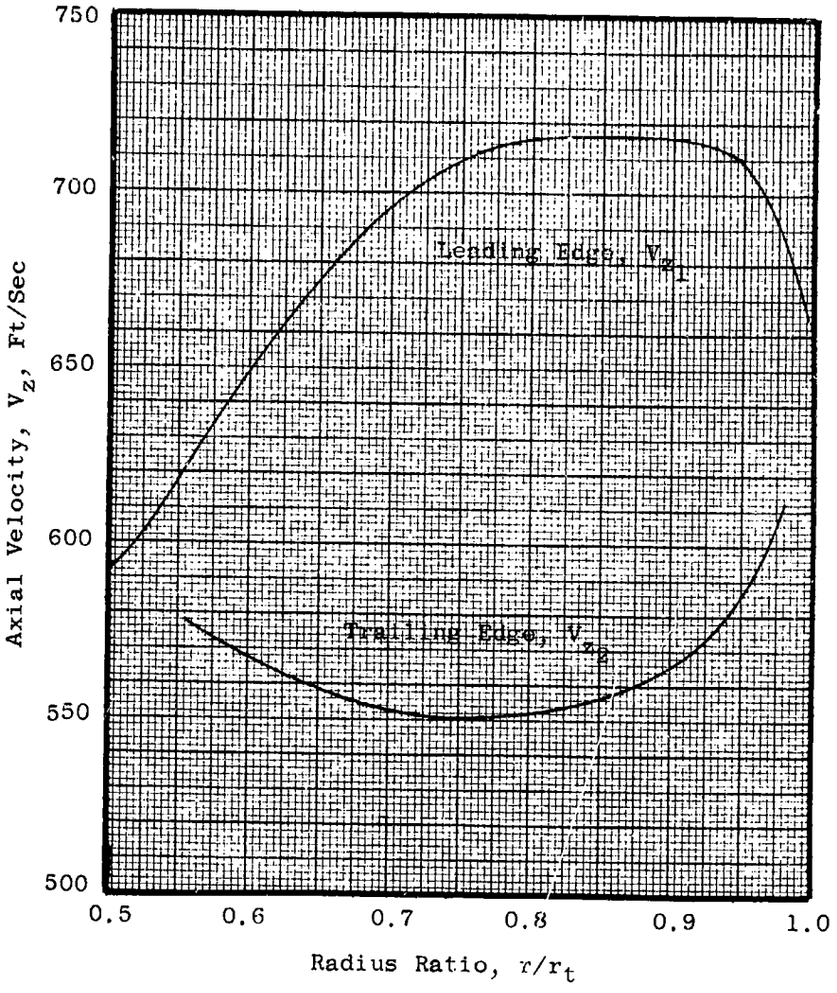

Figure 8. Rotor Axial Velocities at Blade Edges

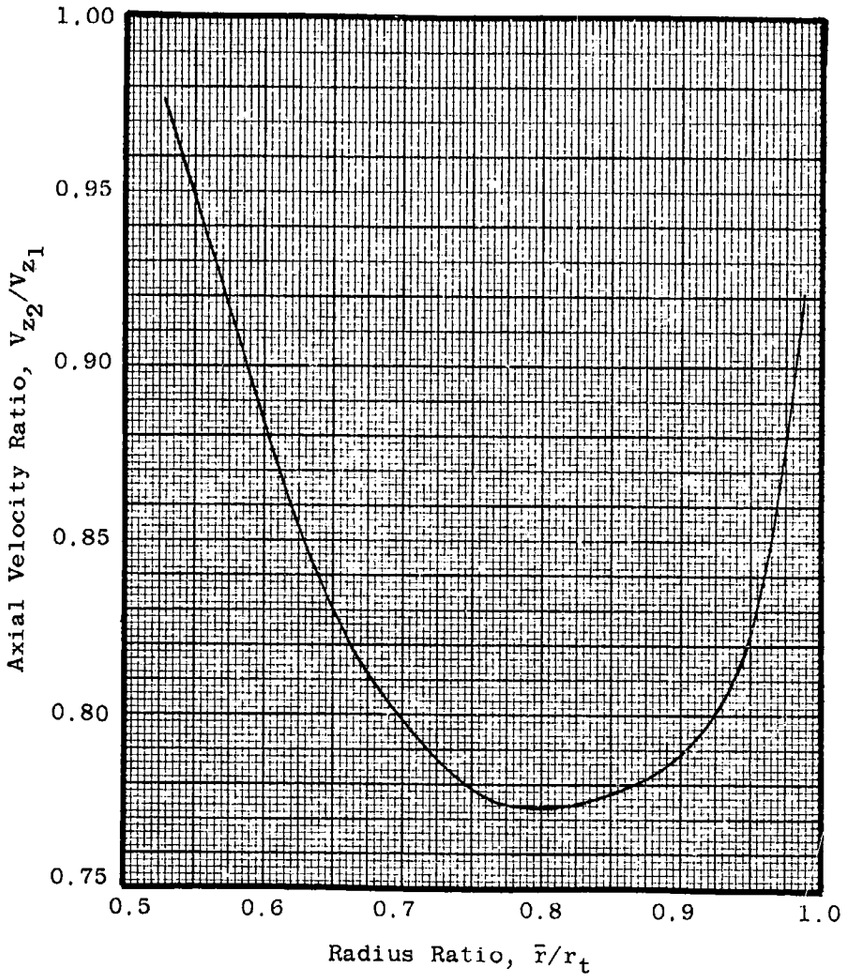

Figure 9. Radial Variation of Rotor Axial Velocity Ratio, Leading Edge to Trailing Edge

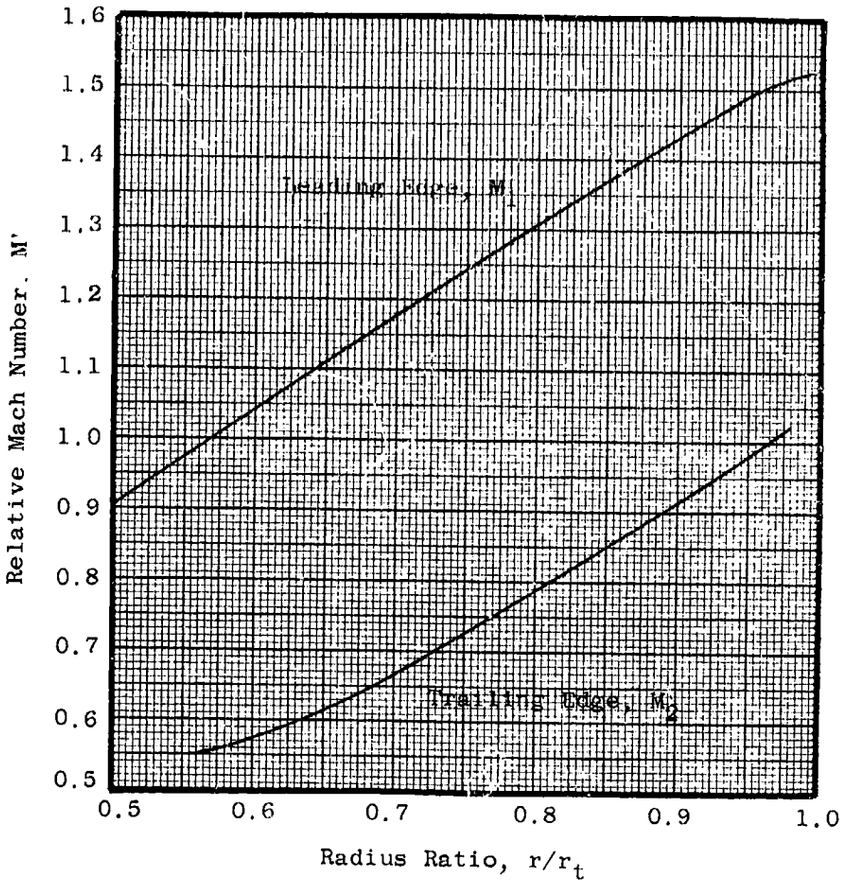

Figure 10. Distribution of Rotor Relative Mach Number at Blade Edges

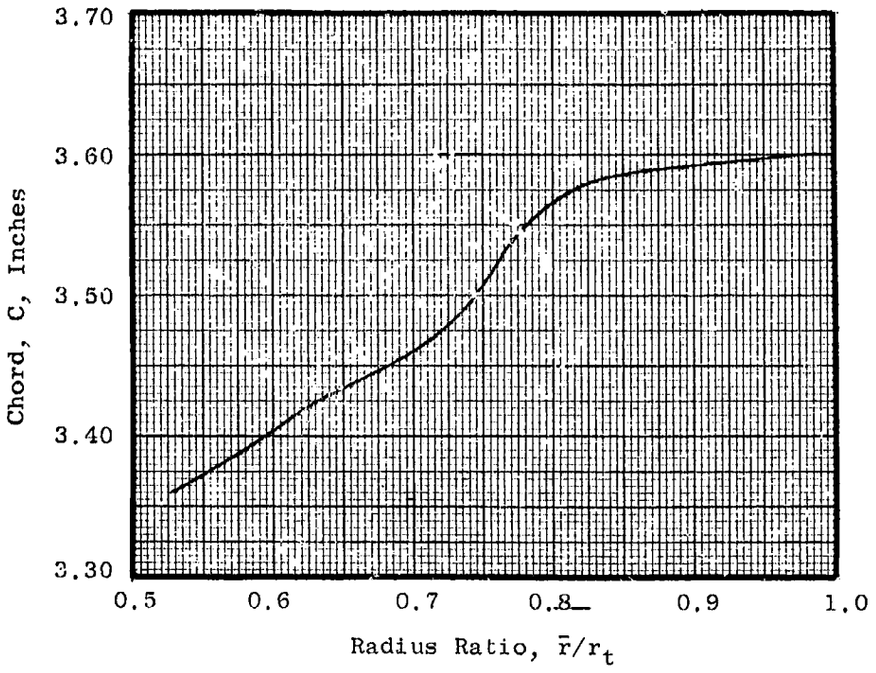

Figure 11. Radial Variation of Rotor Chord on Cylindrical Sections

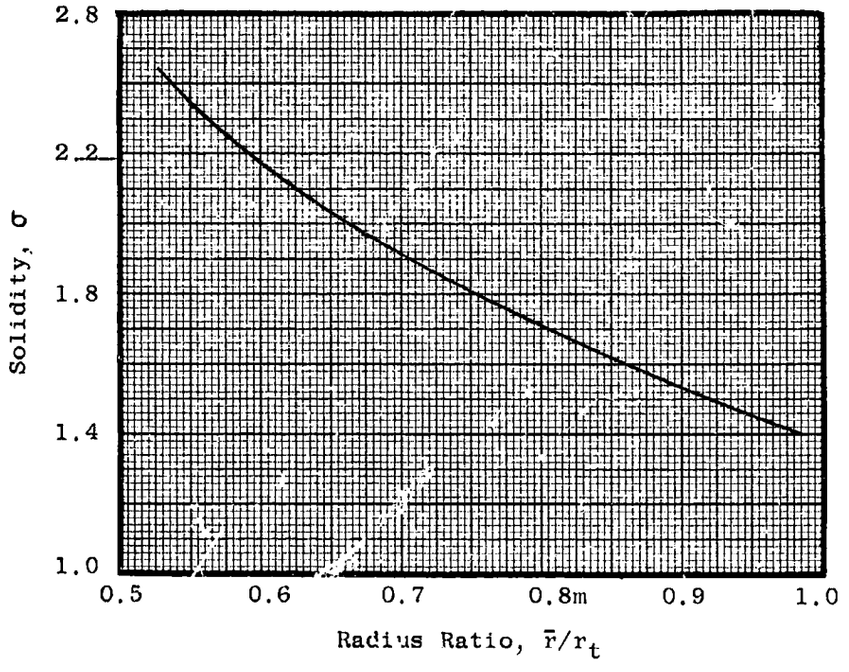

Figure 12. Distribution of Rotor Solidity

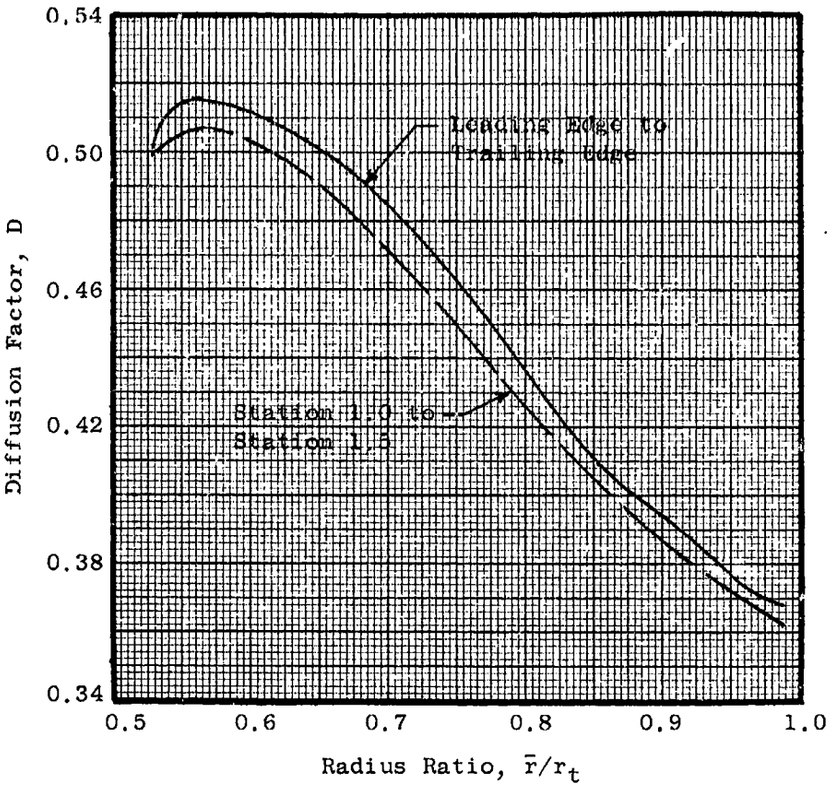

Figure 13. Rotor Diffusion Factor Distribution

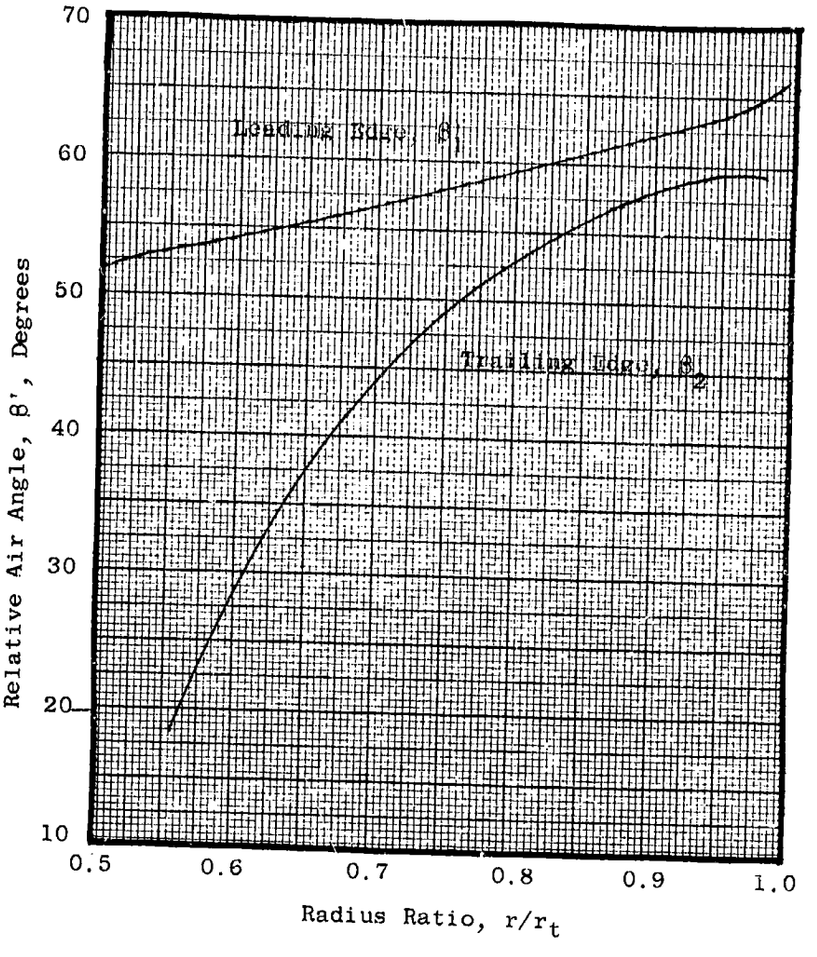

Figure 14. Radial Variations of Rotor Relative Air Angle at Blade Edges

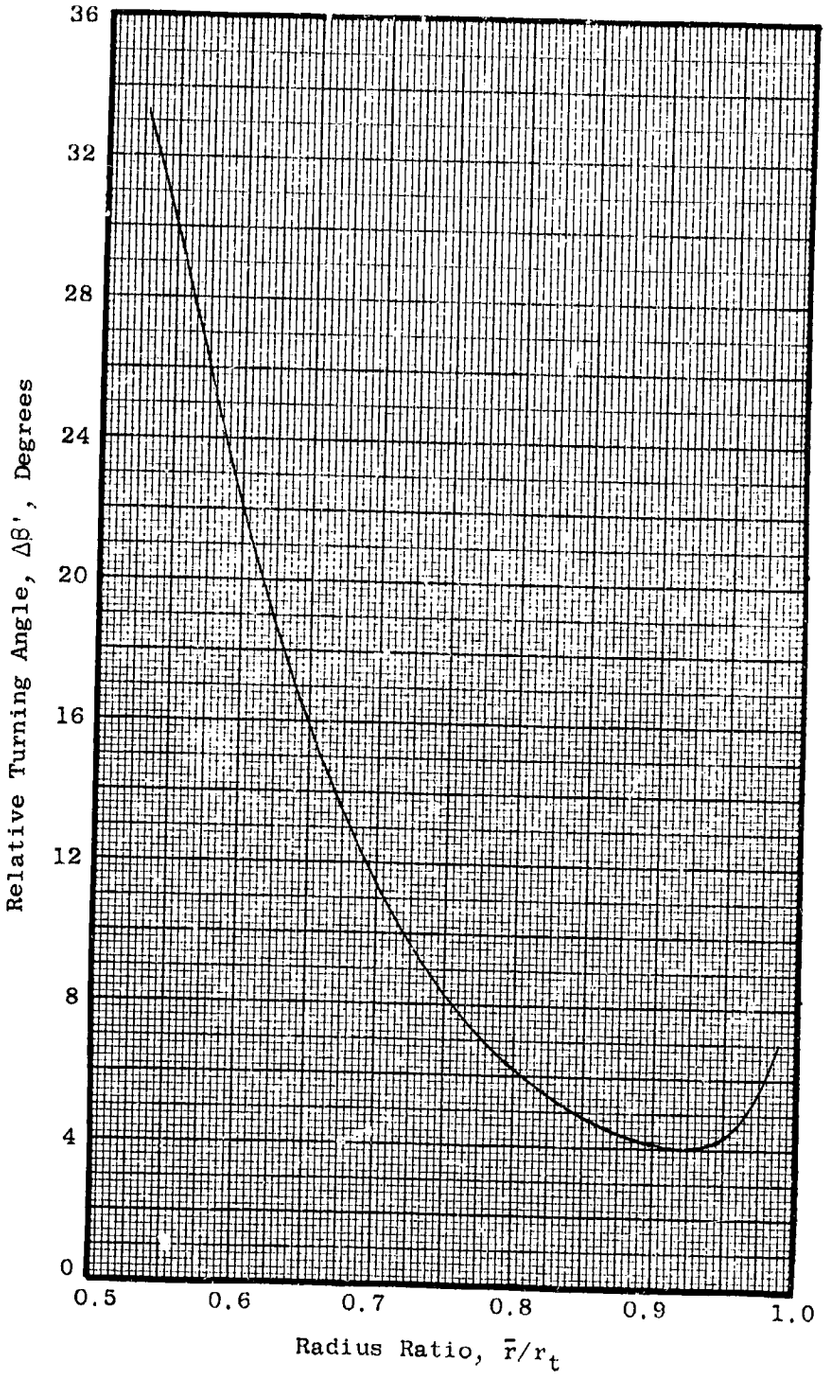

Figure 15. Rotor Relative Turning Angle Distribution

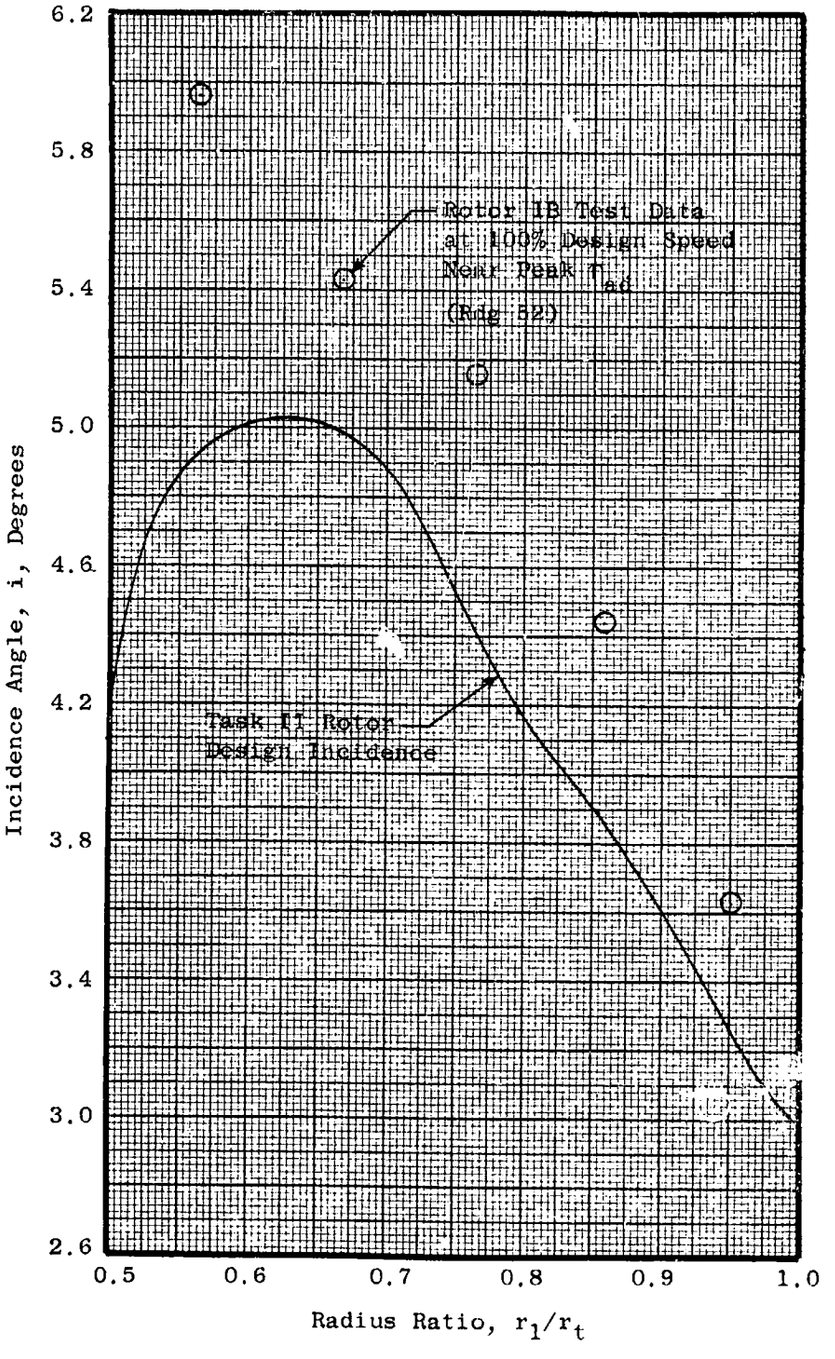

Figure 16. Rotor Incidence Angle Distribution

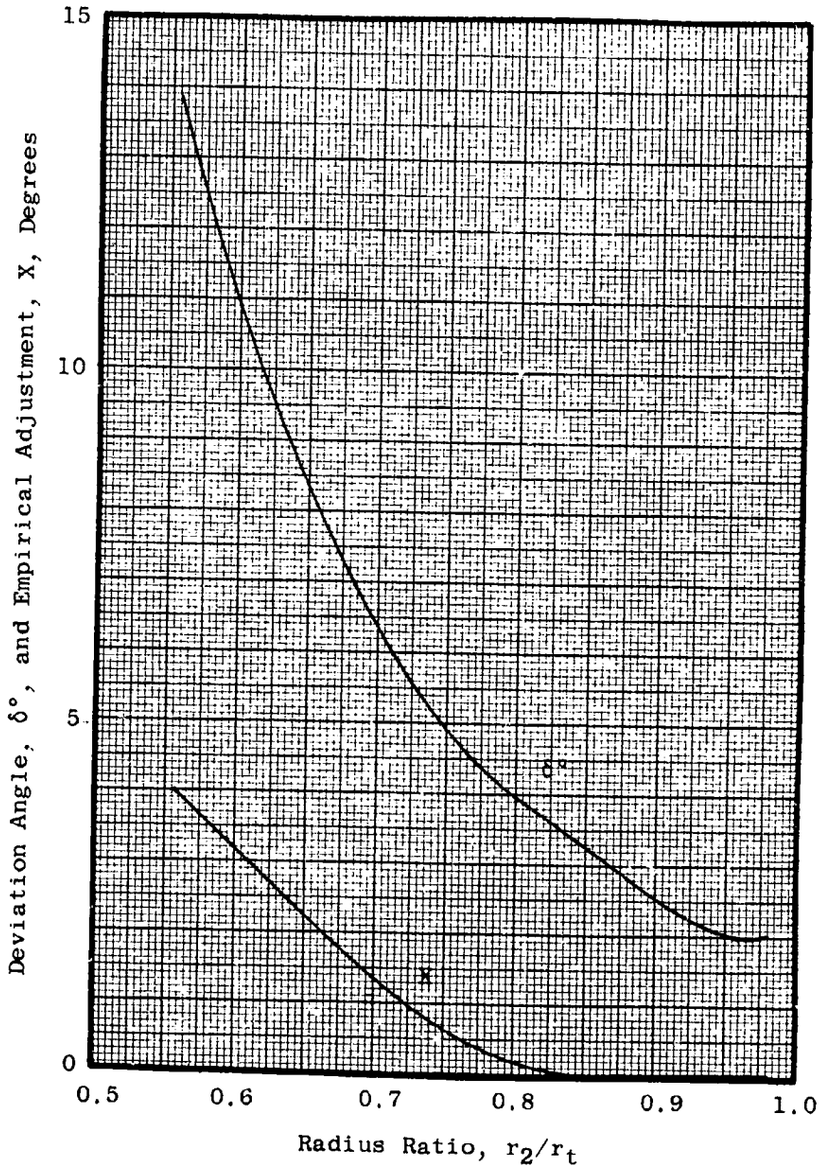

Figure 17. Radial Variation of Rotor Deviation Angle and Empirical Adjustment

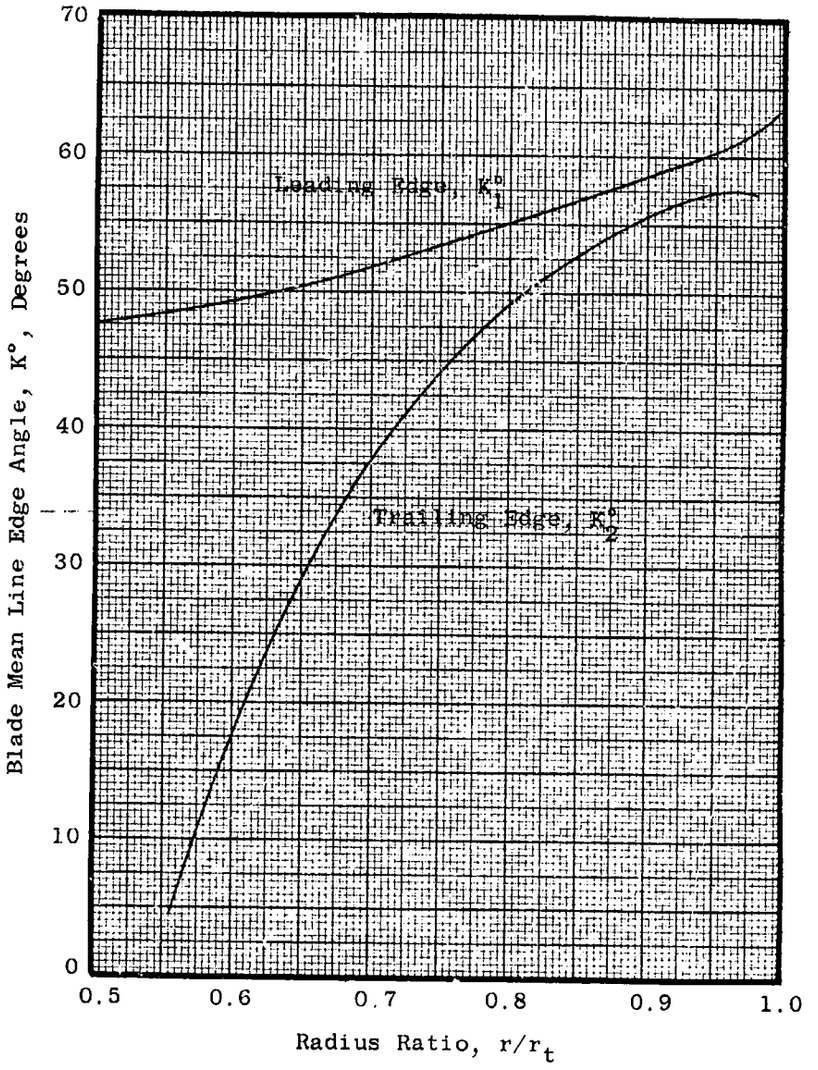

Figure 18. Distributions of Rotor Mean Line Angle at Blade Edges

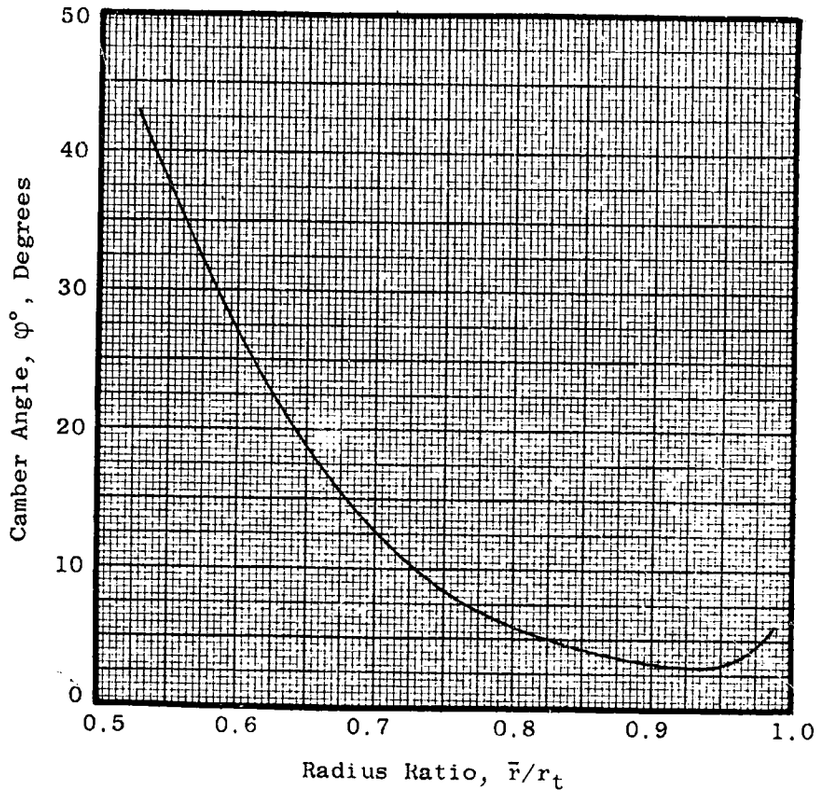

Figure 19. Rotor Camber Angle Distribution

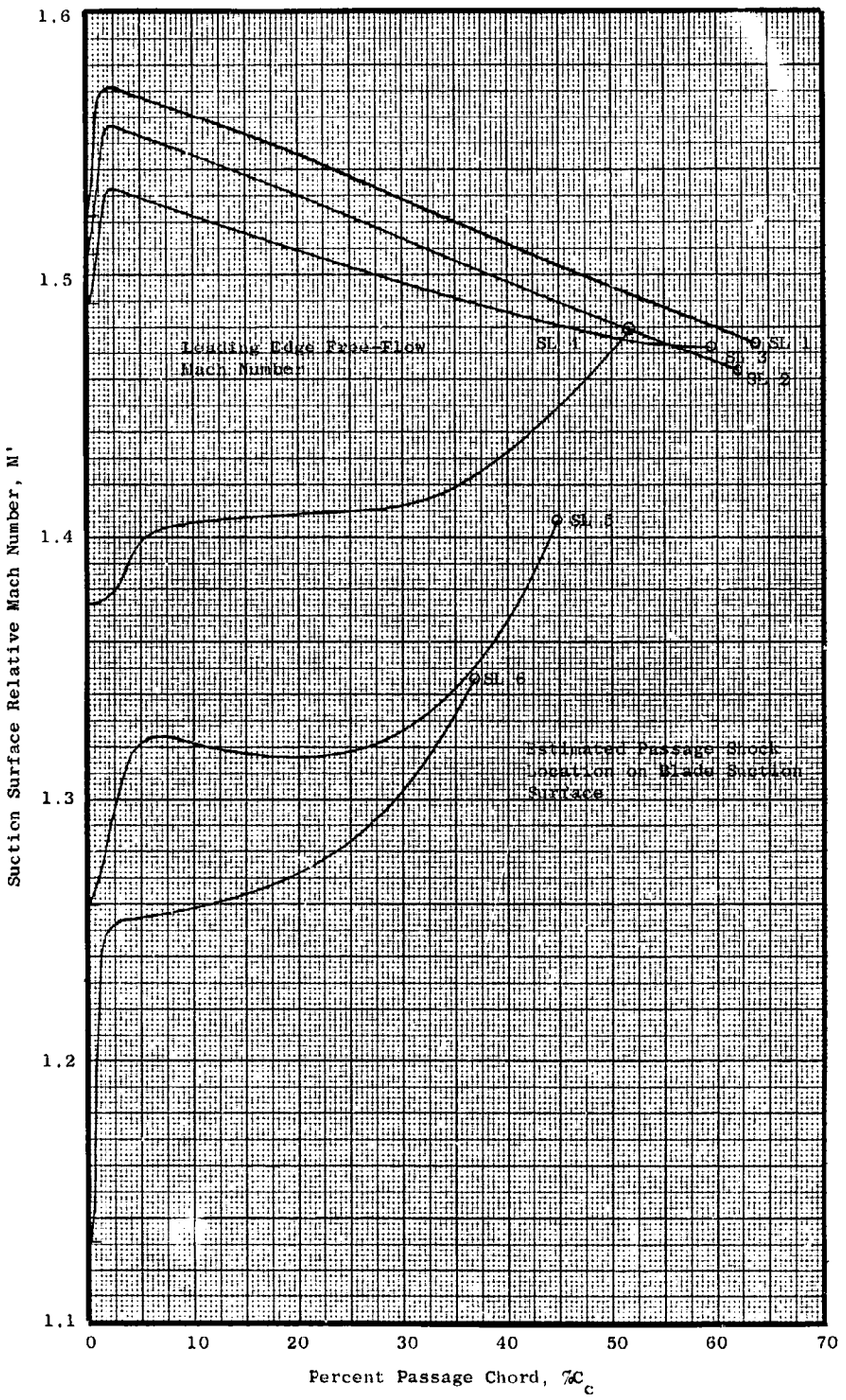

Figure 20. Rotor Suction Surface Mach Number Distributions

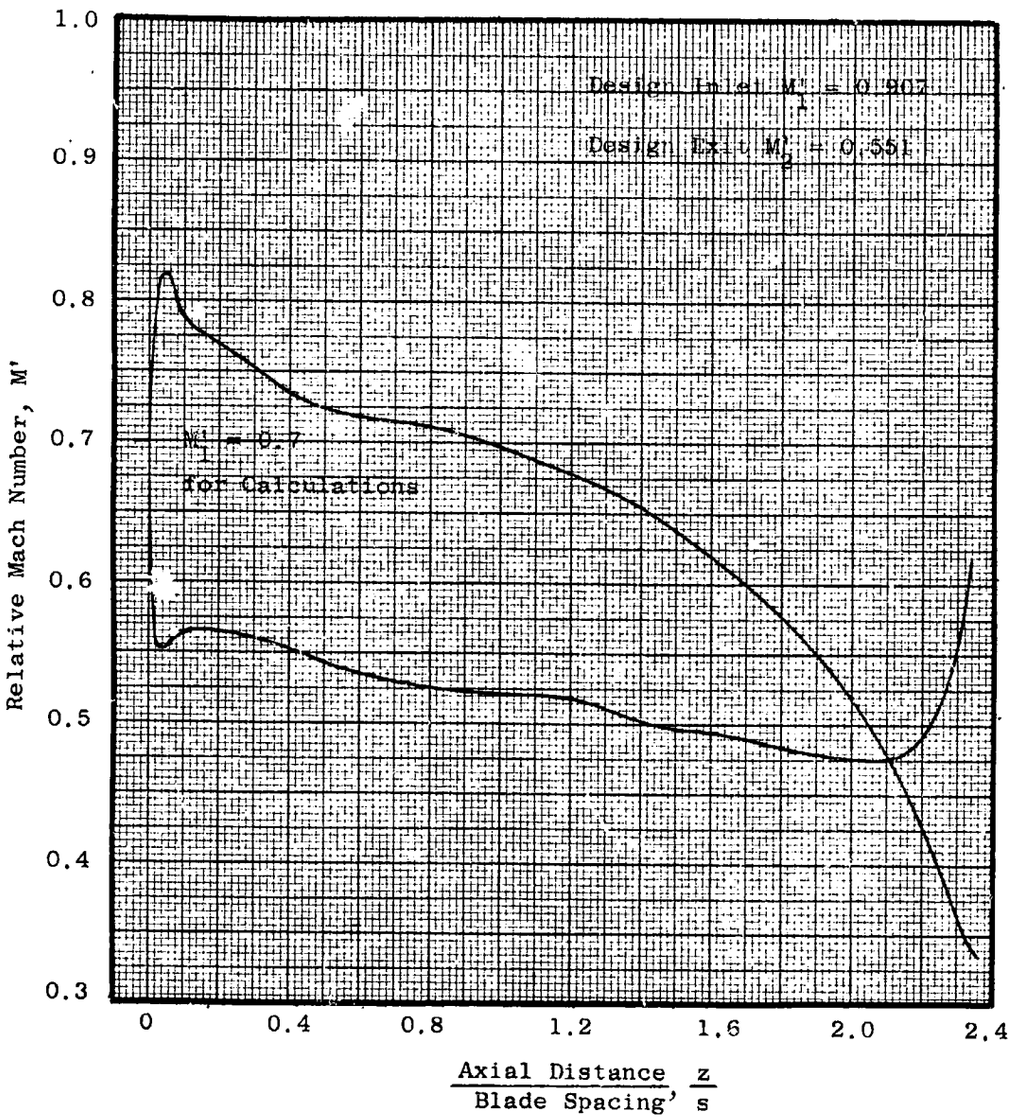

Figure 21. Rotor Hub Section Surface Relative Mach Number Distribution for 0.7 Inlet Relative Mach Number

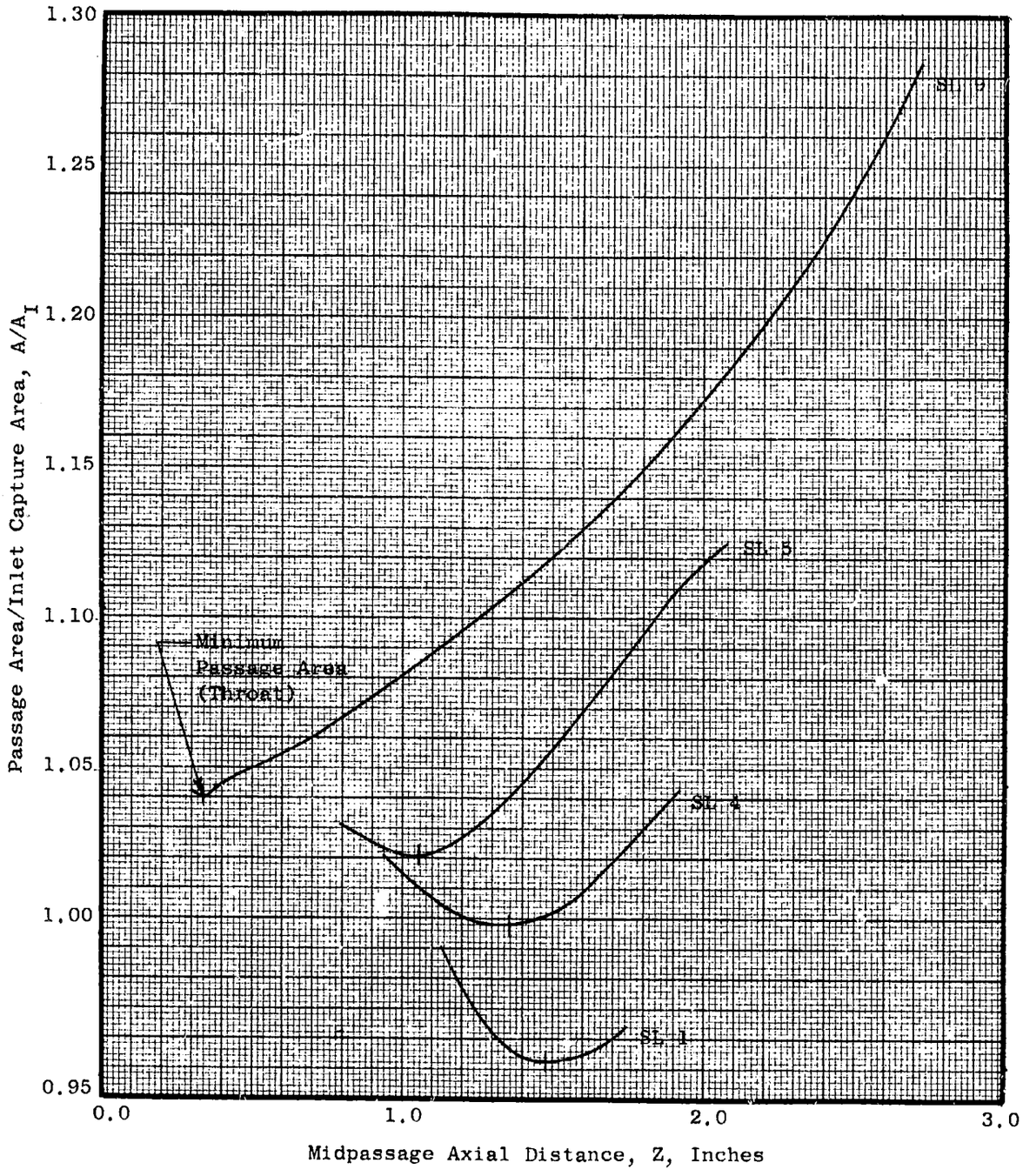

Figure 22. Rotor Passage Area Distributions

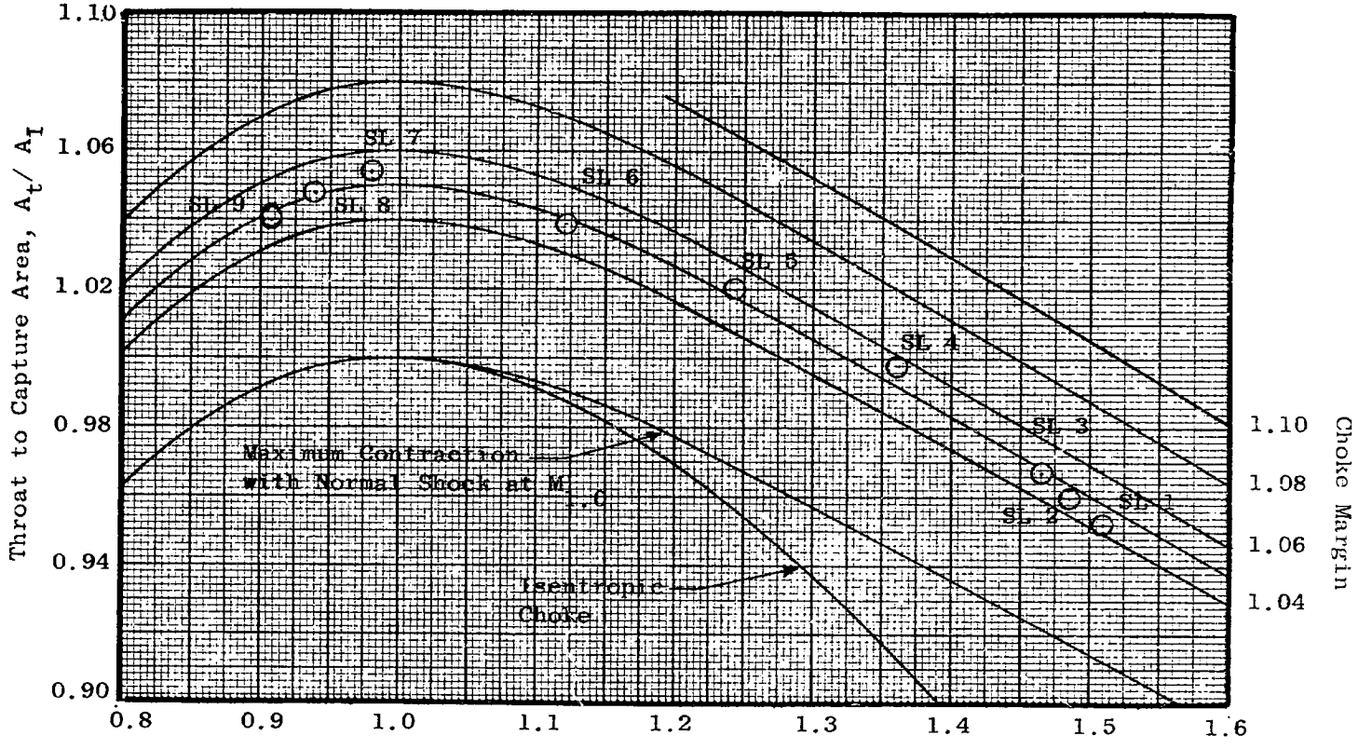

Figure 23. Rotor Throat Areas and Choke Margin

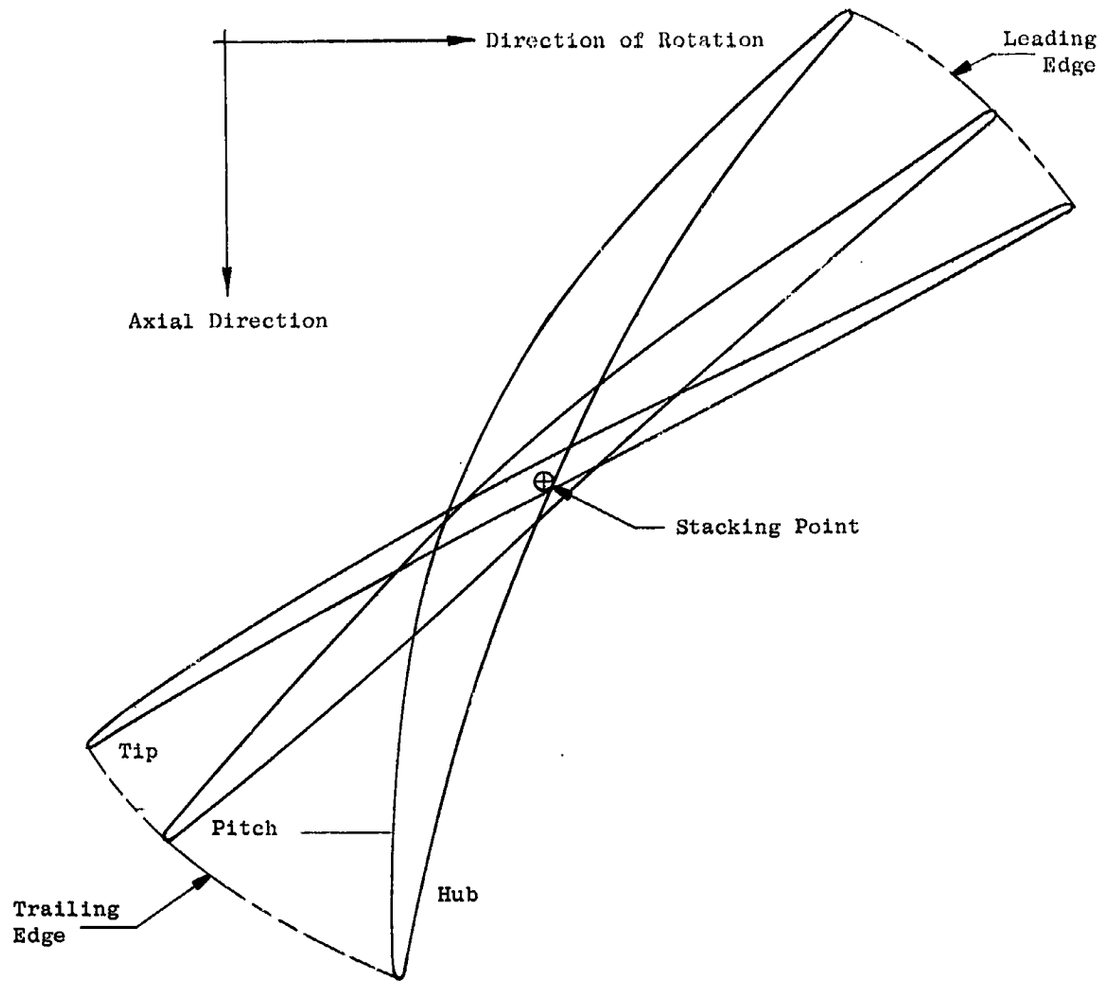

Figure 24. Rotor Blade Cascade Sections

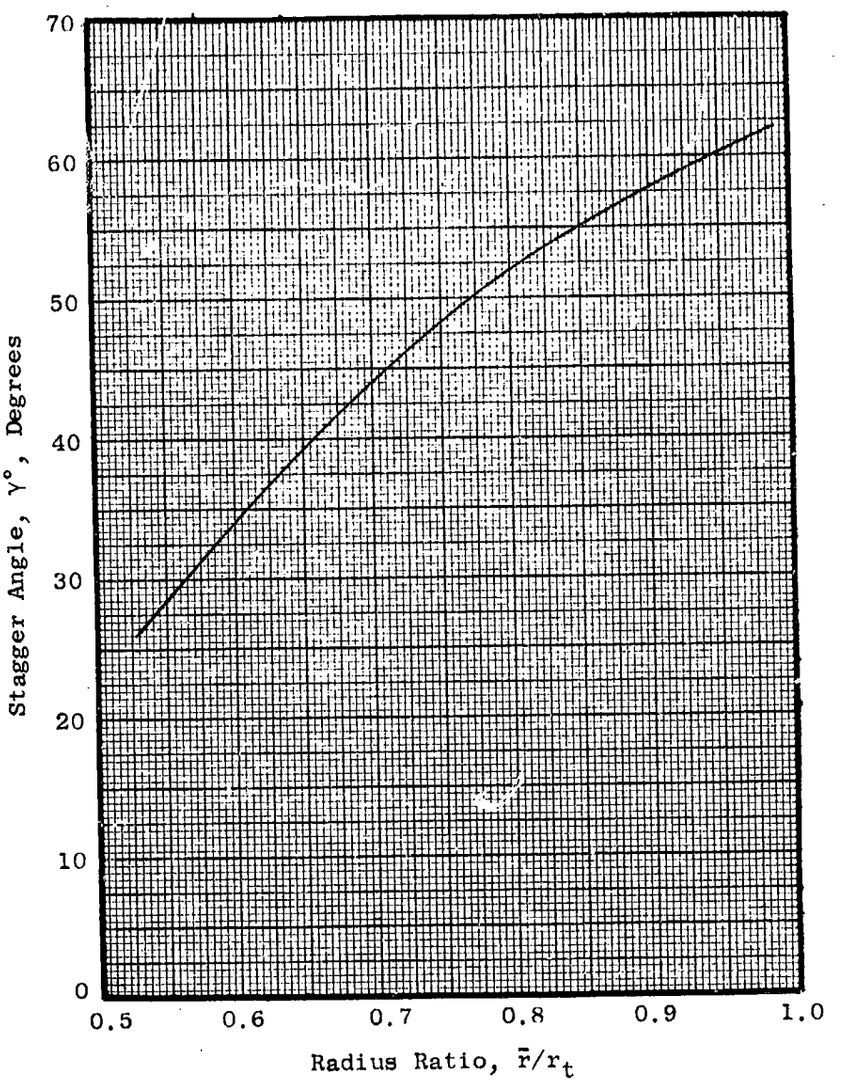

Figure 25. Radial Variation of Rotor Stagger Angles in Cascade Projection

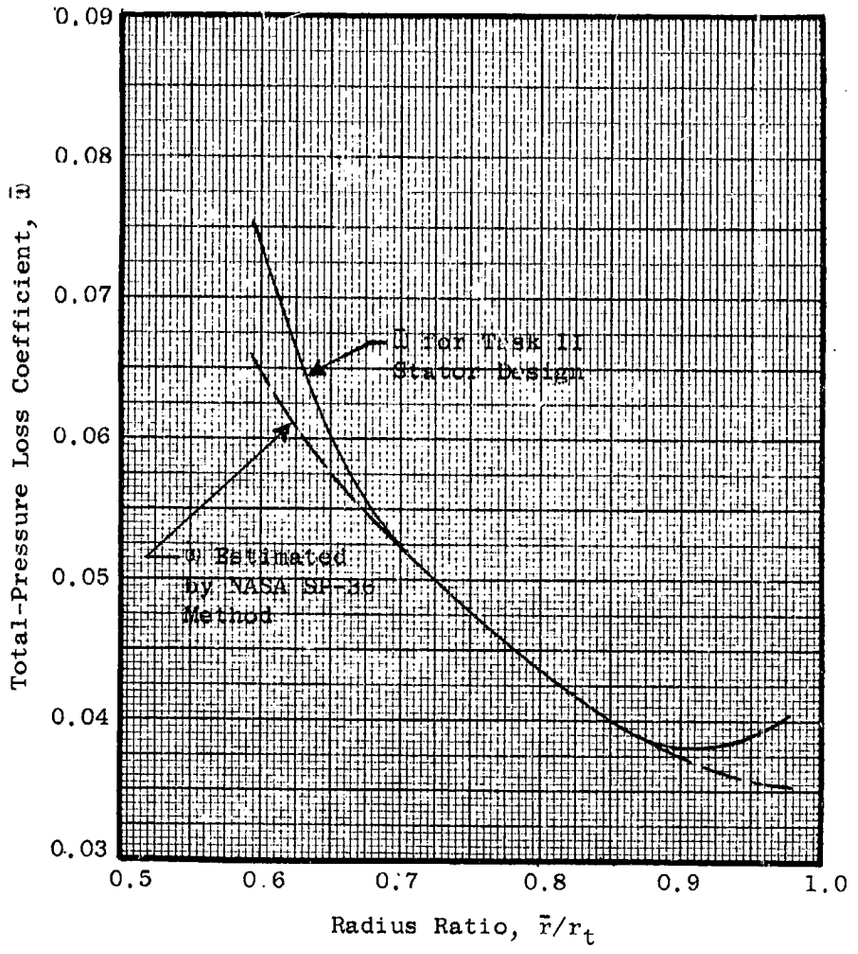

Figure 26. Stator Total-Pressure Loss Coefficient Distribution

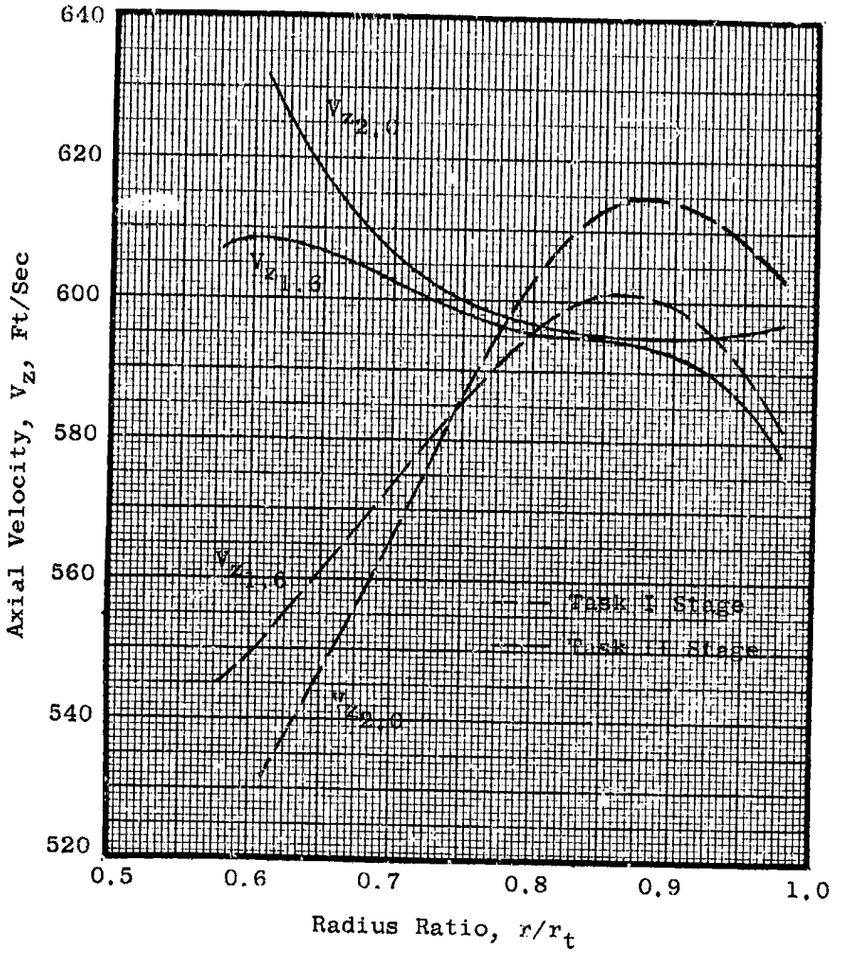

Figure 27. Radial Variations of Stator Axial Velocity at Inlet and Exit Stations

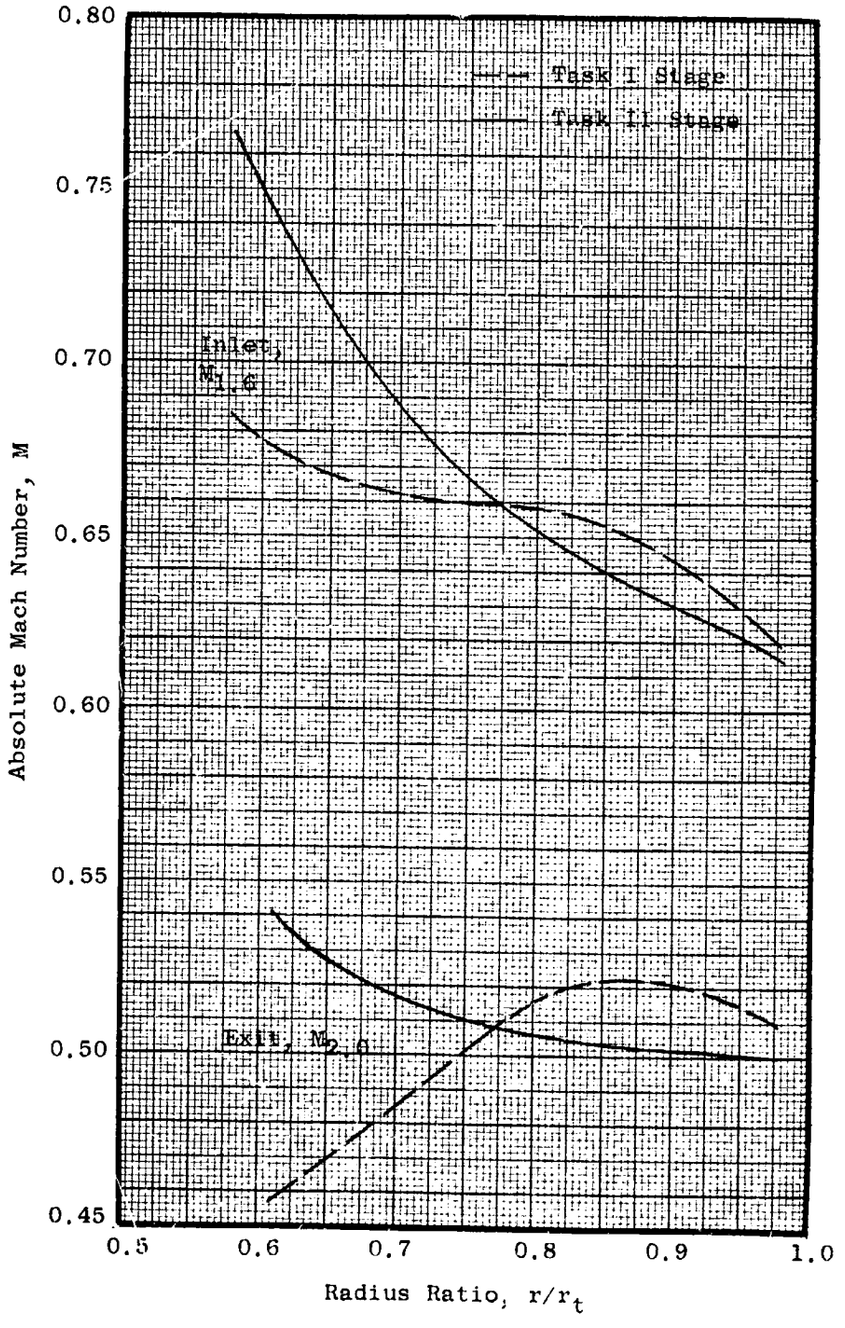

Figure 28. Stator Mach Number Distributions at Inlet and Exit Stations

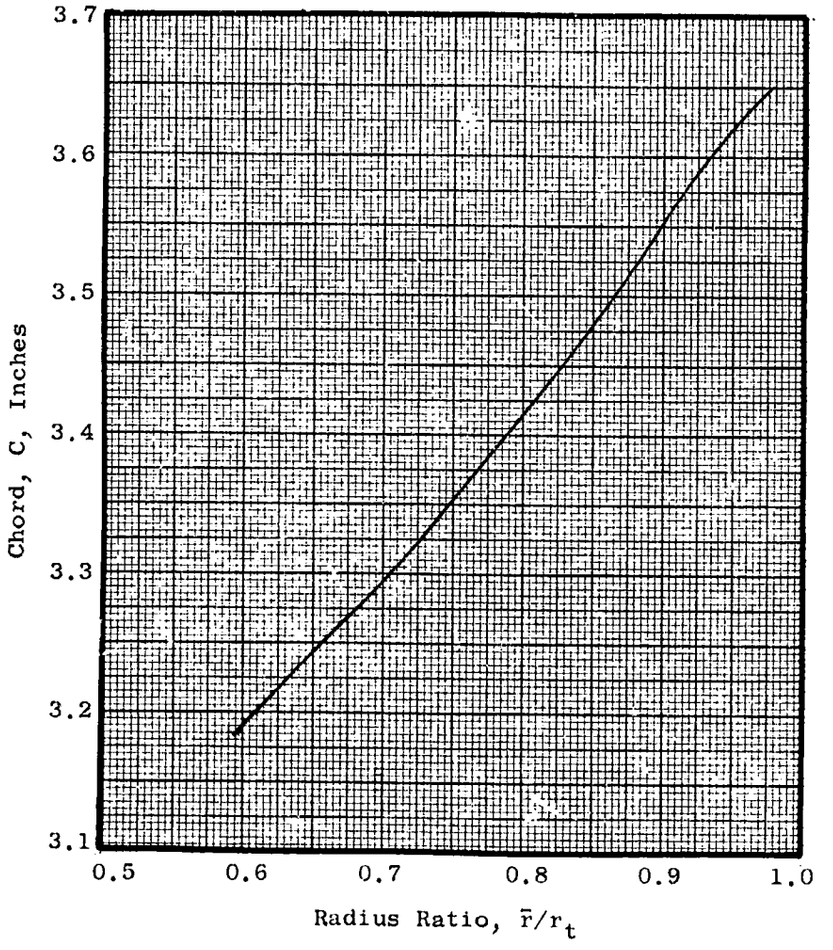

Figure 29. Radial Variation of Stator Chord on Cylindrical Sections

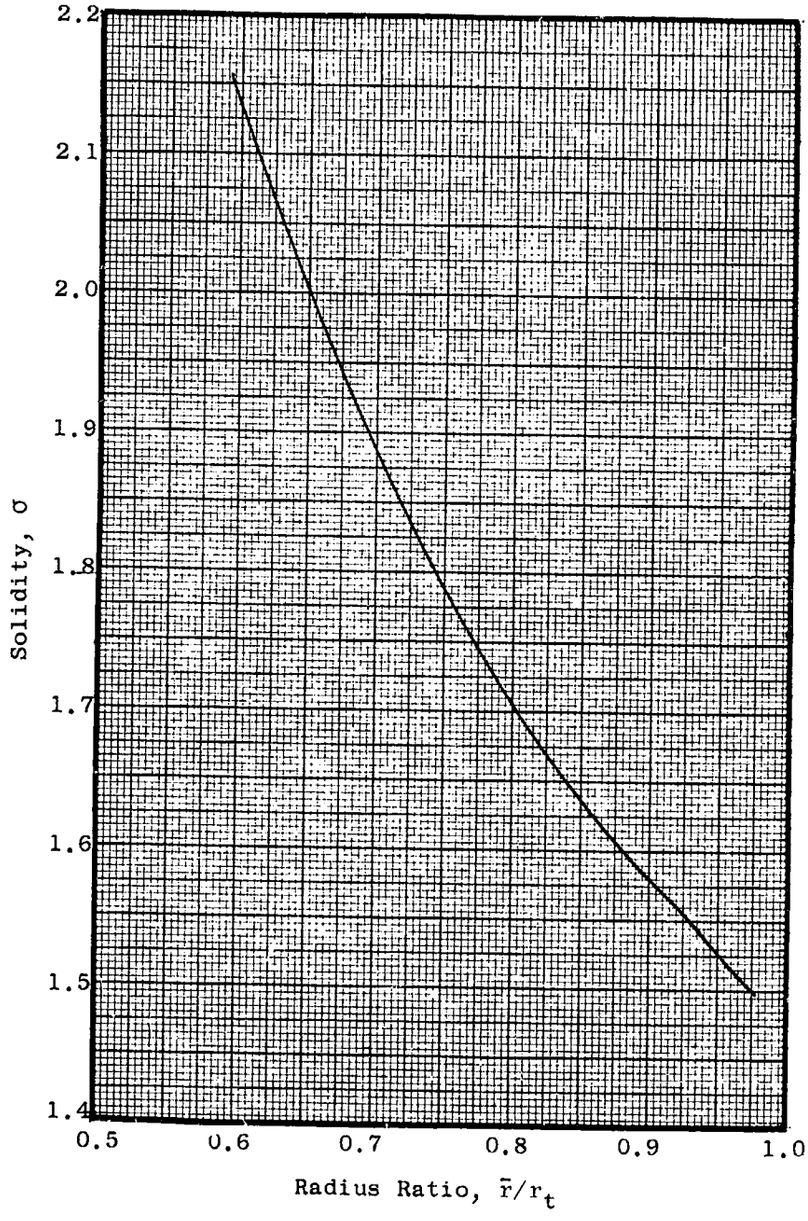

Figure 30. Stator Solidity Distribution

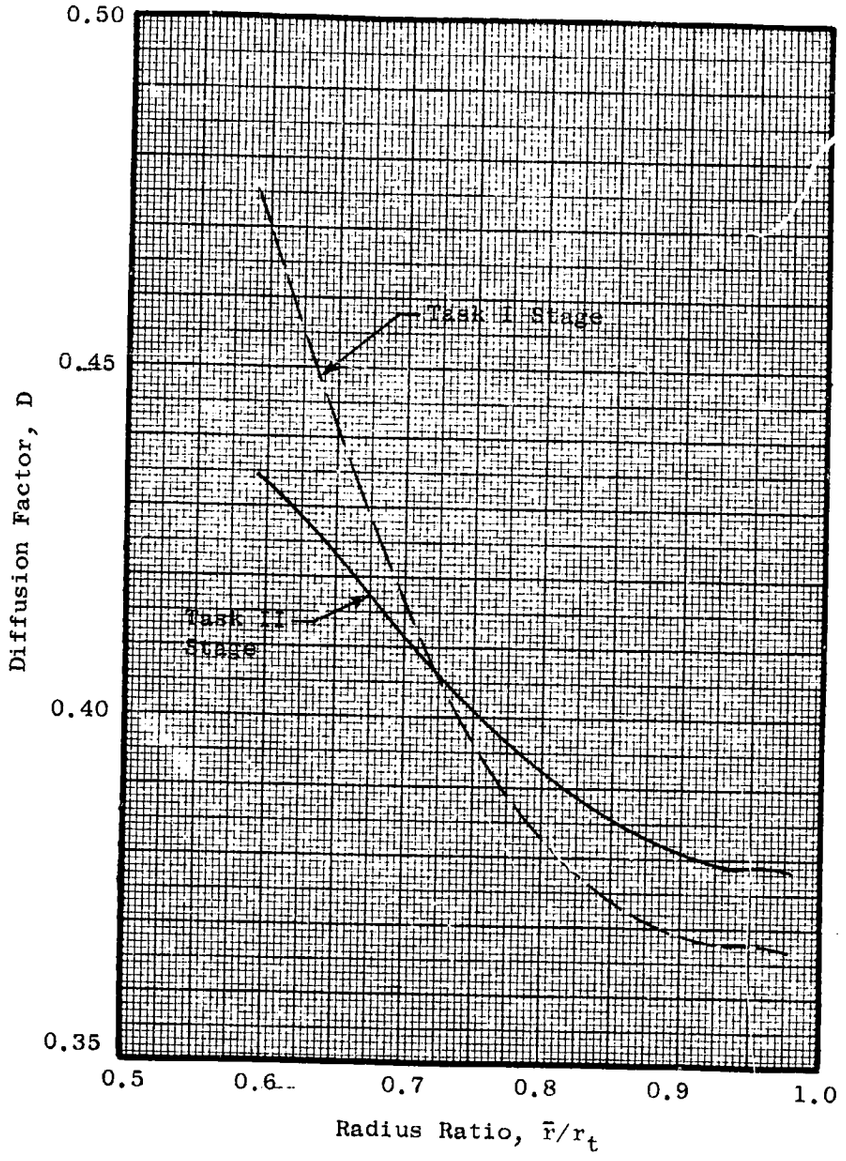

Figure 31. Radial Variation of Stator Diffusion Factor Between Inlet and Exit Stations

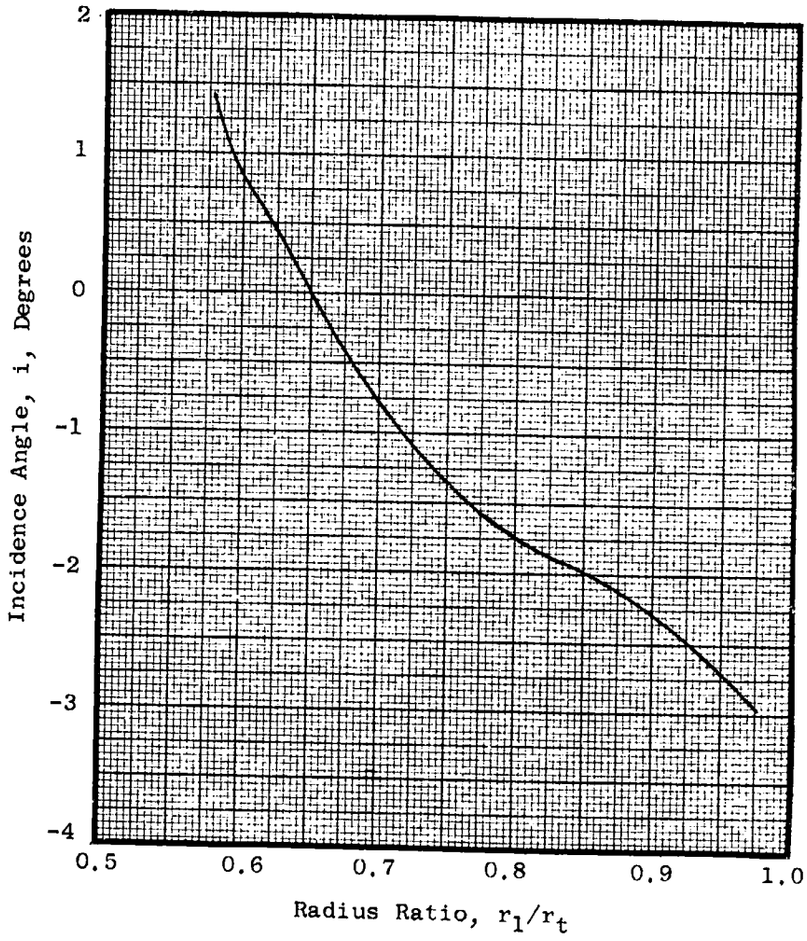

Figure 32. Stator Incidence Angle Distribution

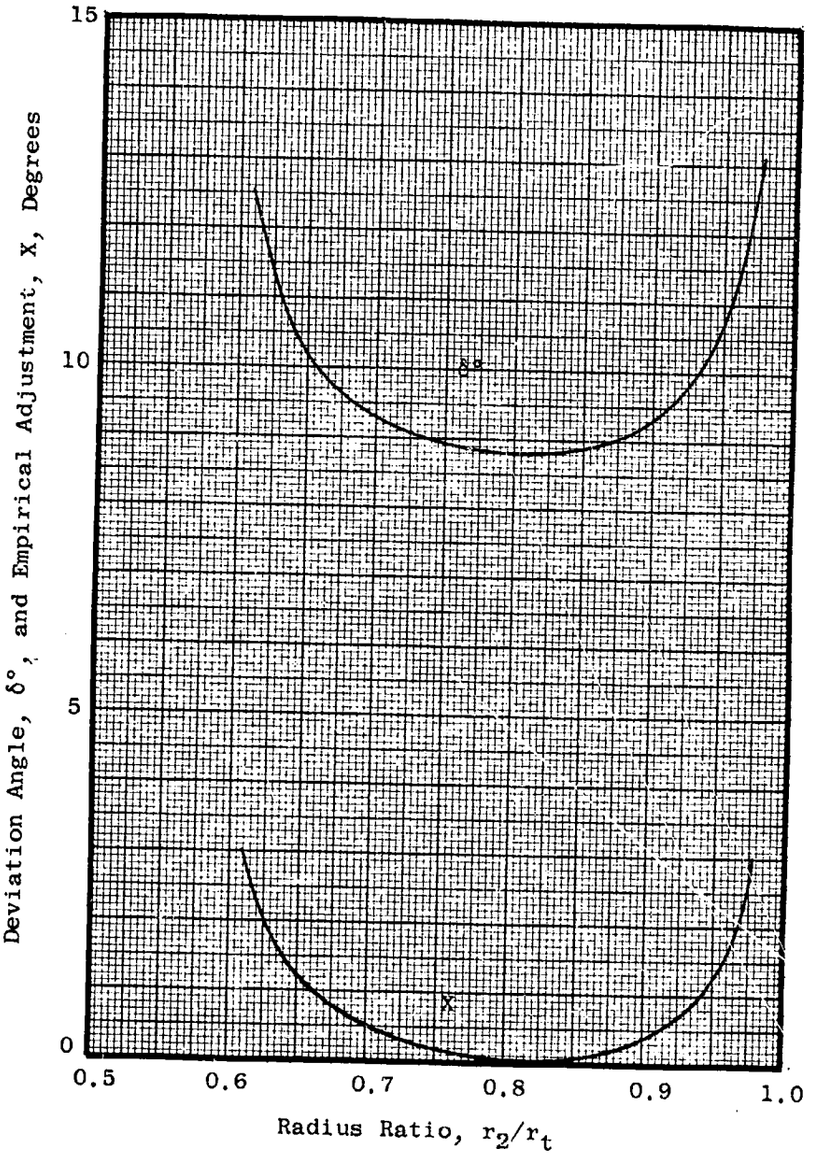

Figure 33. Distributions of Stator Deviation Angle and Empirical Adjustment

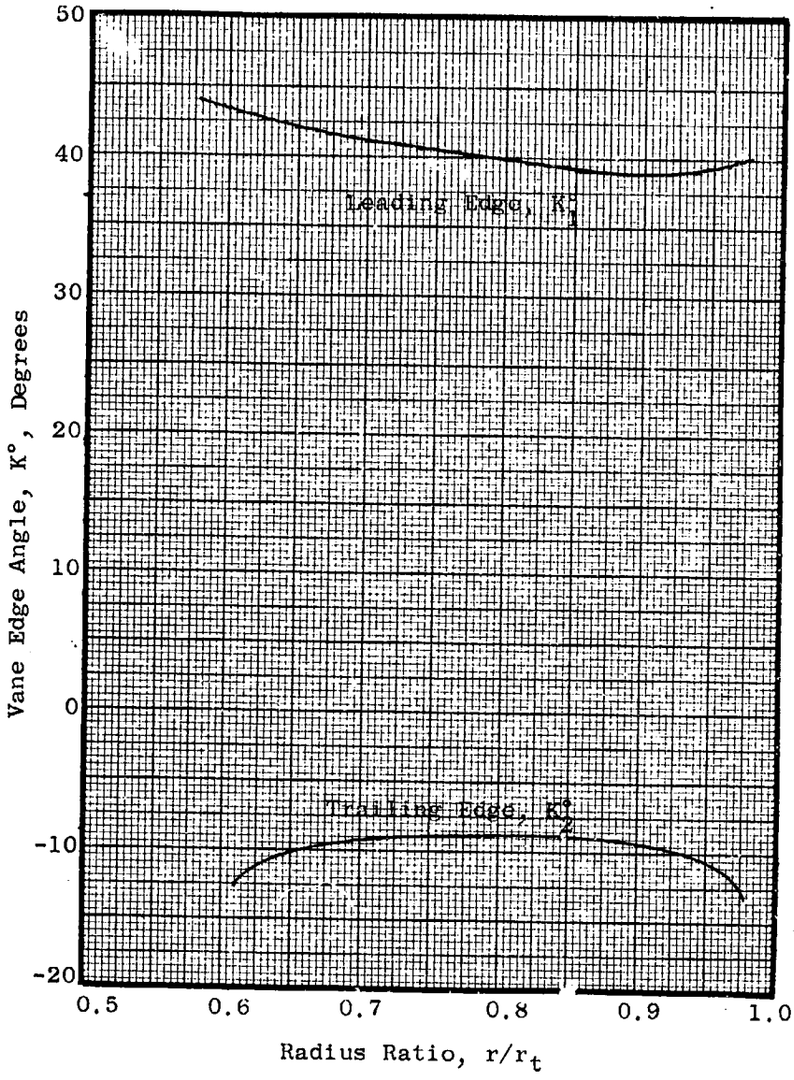

Figure 34. Stator Mean Line Angle Distributions at Vane Edges

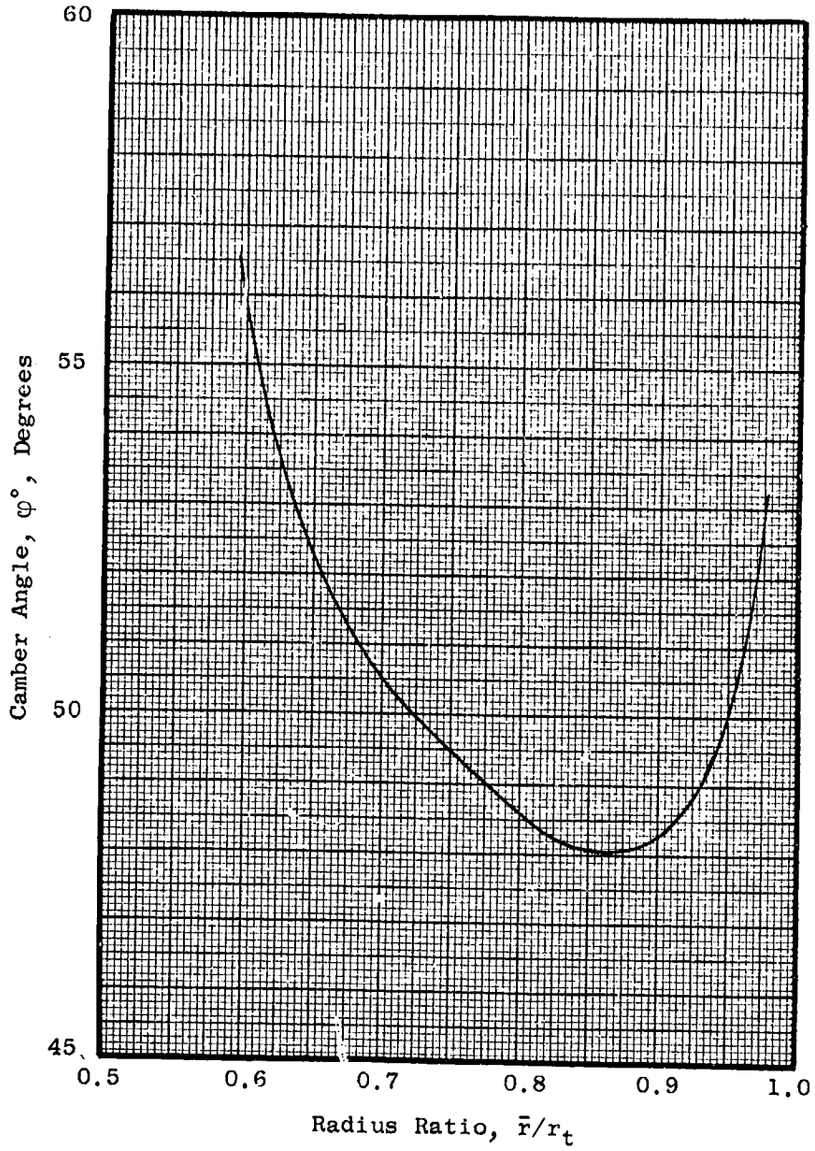

Figure 35. Radial Variation of Stator Camber Angle in Cascade Projection

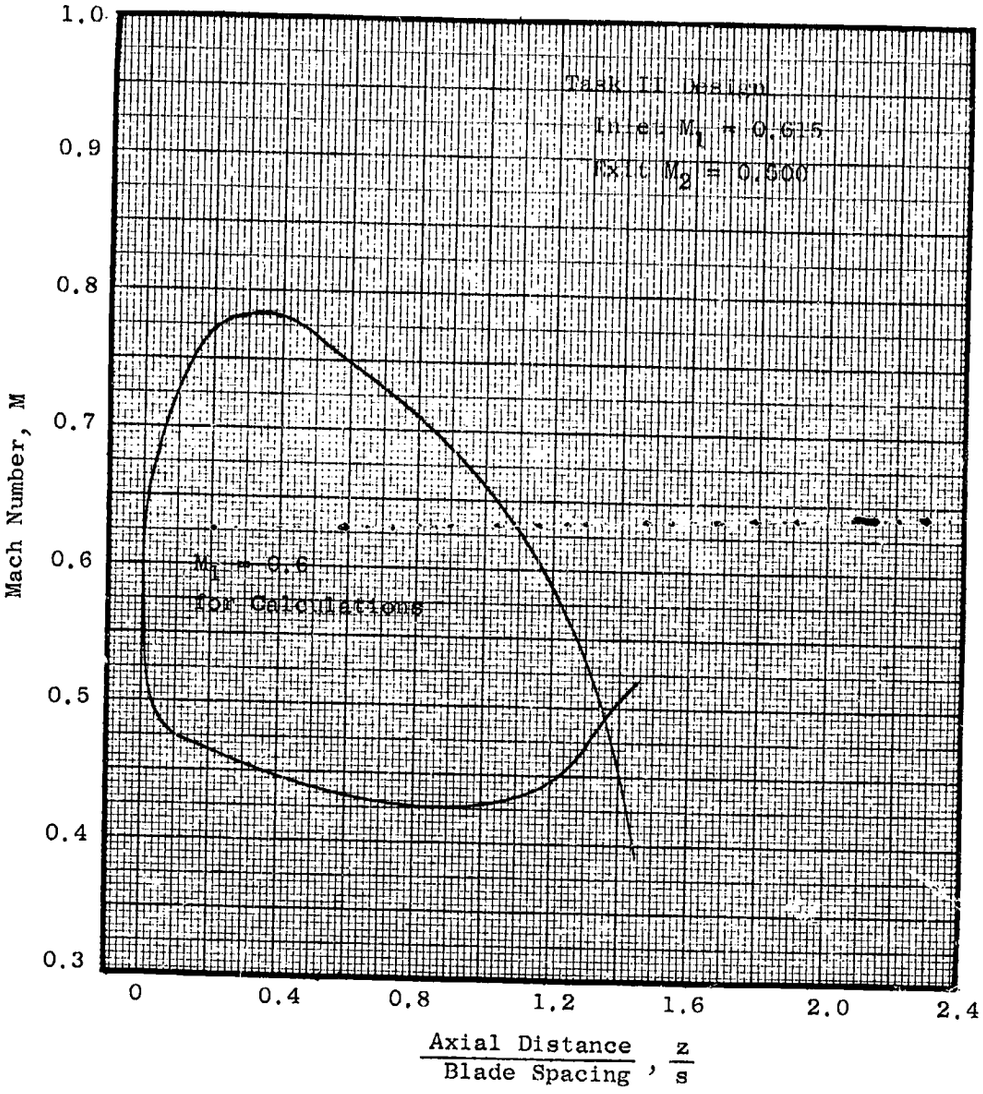

Figure 36. Stator Tip Section Surface Mach Number Distribution for 0.6 Inlet Mach Number

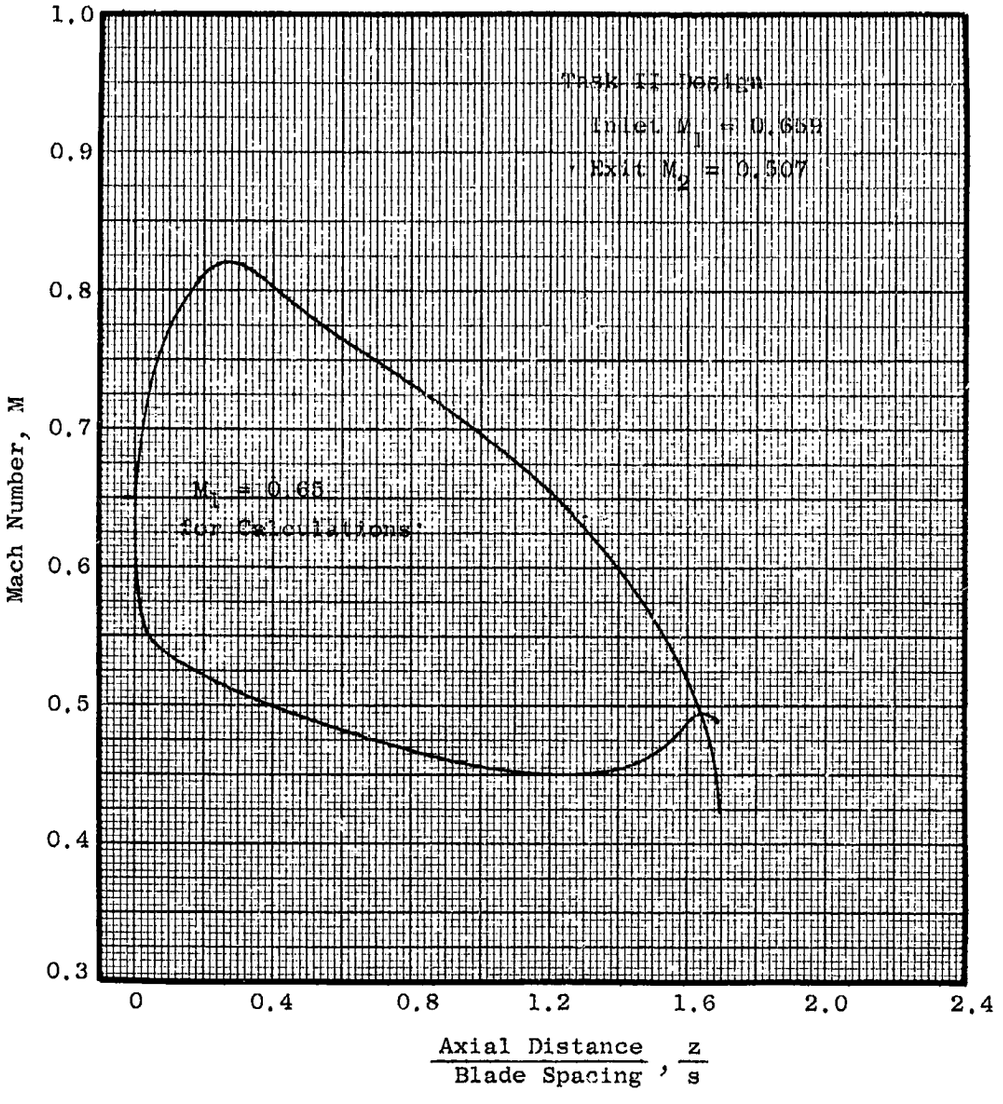

Figure 37. Stator Pitch Section Surface Mach Number Distribution for 0.65 Inlet Mach Number

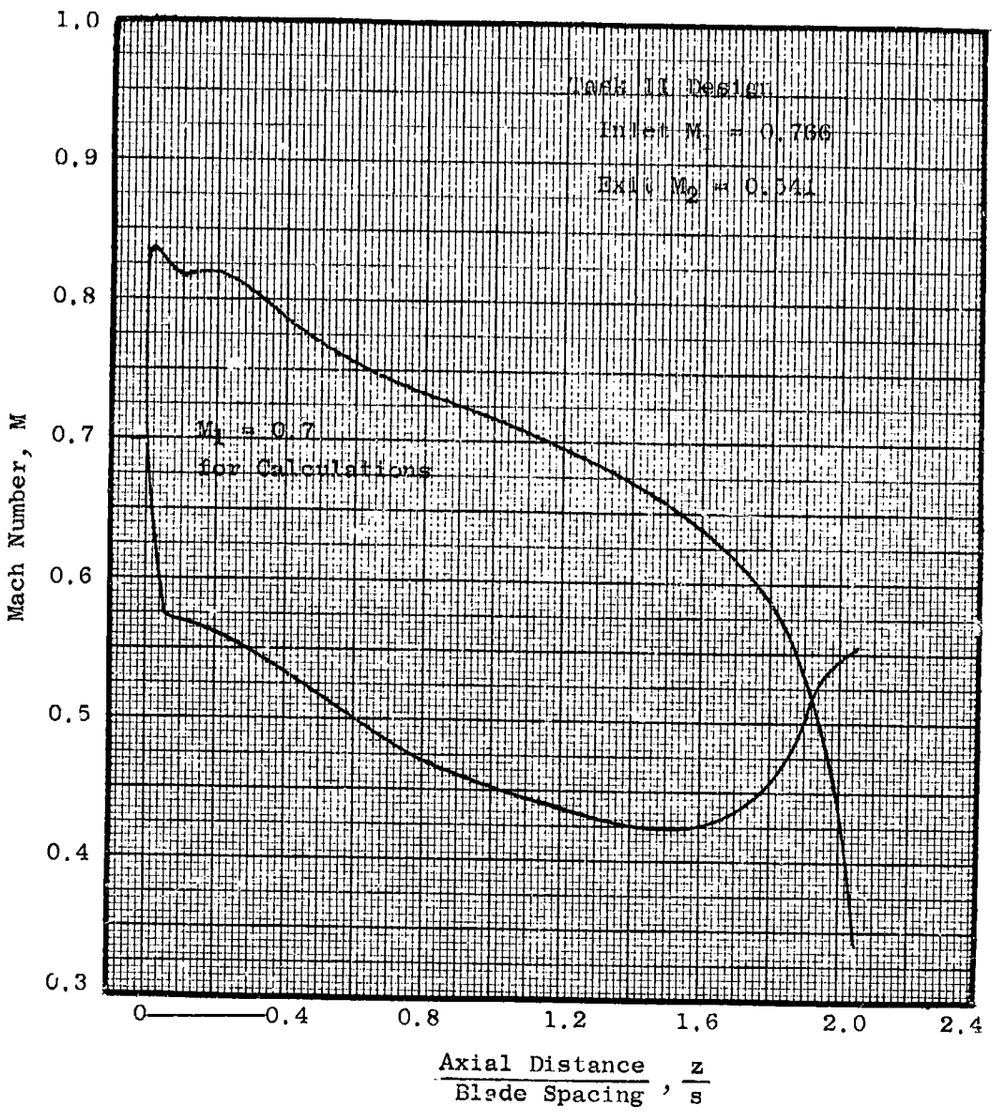

Figure 38. Stator Hub Section Surface Mach Number Distribution for 0.7 Inlet Mach Number

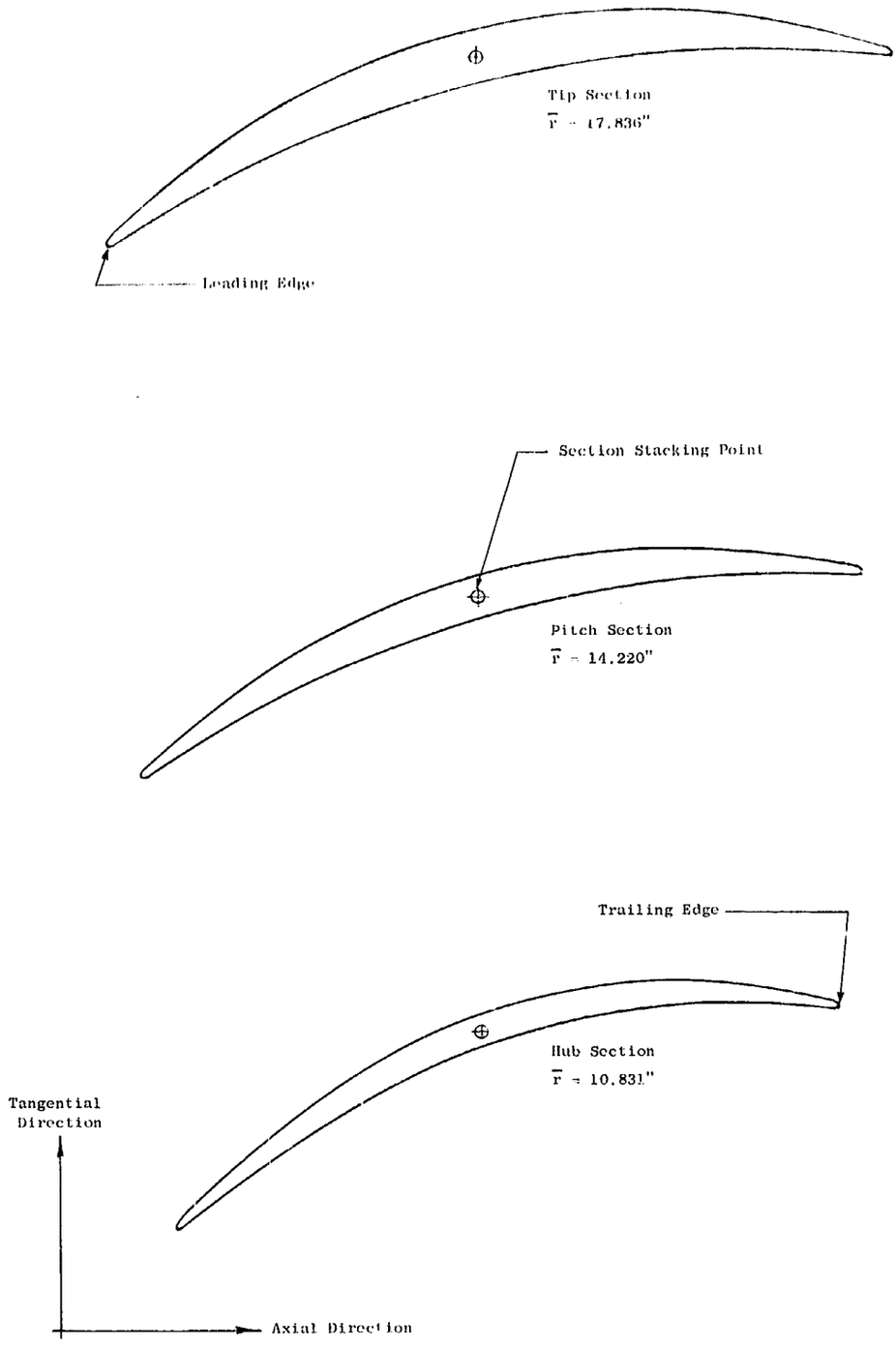

Figure 39. Stator Vane Cascade Sections

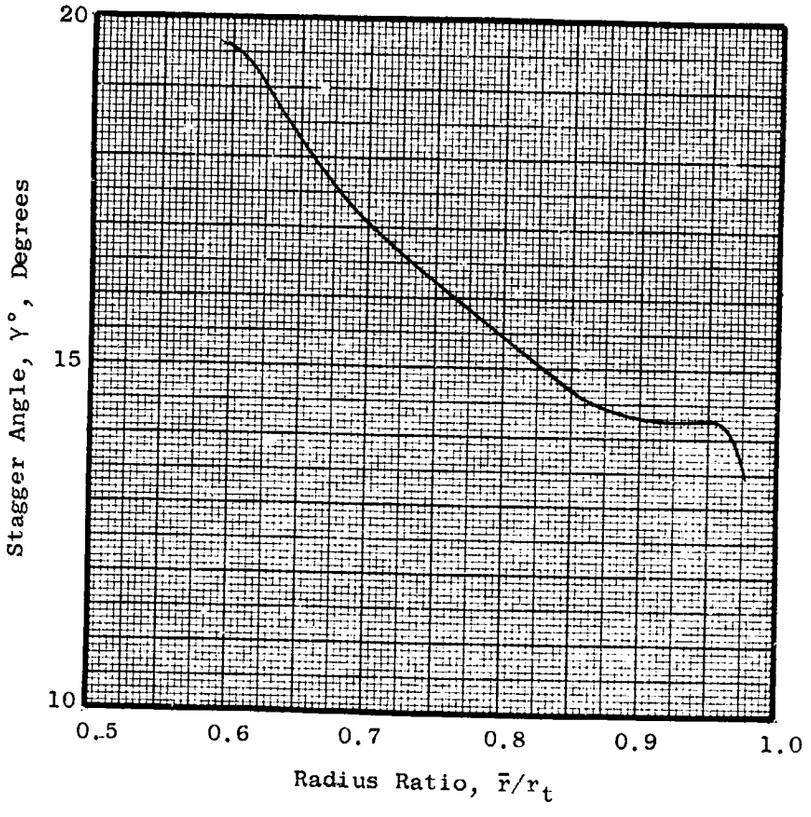

Figure 40. Radial Variation of Stator Stagger Angle in Cascade Projection

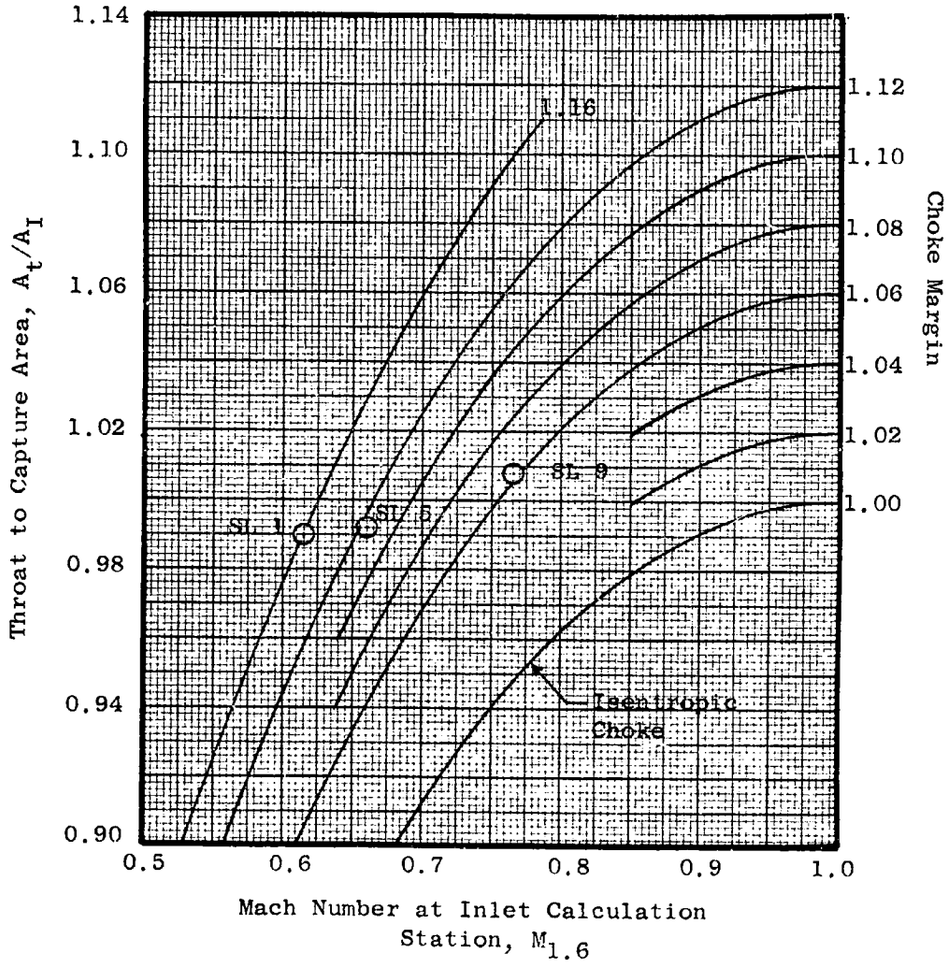

Figure 41. Stator Throat Areas and Choke Margin

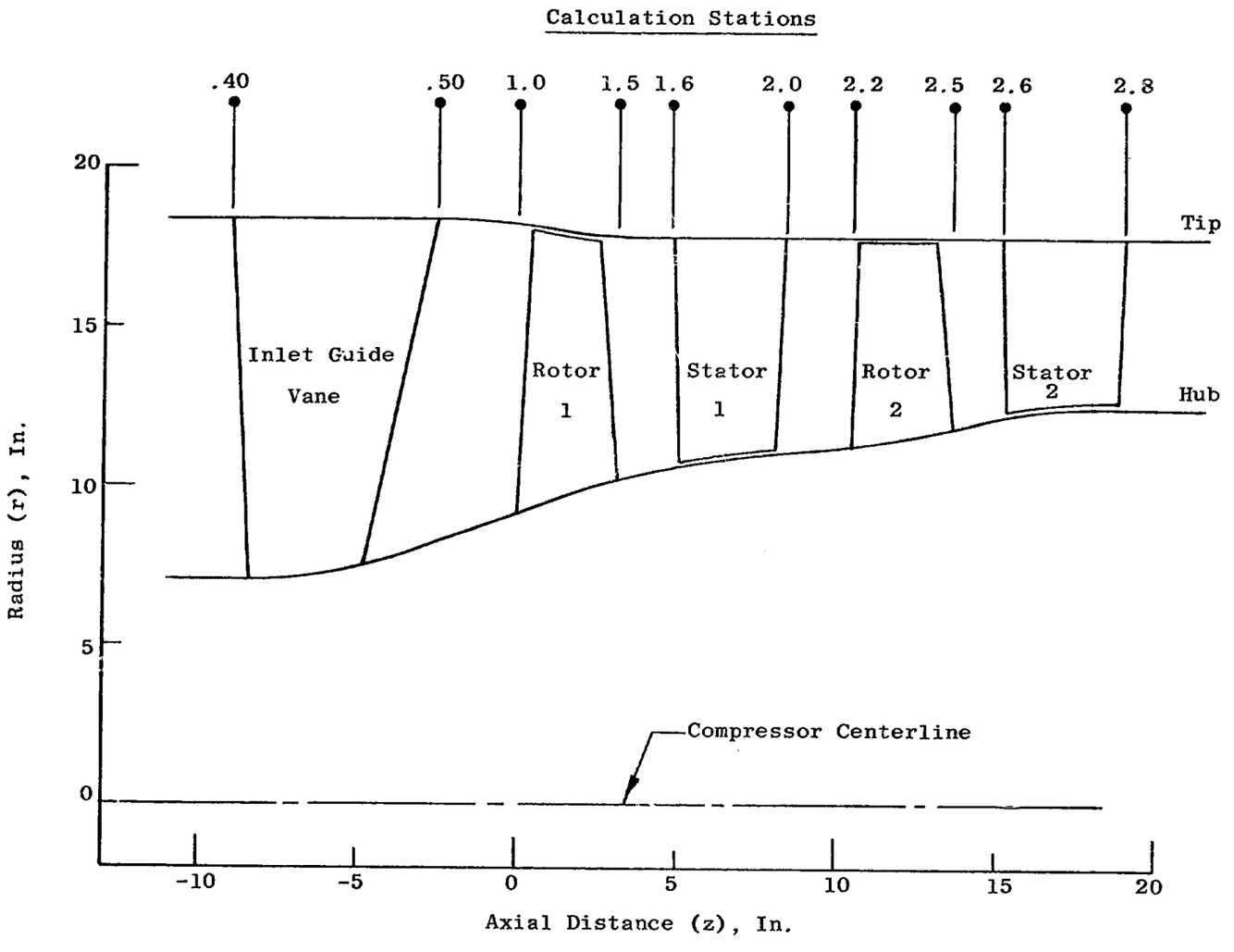

Figure 42. Compressor Flowpath for Preliminary Off-Design Analysis

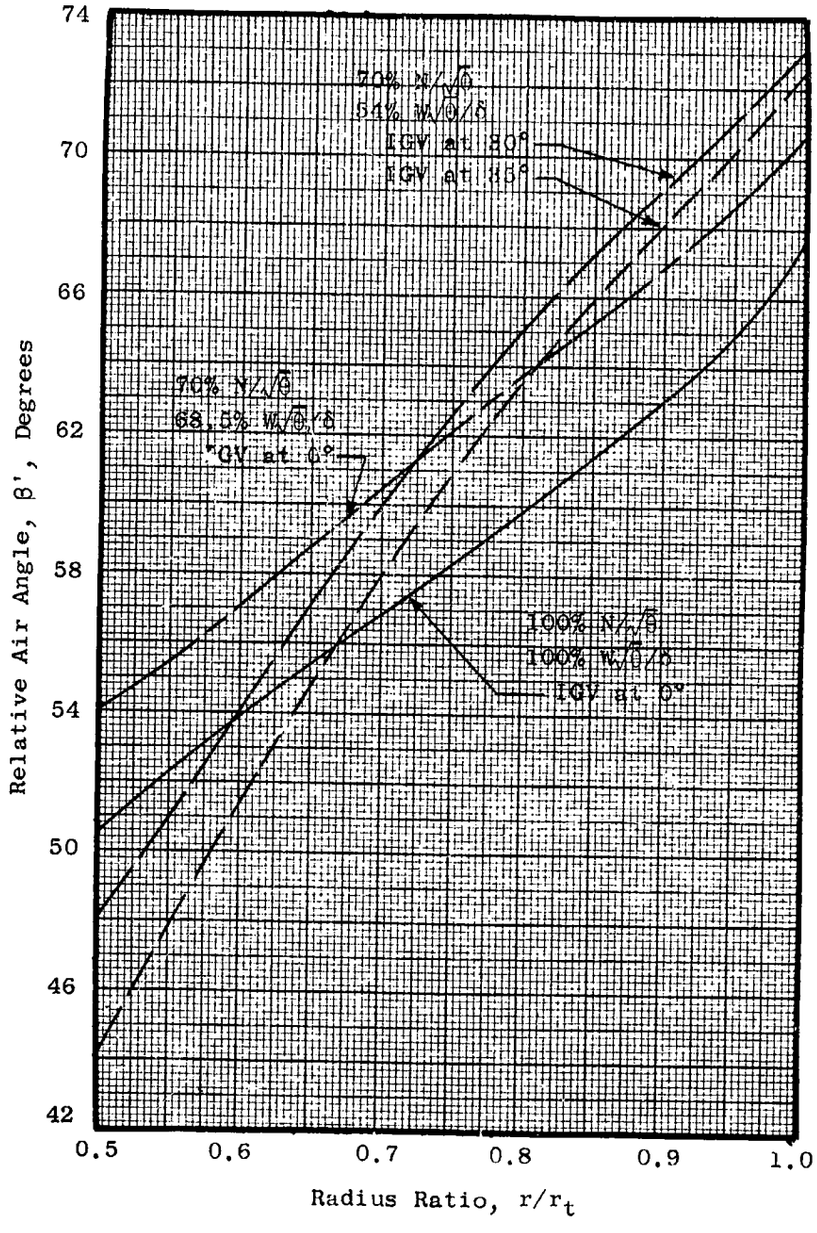

Figure 43. Distributions of First Rotor Inlet Relative Air Angles at Station 1.0

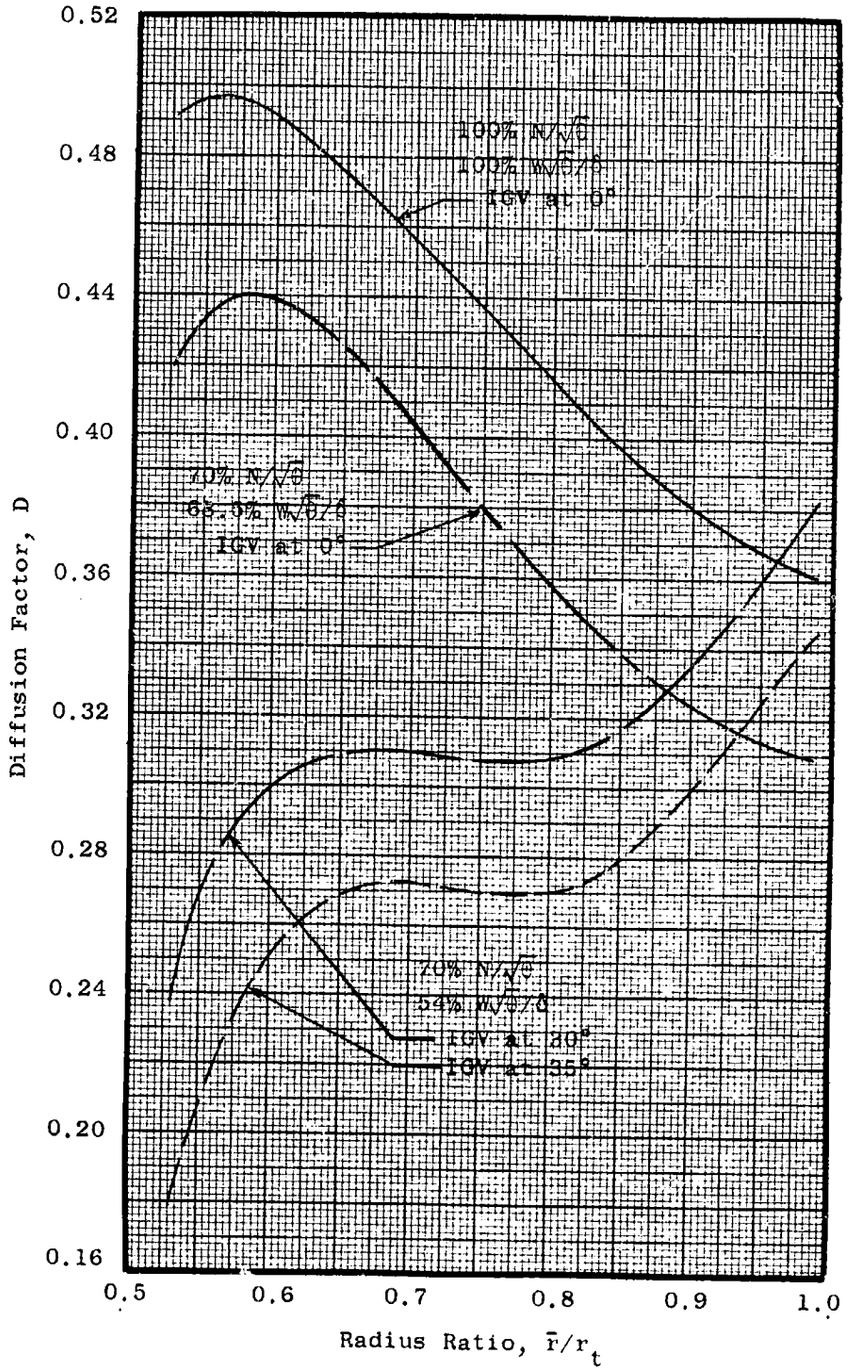

Figure 44. Radial Variations of First Rotor Diffusion Factor

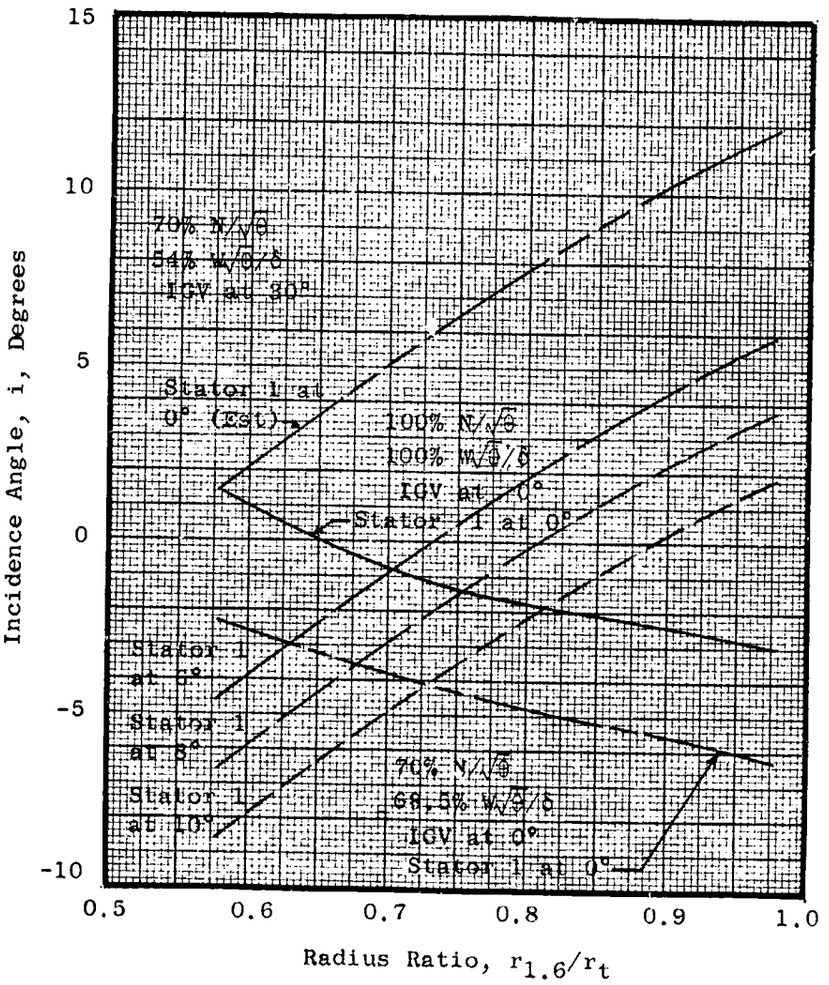

Figure 45. First Stator Incidence Angle Distributions at Plane 1.60

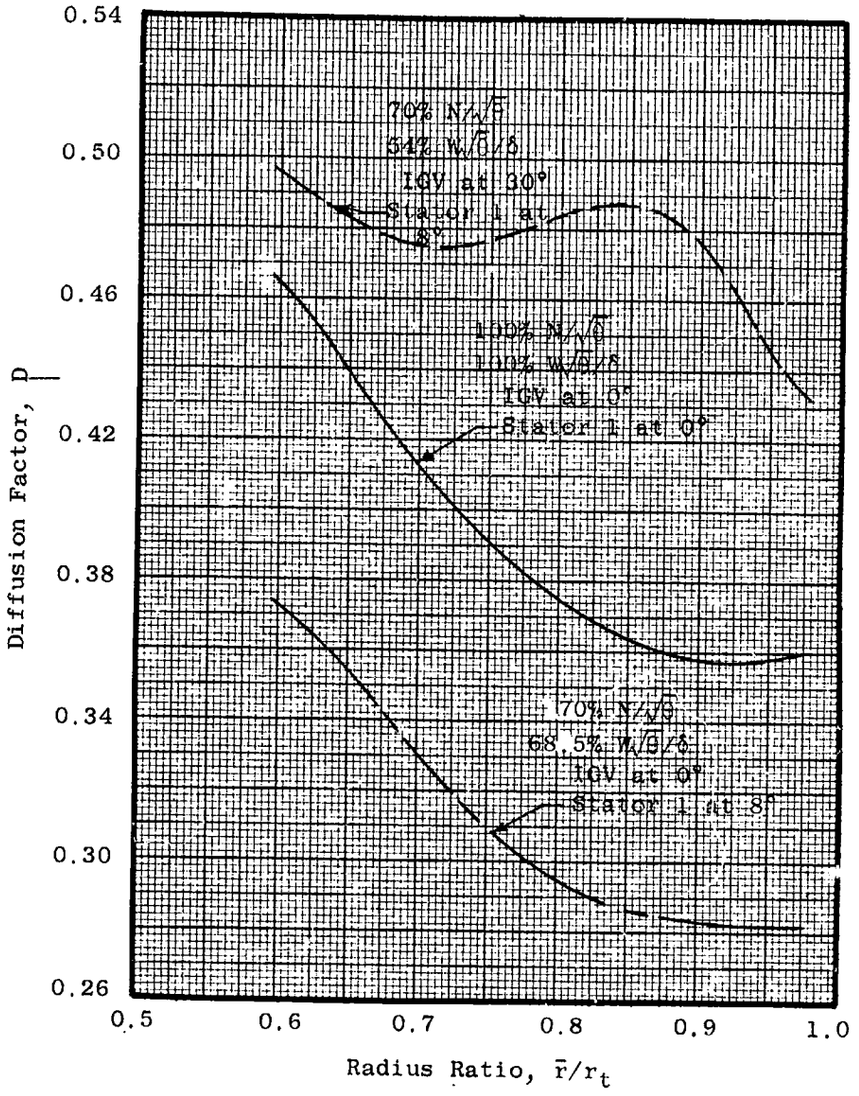

Figure 46. Radial Variations of First Stator Diffusion Faltor

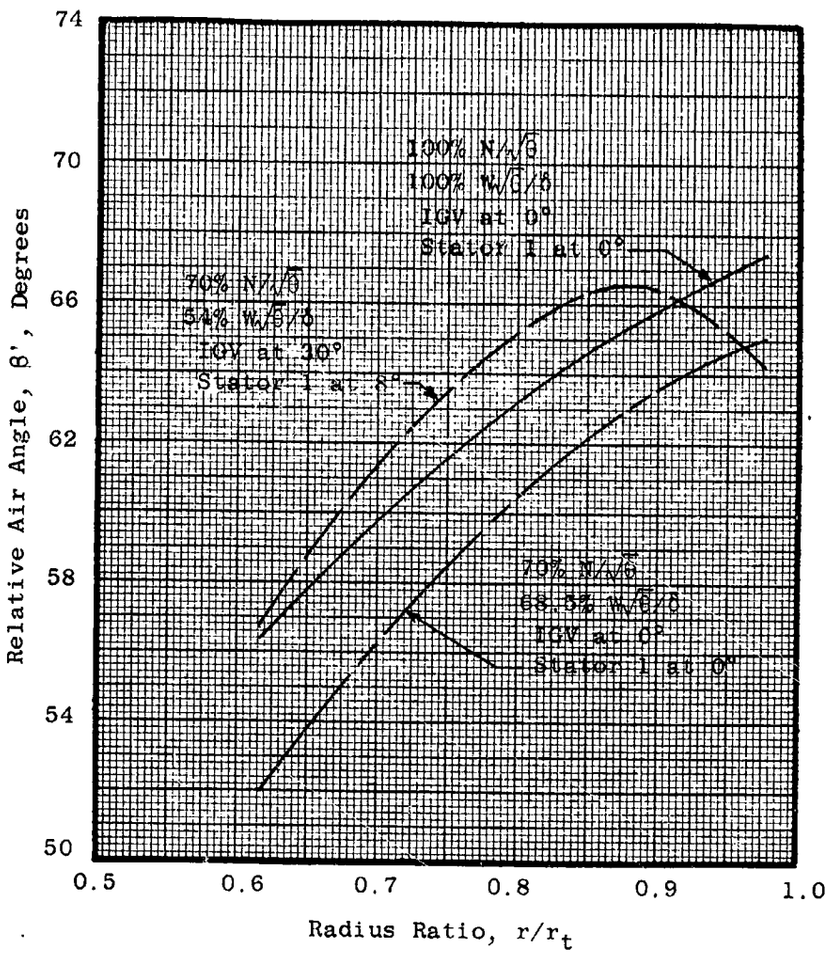

Figure 47. Second Rotor Inlet Relative Air Angle Distributions at Station 2.20

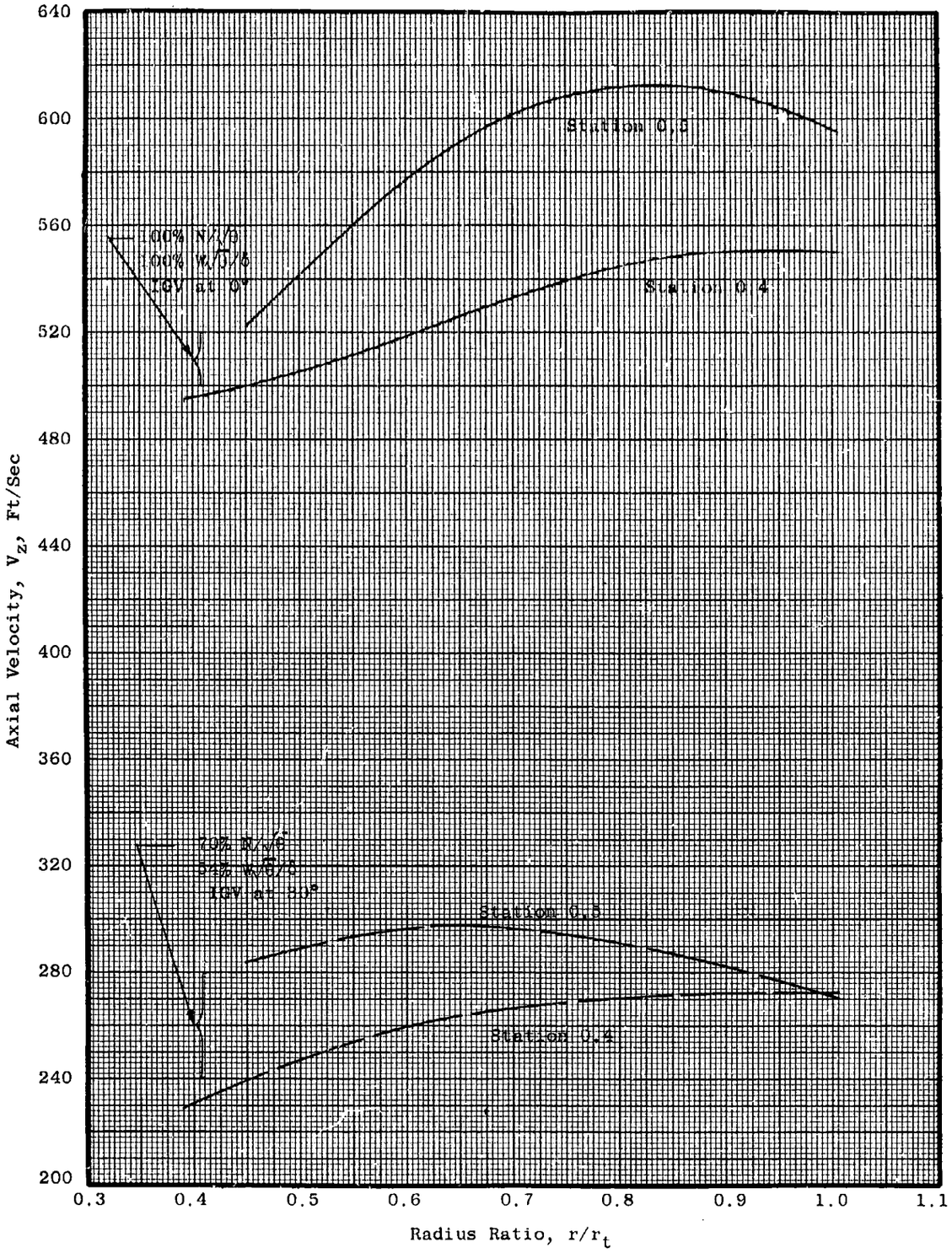

Figure 48. Distributions of Inlet Guide Vane Axial Velocity

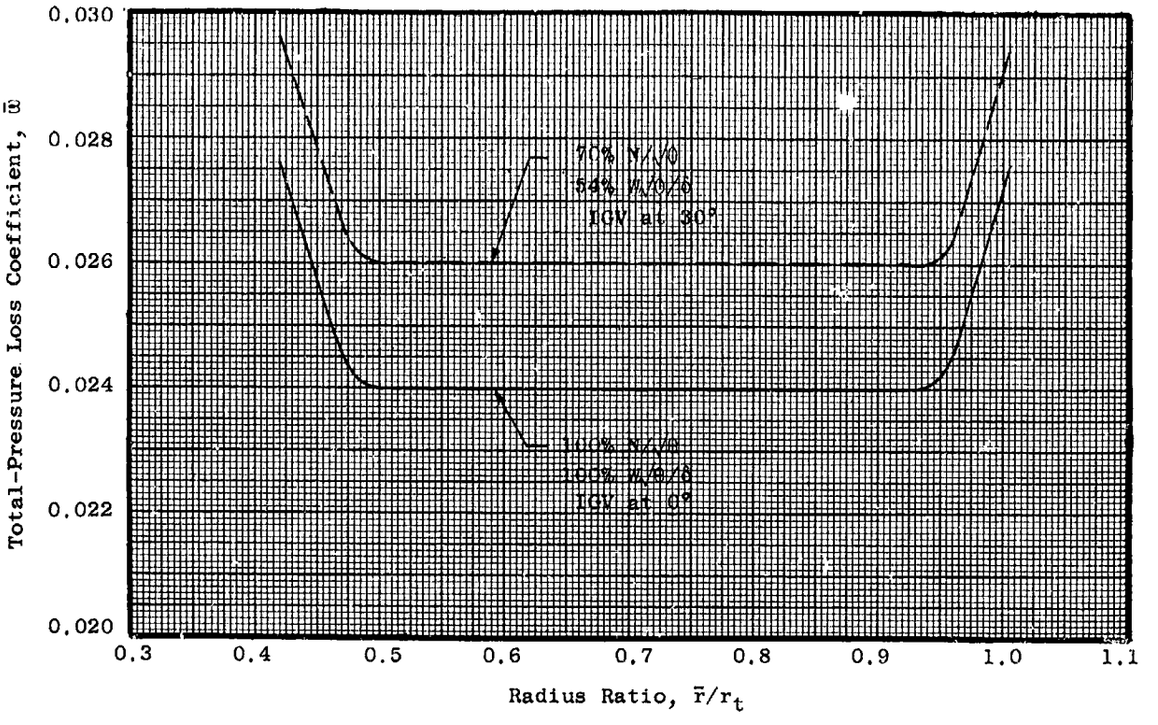

Figure 49. Inlet Guide Vane Total-Pressure Loss Coefficient Distributions

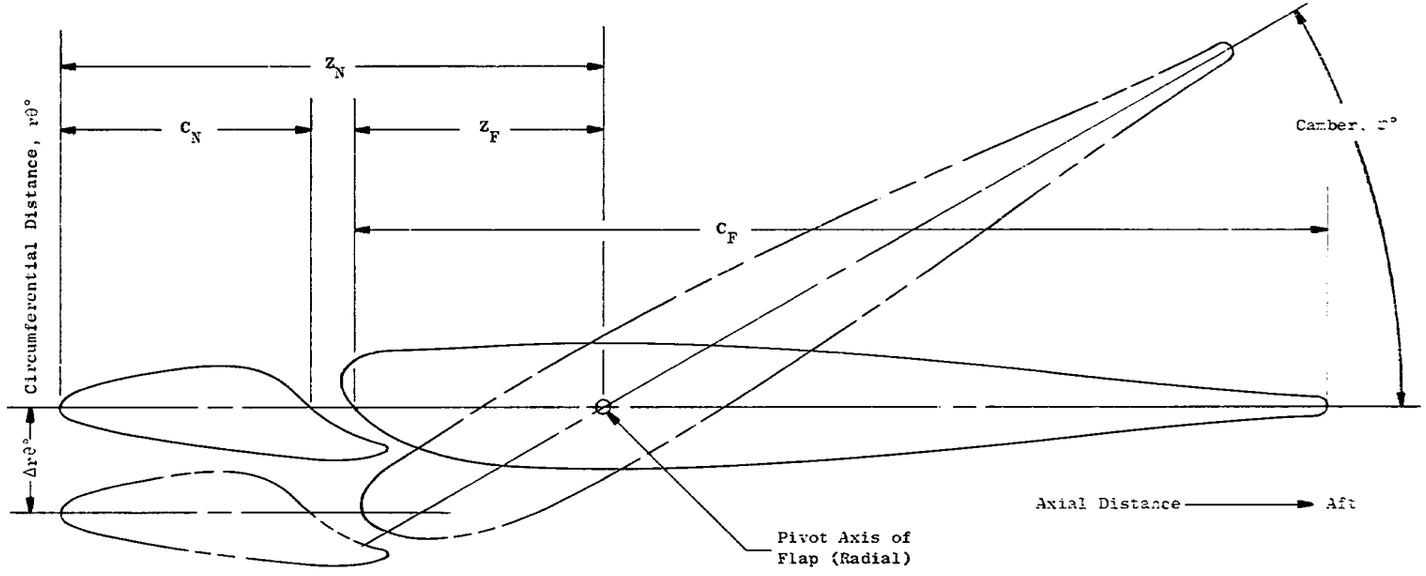

Figure 50. Variable Camber Inlet Guide Vane Pitch Section at Zero and 30° Turning

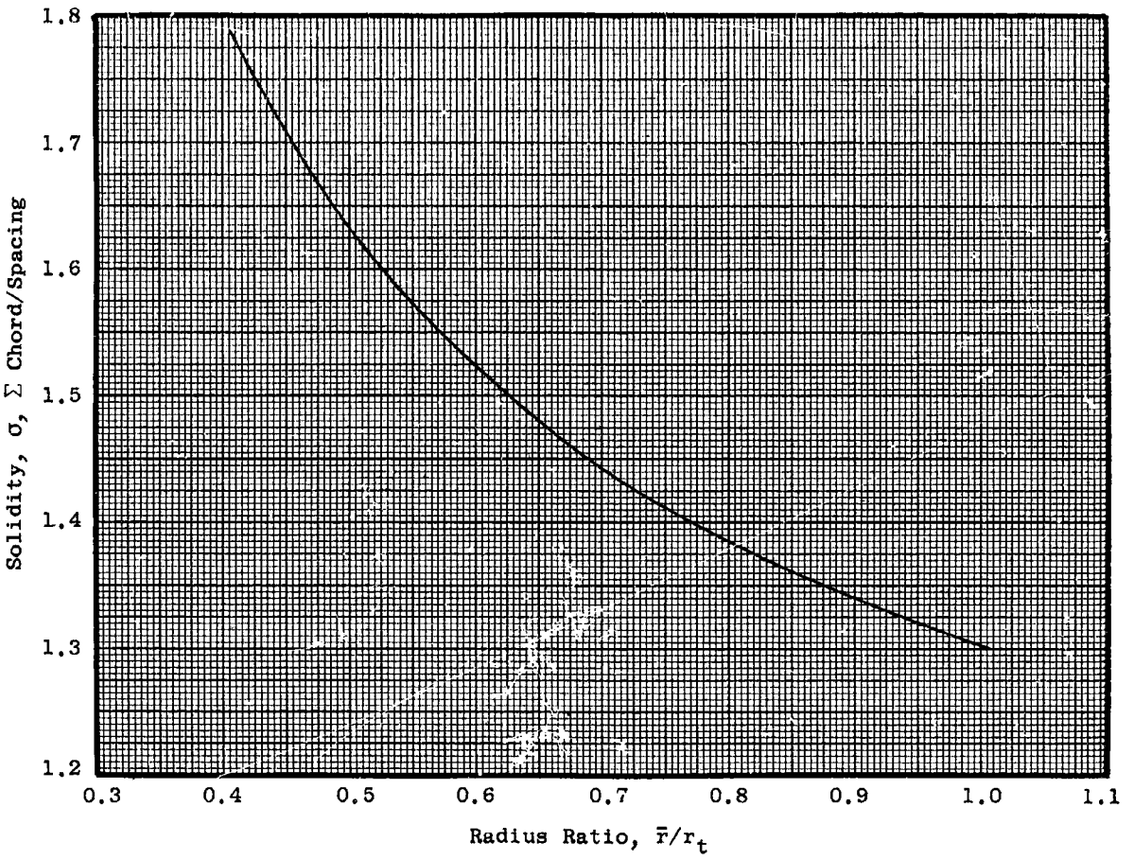

Figure 51. Inlet Guide Vane Solidity Distribution

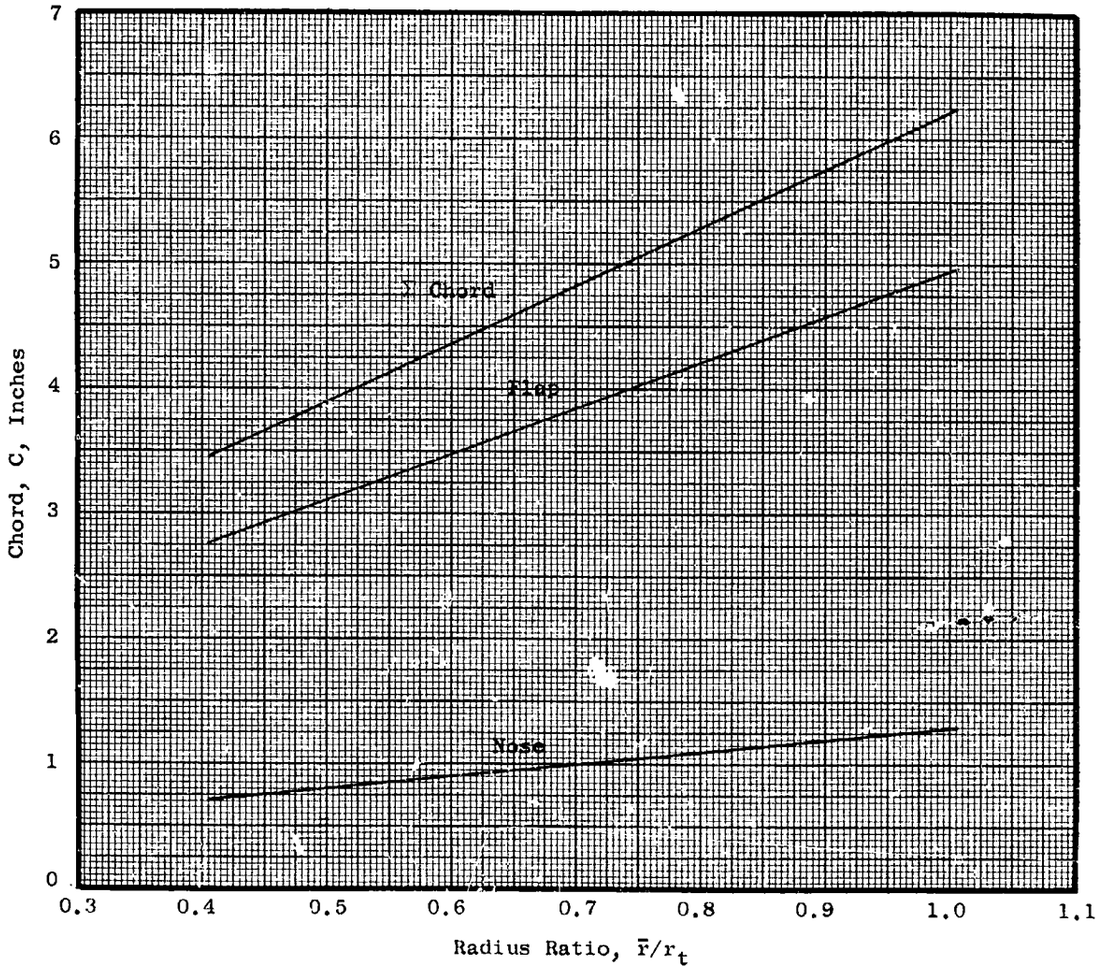

Figure 52. Radial Variations of Inlet Guide Vane Chord on Cylindrical Sections

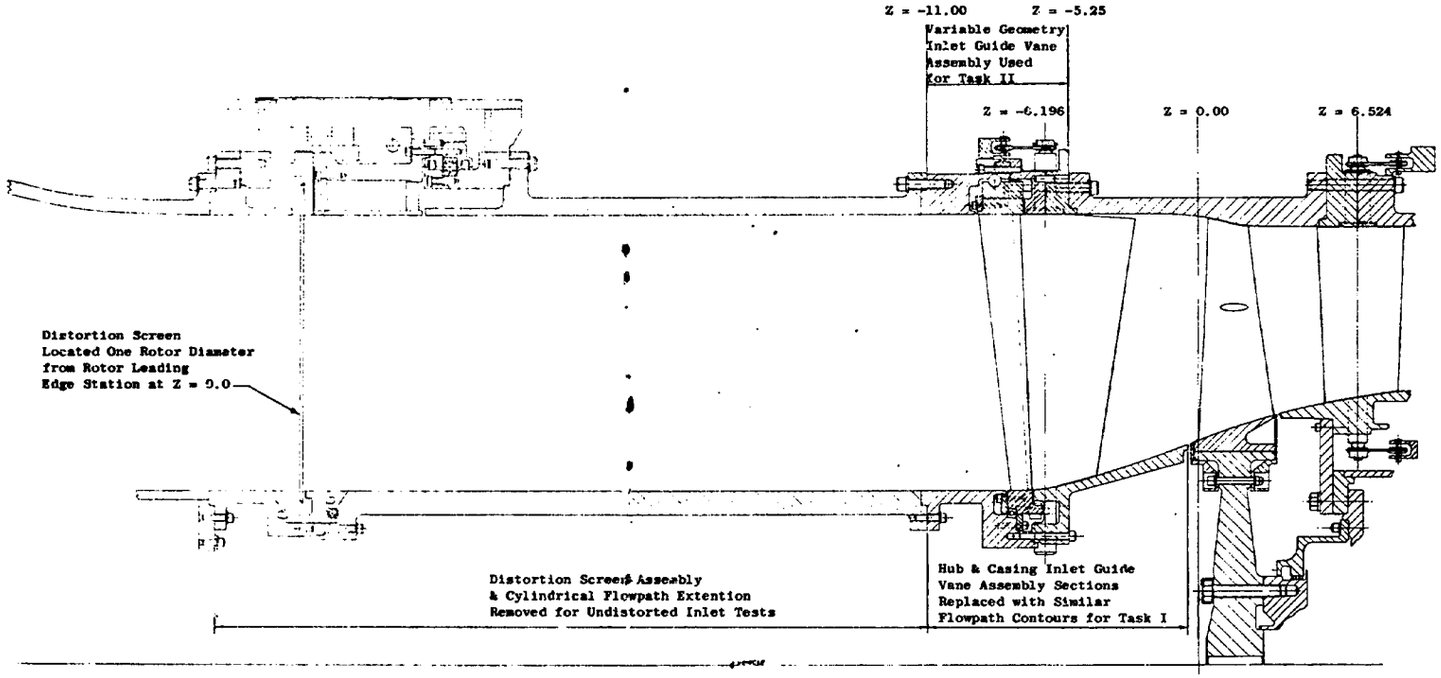

Figure 53. Assembly of NASA Tasks I and II Compressor Vehicles

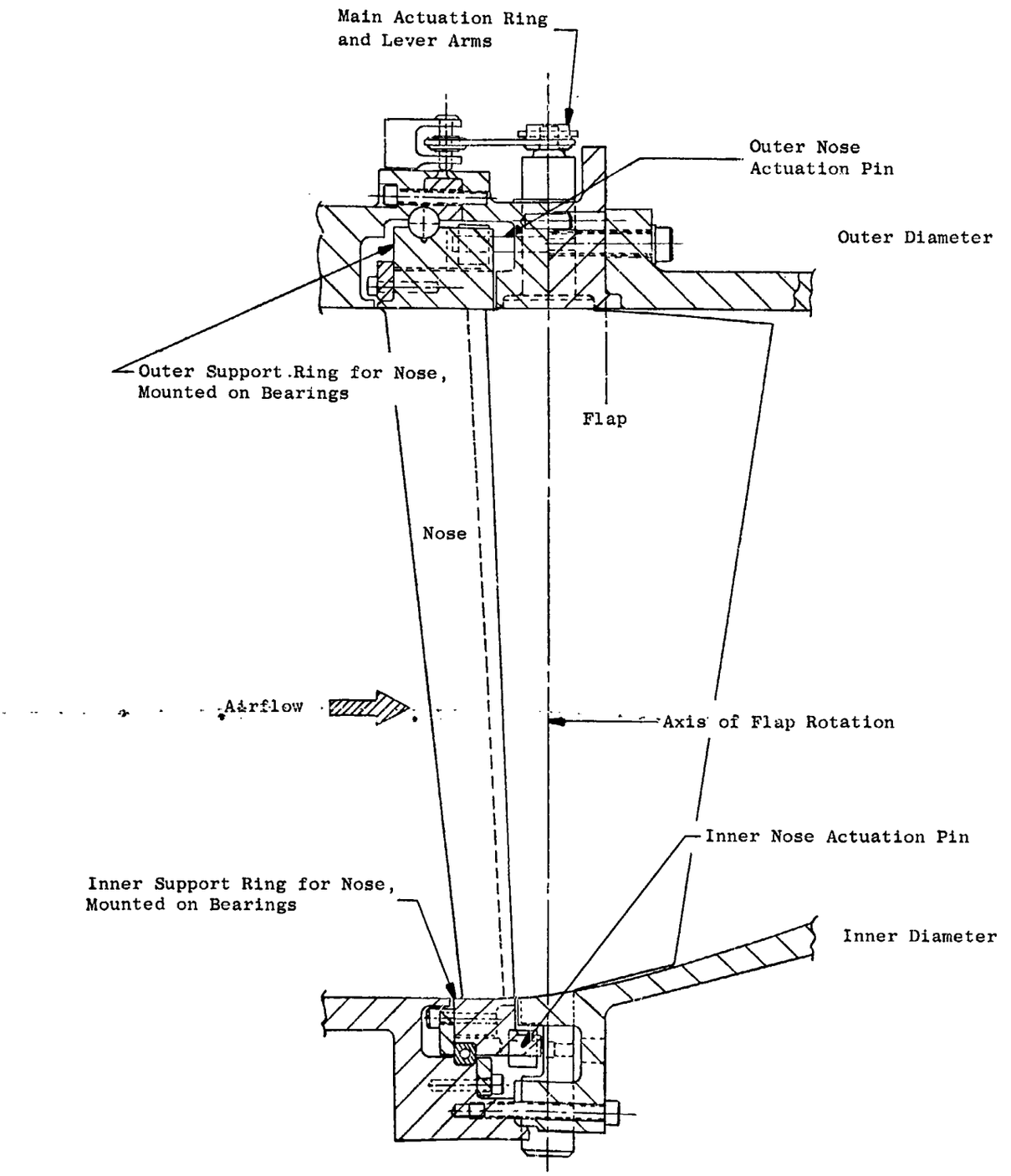

Figure 54. NASA Task II Variable Camber Inlet Guide Vane

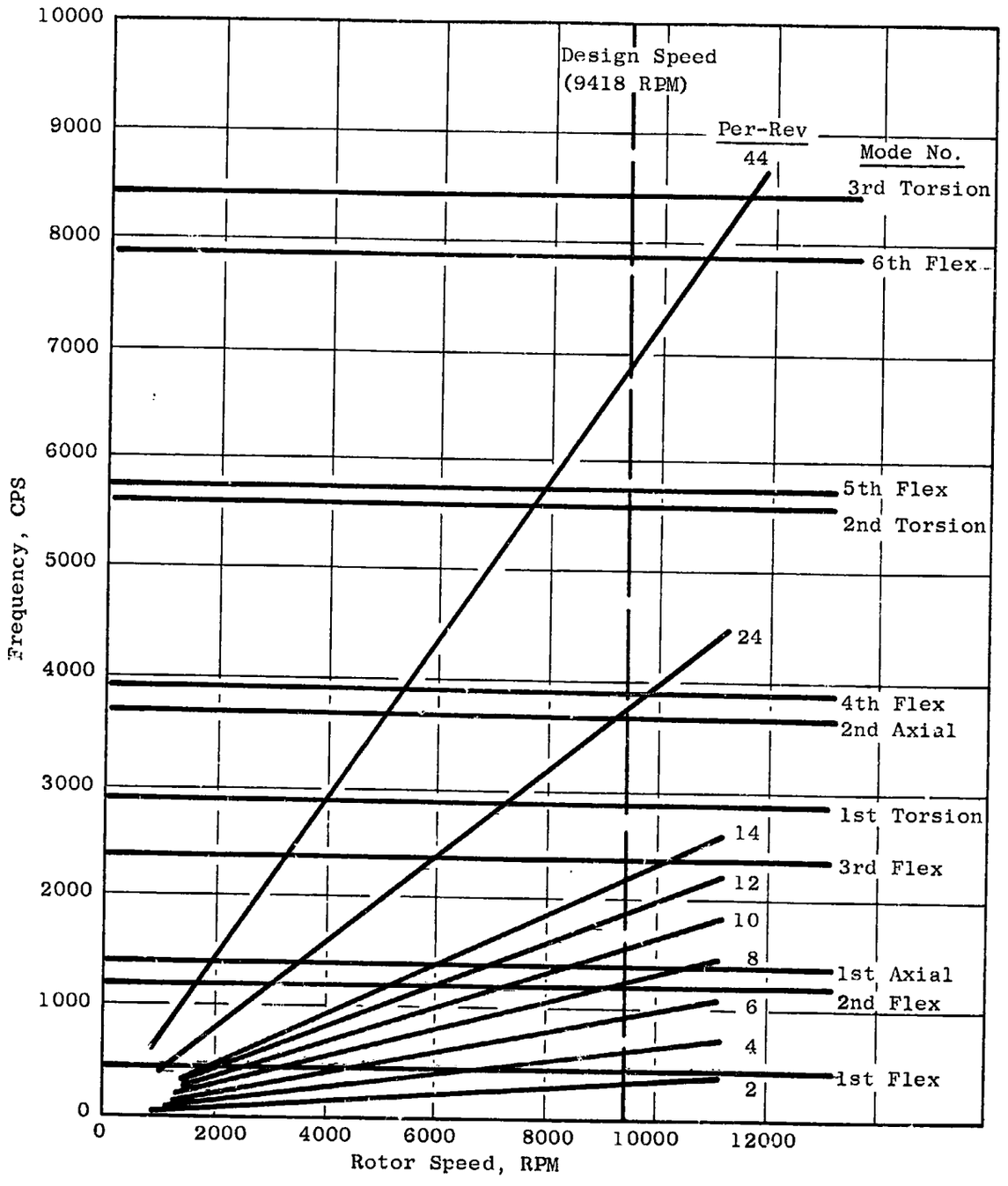

Figure 55. NASA Variable-Camber IGV Forward Vane (Nose) Campbell Diagram

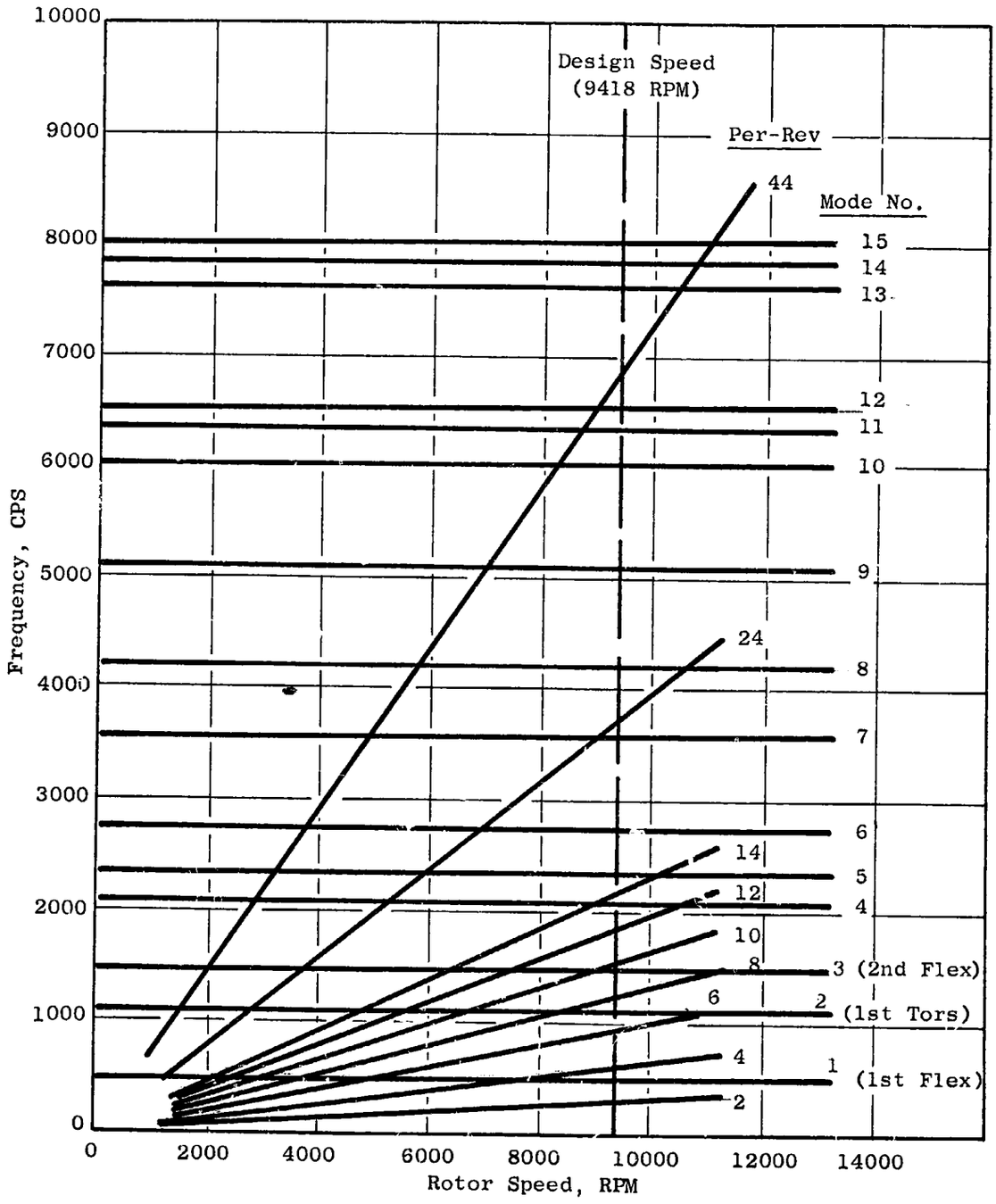

Figure 56. NASA Variable-Camber IGV Aft Vane (Flap) Campbell Diagram

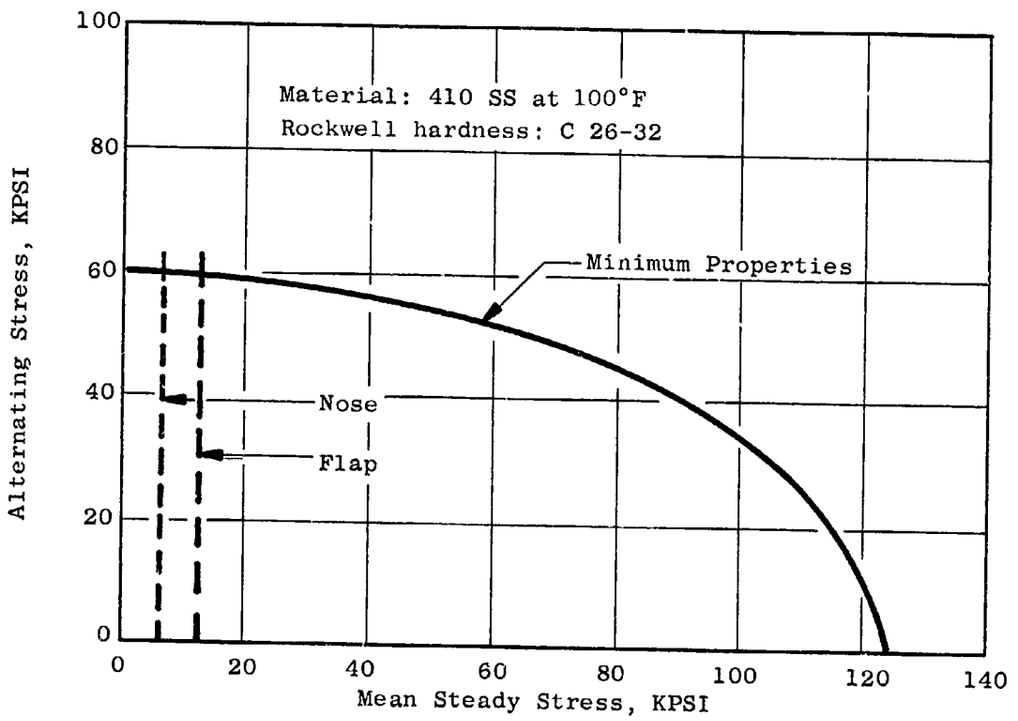

Figure 57. Stress Range Diagram for Variable-Camber IGV and Stator Vanes

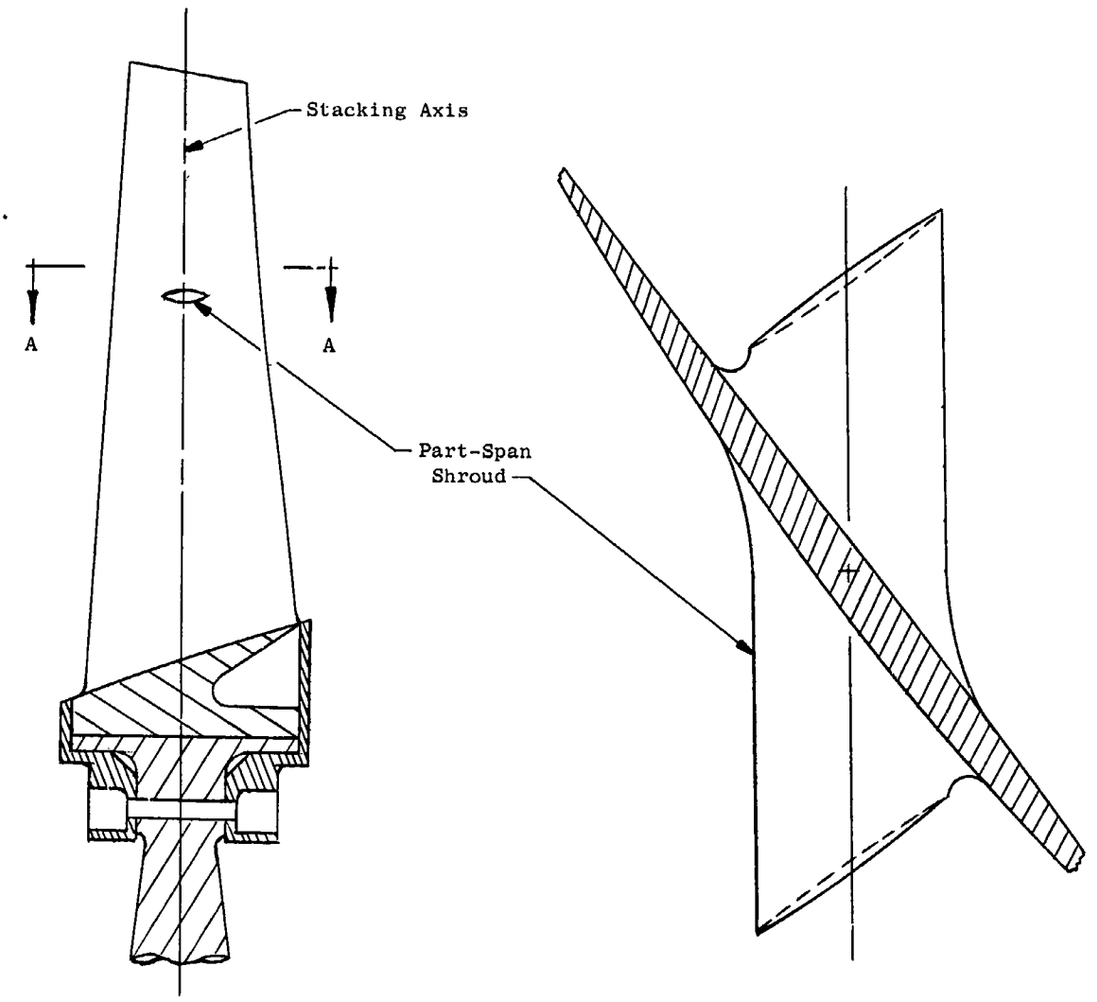

Figure 58. NASA Task II Rotor Blade

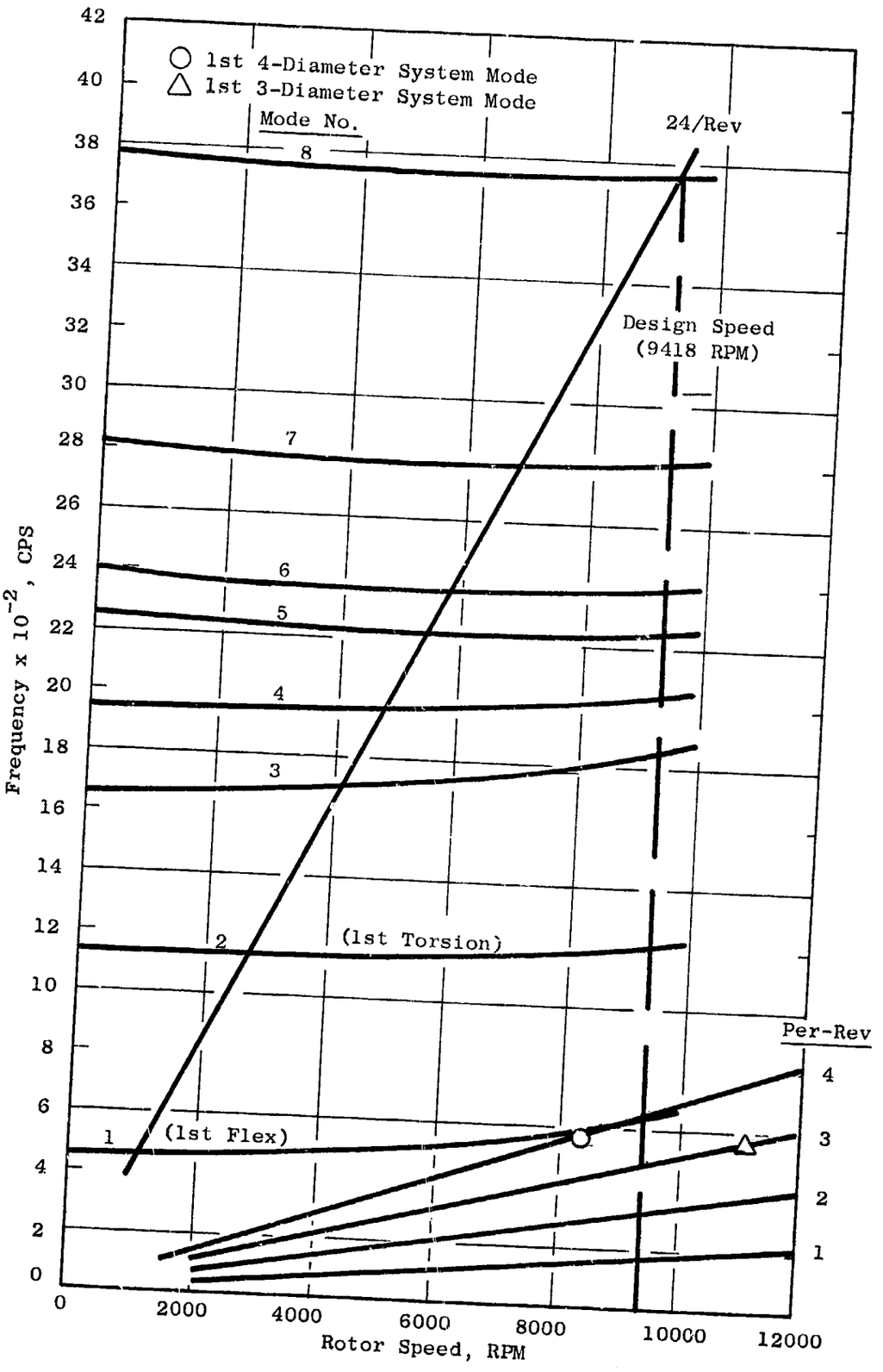

Figure 59. NASA Task II Rotor Blade Campbell Diagram

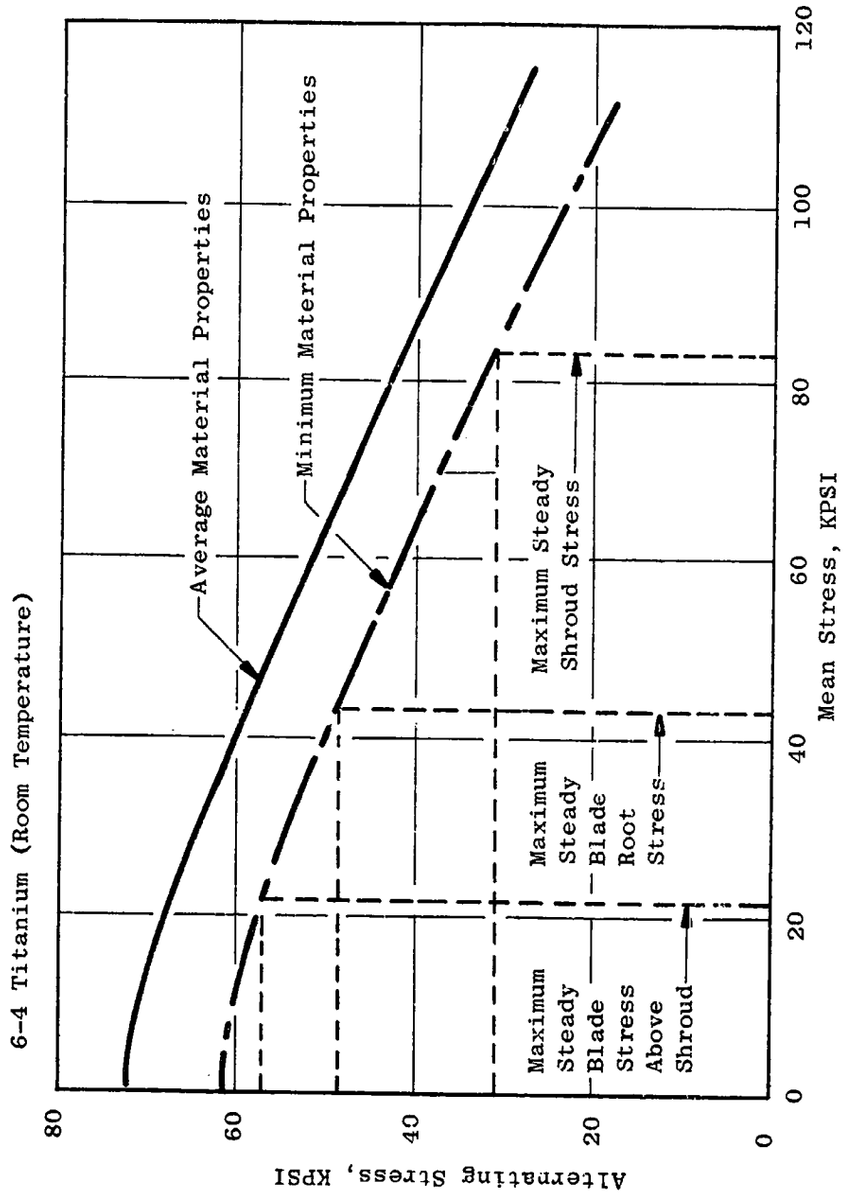

Figure 60. Stress-Range Diagram for Task II Rotor

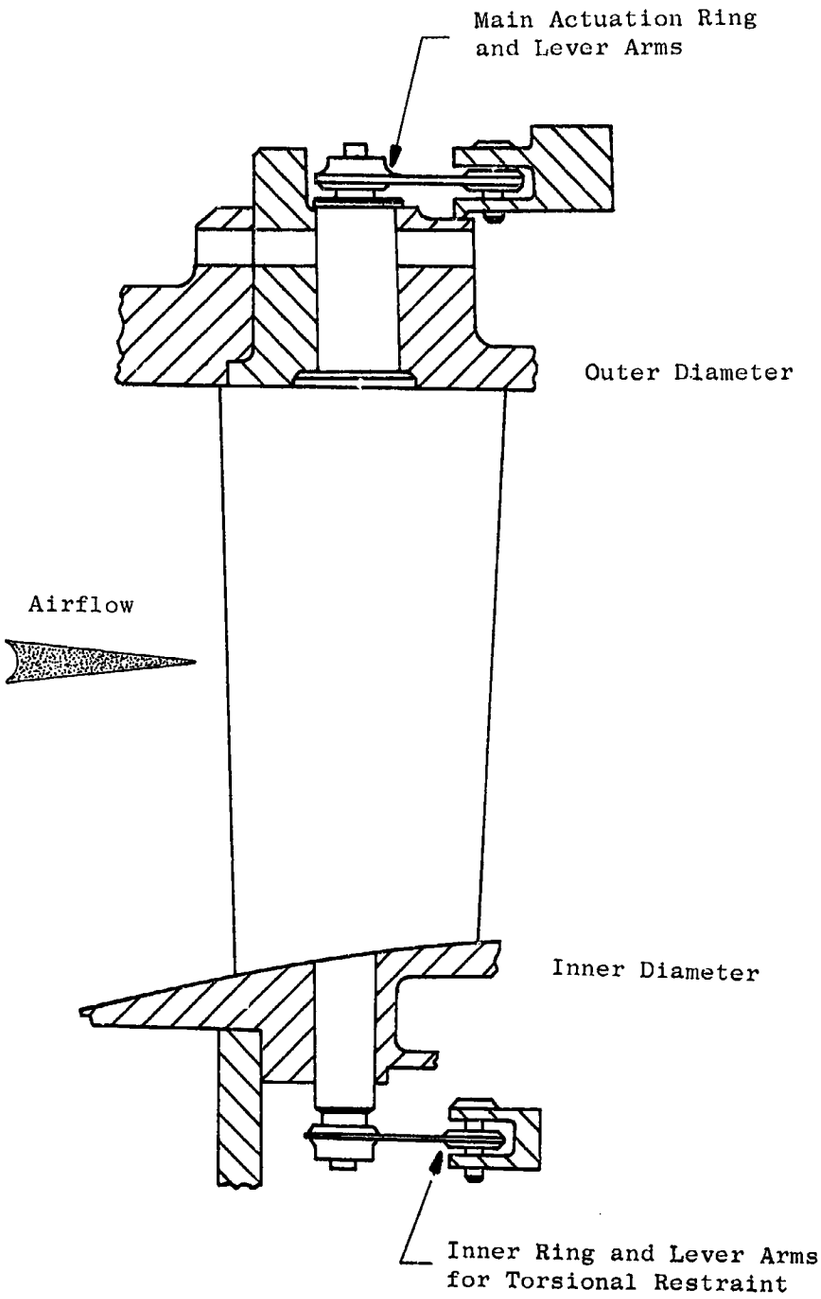

Figure 61. NASA Task II Stator Vane

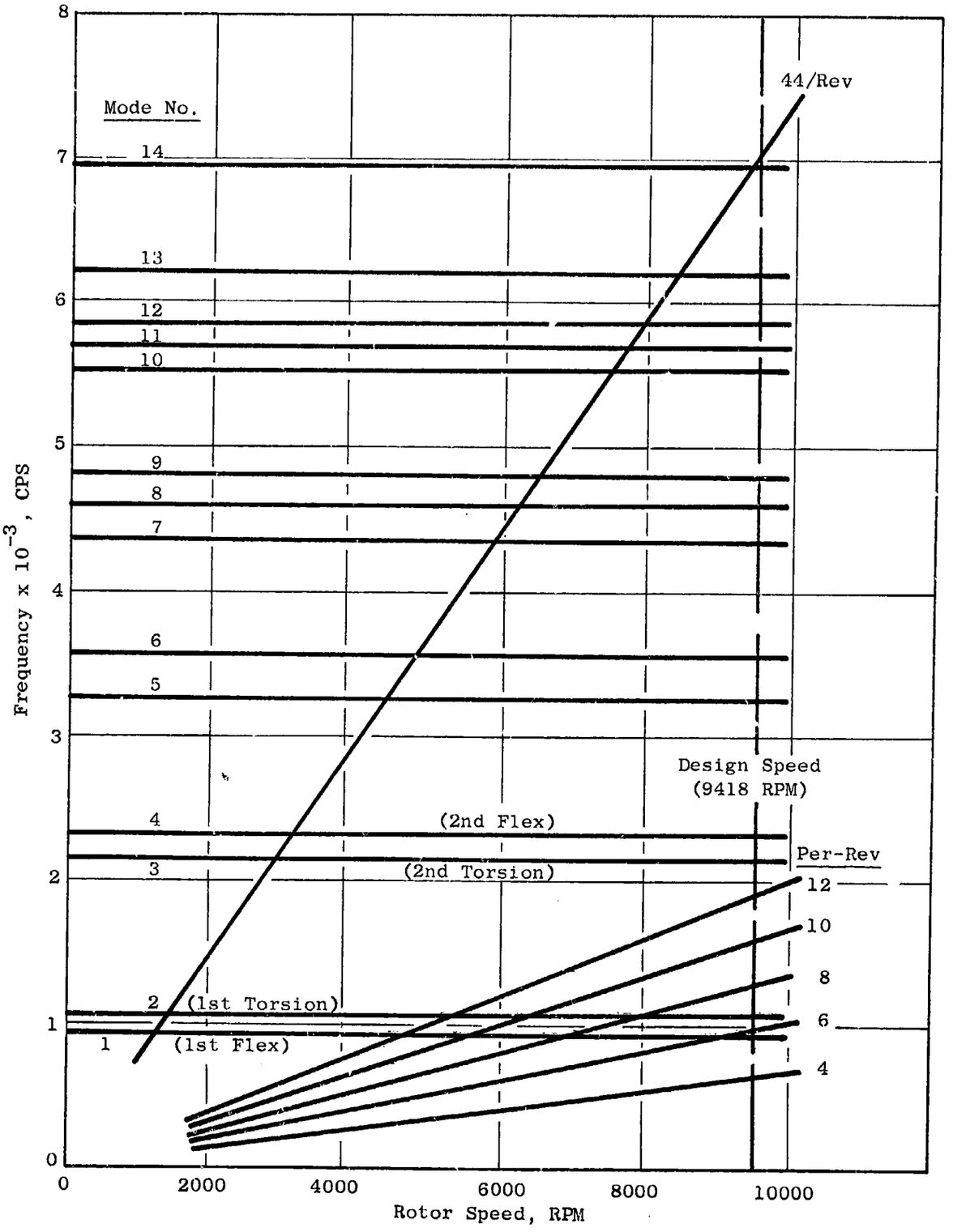

Figure 62. Campbell Diagram for NASA Task II Stator Vanes